TRANSPORTATION RESEARCH RECORD 827

General Soils Problems

TRANSPORTATION RESEARCH BOARD

COMMISSION ON SOCIOTECHNICAL SYSTEMS
NATIONAL RESEARCH COUNCIL

NATIONAL ACADEMY OF SCIENCES
WASHINGTON, D.C. 1981

Transportation Research Record 827
Price $6.20
Edited for TRB by Naomi Kassabian

modes
1 highway transportation
3 rail transportation
4 air transportation

subject areas
24 pavement design and performance
62 soil foundations
63 soil and rock mechanics
64 soil science

Library of Congress Cataloging in Publication Data
National Research Council (U.S.). Transportation Research Board. Meeting (60th: 1981: Washington, D.C.)
General soils problems.

(Transportation research record; 827)
Reports presented at the 60th annual meeting of the Transportation Research Board.
1. Pavements—Addresses, essays, lectures. 2. Soil mechanics—Addresses, essays, lectures. I. Title. II. Series.
TE7.H5 no. 827 [TE250] 380.8s [625.7'3] 82-3545
ISBN 0-309-03269-5 ISSN 0361-1981 AACR2

Sponsorship of the Papers in This Transportation Research Record

DIVISION A—REGULAR TECHNICAL ACTIVITIES
Lawrence D. Dahms, Metropolitan Transportation Commission, chairman

Committee on Low Volume Roads
Melvin B. Larsen, Illinois Department of Transportation, chairman
Richard G. Ahlvin, John A. Alexander, J.R. Bell, Mathew J. Betz, A.S. Brown, Everett C. Carter, Paul E. Conrad, Robert C. Deen, Martin C. Everitt, Asif Faiz, Gordon M. Fay, Raymond J. Franklin, Marian T. Hankerd, Clell G. Harral, William G. Harrington, Raymond H. Hogrefe, J.M. Hoover, Lynne H. Irwin, Delano S. Jespersen, Clarkson H. Oglesby, Adrian Pelzner, George B. Pilkington II, George W. Ring III, Eldo W. Schornhorst, Eugene L. Skok, Jr., Nelson H. Taber, Ronald L. Terrel, Eldon J. Yoder, John P. Zedalis

GROUP 2—DESIGN AND CONSTRUCTION OF TRANSPORTATION FACILITIES
R.V. LeClerc, Washington State Department of Transportation, chairman

Stabilization Section
Marshall R. Thompson, University of Illinois at Urbana-Champaign, chairman

Committee on Chemical Stabilization of Soil and Rock
Hassan A. Sultan, University of Arizona, chairman
Kandiah Arulanandan, Wallace Hayward Baker, William D. Bingham, Gail C. Blomquist, Robert C. Deen, Conan P. Furber, Edward D. Graf, T. Allan Haliburton, Darryl L. Hearn, Charles M. Higgins, Eugene Y. Huang, B. Dan Marks, James K. Mitchell, Raymond K. Moore, Thomas M. Petry, Marian E. Poindexter, Chester I. Schlarb, Walker L. Shearer, C.K. Shen, Andrew Sluz, Daniel R. Turner, Wilfred W. Wong

Soil Mechanics Section
Lyndon H. Moore, New York State Department of Transportation, chairman

Committee on Foundations of Bridges and Other Structures
Bernard E. Butler, New York State Department of Transportation, chairman
Arnold Aronowitz, Michael Bozozuk, W. Dale Carney, Harry M. Coyle, Gerald F. Dalquist, M.T. Davisson, Albert F. Dimillio, Bengt H. Fellenius, Frank M. Fuller, G.G. Goble, Richard J. Goettle III, Stanley Gordon, Stanley Haas, Hal W. Hunt, Philip Keene, Clyde N. Laughter, G.A. Leonards, Alex Rutka, Richard J. Suedkamp, Aleksandar S. Vesic, John L. Walkinshaw, James Doyle Webb, William J. Williams

Committee on Subsurface Drainage
Lyle K. Moulton, West Virginia University, chairman
Robert G. Carroll, Jr., Barry J. Dempsey, Eugene B. Drake, Wilbur M. Haas, William E. Harrison, Kent A. Healy, Gary L. Hoffman, S. Bennett P. John, Gary L. Klinedinst, B. Dan Marks, John E. Merten, S. Paul Miller, Lyndon H. Moore, Willard G. Puffer, Hallas H. Ridgeway, George W. Ring III, Gary A. Shepherd, William D. Trolinger, Hugh L. Tyner, Walter C. Waidelich, Clayton E. Warner, David C. Wyant, Thomas F. Zimmie

Geology and Properties of Earth Materials Section
David L. Royster, Tennessee Department of Transportation, chairman

Committee on Physicochemical Phenomena in Soils
Dwight A. Sangrey, Carnegie-Mellon University, chairman
George R. Glenn, Joakim G. Laguros, C. William Lovell, Charles A. Moore, Edward Belk Perry, Robert M. Quigley

John W. Guinnee, Transportation Research Board staff

Sponsorship is indicated by a footnote at the end of each report. The organizational units, officers, and members are as of December 31, 1980.

Contents

Authors of the Papers in This Record

Ahmed, Samir A., School of Civil Engineering, Oklahoma State University, Stillwater, OK 74078
Bell, J.R., Department of Civil Engineering, Oregon State University, Corvallis, OR 97331
Blair, J.C., Forest Service, U.S. Department of Agriculture, Wasatch National Forest, 8226 Federal Building, 125 South State, Salt Lake City, UT 84138
Das, Braja M., Civil Engineering Department, University of Texas at El Paso, El Paso, TX 79968
Greenstein, Jacob, Louis Berger International, Inc., 100 Halsted Street, East Orange, NJ 07019
Handfelt, L.D., Dames and Moore, 1100 Glendon Avenue, Los Angeles, CA 90024
Hicks, R.G., Department of Civil Engineering, Oregon State University, Corvallis, OR 97331
Hoover, J.M., Geotechnical Research Laboratory, Iowa State University, Ames, IA 50011
Livneh, Moshe, Department of Civil Engineering, Technion-Israel Institute of Technology, Haifa, Israel
Lovell, C.W., School of Engineering, Grissom Hall, Purdue University, West Lafayette, IN 47907
McDowell, Chester, Consulting Engineer, 703 E. 43rd Street, Austin, TX 78751
Moore, John C., Oklahoma State University, Stillwater, OK 74978 (deceased)
Pitt, J.M., Geotechnical Research Laboratory, Iowa State University, Ames, IA 50011
Siddiqi, Razi A., Garyounis University, P.O. Box 9476, Bengazi, Libya
Stanley, R.L., Ames Engineering and Testing Company, 1212 McCormick, Ames, IA 50010
Surendra, M., ATEC Associates, Inc., 5150 East 65th Street, Indianapolis, IN 46220
Wood, L.E., School of Engineering, Grissom Hall, Purdue University, West Lafayette, IN 47907

Permeability Testing of Geotextiles

J.C. BLAIR, J.R. BELL, AND R.G. HICKS

In recent years, geotextiles (filter fabrics) have been used extensively as filters for drainage systems. Unfortunately, the increase in use has not been accompanied by the development of suitable testing methods or specifications. This paper investigates fabric permeability tests and factors that affect the measurement of permeability and provides recommendations for a method to measure permeability. Both water and air permeability tests were evaluated by using nine geotextiles. For the water tests, a falling-head permeameter was used. The results indicated that the permeability of geotextiles was quite variable both within and between lots and the effect of the hydraulic gradient in the water test was significant. Data were also obtained to show the effects of sample size and operator and the number of samples needed to ensure a given level of accuracy. The term "permittivity," or permeability divided by fabric thickness, is presented. Fabrics that have high permeability do not always have high permittivity. Also, there is a linear relation between permittivity measured by the air and by the water tests. Because of its simplicity, the falling-head permeameter is recommended for adoption. The air-permeability test also shows potential for providing accurate results.

Control of subsurface water is often a problem during and after construction of an engineering project. Drainage must be provided so that excessive water pressures or seepage forces do not develop. Inadequate drainage may result in the instability of a soil mass and subsequent structural failure.

The need for adequate drainage of highways has become especially apparent in recent years because of the increasing number of pavement failures attributed to poor drainage (1). Conventional drainage design specifies graded aggregate filters so that soil movement into hydraulic structures is prevented. However, due to recent technological advances in the textile industry, geotextiles (filter fabrics) have gained increased acceptance as effective filters in drainage systems (2). The replacement of conventional aggregate filters with fabric reduces the amount of aggregate needed, eliminates the need for strict gradation control during filter placement, provides greater ease of construction, and, in most cases, reduces the overall cost of the drain.

Unfortunately, the rapid increase in fabric use has not been accompanied by the development of suitable design, testing, and evaluation technology. Basically, it is known that the geotextile must satisfy two requirements in filtration applications. First, the fabric must be sufficiently permeable to allow removal of groundwater without the buildup of excessive water pressures. Second, the fabric must be able to prevent piping or subsurface erosion of the soil mass being drained. Recent studies suggest that design for the retention of soil particles suspended in water might be accomplished through the use of relationships between soil grain size and the coefficient of permeability (3,4). Thus, the importance of geotextile permeability in drainage design is to permit the removal of groundwater without the buildup of excessive water pressures and to prevent the erosion of soil particles.

Several studies have been conducted to evaluate the permeability of systems of soil and fabric in direct contact (5-8). However, to provide a simple comparison of permeability of different geotextiles, the fabrics must be evaluated in isolation to eliminate variations due to different soil characteristics.

The purposes of this paper are (a) to investigate fabric permeability tests and factors that affect the measurement of permeability and (b) to recommend a method for measuring fabric permeability. The scope is limited to testing fabrics in isolation. Mechanisms of filtration of soil particles are not considered nor is the influence of biological growth or chemical deposits and chemical, biological, or mechanical degradation on hydraulic behavior.

PERMEABILITY TESTING

Permeability is normally expressed in the form of Darcy's law, which assumes laminar flow. Then

$$k = q/(iA) \quad (1)$$

where

- k = coefficient of permeability,
- q = volume of flow per unit time,
- i = hydraulic gradient (= h/L, where h is head loss and L is thickness of fabric), and
- A = cross-sectional area (9).

When turbulence occurs, a linear relationship between velocity and hydraulic gradient no longer exists. Darcy's law may be modified to account for turbulence as follows:

$$v^n = ki \quad (2)$$

where n is the turbulence coefficient (10,11). Values of n are greater than 1 for turbulent flow.

Fabric permeability testing by using water as the fluid has been performed by others (11-13; personal communication from J.P. Giroud, Woodward-Clyde Consultants of Chicago, IL). Both constant and falling-head test methods have been employed. In most cases, the number of specimens tested was small; however, several significant factors that affect test results were noted. These included turbulence, air in the system, and fabric compressibility.

Variation in fabric types is also a major factor that must be considered in test evaluation. Fabric characteristics that can affect test results are fiber diameter, type of construction, thickness, fiber density, and rigidity of structure.

Because the geotextiles are thin, it may be more meaningful to relate the flow through the fabric to the total hydraulic head loss across the fabric rather than to permeability. The permittivity (P), which is the ratio of the permeability to the geotextile thickness (k/L), provides this alternative. Permittivity is the volume of water that will flow per unit area of geotextile in a unit of time with a unit head loss across the fabric.

Numerous factors deserve consideration in geotextile permeability (permittivity) testing. As in all testing, the sample size and selection must be appropriate (sufficient specimens) to represent the material with the desired accuracy. There are also the usual permeability testing problems of deairing the water, the specimen, and the system; controlling or measuring temperature; and providing water of adequate quality. Further, the apparatus and procedure should not be sensitive to operator skill.

The combination of high permeability and small thickness creates special problems for testing geotextiles in a water-permeability test. With moderate gradients the flow rate is very high in a constant-head device. This requires large volumes of water, which creates supply problems if deaired

Table 1. Geotextiles tested.

Identification No.	Fiber Polymer(s)	Construction	Nominal Weight (g/m^2)	Average Thickness (mm)
Nonwoven Geotextile				
NW-1(3)	Polyester	Resin-bonded staple filament	100	0.86
NW-2(4)	Polypropylene and polyamide	Heat-bonded continuous filament	140	0.74
NW-3(4)	Polypropylene	Heat-bonded continuous filament	140	0.38
NW-4(8)	Polyester	Needle-punched continuous filament	270	3.00
NW-5(13)	Polypropylene	Needle-punched continuous filament	400	5.16
Woven Geotextile				
W-1(4)	Polyamide	Woven multifilament	240	0.51
W-2(7)	Polypropylene	Woven monofilament	220	0.41
W-3(8)	Polypropylene	Woven slit film	150	0.56
Combination Geotextile				
C-1(4)	Polypropylene	Woven slit film with needle-punched nap	140	0.97

Note: 1 gm/m^2 = 0.029 oz/yd^2; 1 mm = 0.004 mil.

Figure 1. Schematic of falling-head test apparatus.

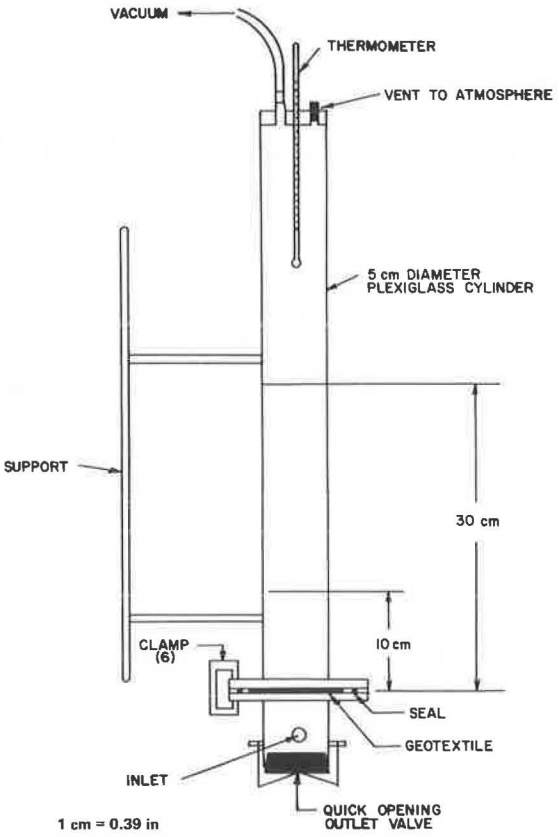

and filtered or distilled water is to be used. The gradient may be reduced by reducing the head loss across the specimen or by stacking several fabric specimens to increase the length of flow. The low head causes problems of accurate control. Stacked specimens create problems with deairing, clamping, and leakage.

A falling-head test solves the problem of needing large volumes of water, but the water level tends to drop very rapidly in the standpipe, which makes accurate time measurement difficult. This can be overcome by selecting a standpipe diameter larger than the specimen diameter. This tends to reduce practical specimen size and requires more tests to obtain a reliable mean. Times and head changes large enough for convenient, accurate determinations result in gradients too large to assure laminar flow.

An alternative to trying to resolve these problems is to use a gas rather than a liquid to measure the permeability. It is theoretically possible to relate gas permeability to water permeability (10).

TEST PROGRAM

Two tests were conducted. An air test was selected to investigate the feasibility of this method for predicting water permeability. A falling-head water test was chosen for comparison because of its simplicity.

Nine geotextiles were investigated. They were selected to represent a range of types and weights commonly used in the United States in 1979. Table 1 lists the fabrics and their thickness, nominal weight, polymer type(s), and construction.

Seven specimens of each fabric were tested by using each method. The means of these tests were used to estimate the sample sizes required for specific desired accuracies. Some studies were also made of the effects of sampling within and between lots. The effects of gradient (turbulence) were also investigated for two geotextiles in the falling-head test by testing stacks of different numbers of specimens.

Air Permeability

Air-permeability tests were performed in accordance with ASTM D737. All fabrics were tested by using a pressure difference equivalent to 1.27 cm (0.5 in) of water across the fabric. The tests were performed by using a United States Testing Company, Inc., Air Flow Tester, Model 9025.

Water Permeability

The falling-head test apparatus consisted of a cylinder 5.08 cm (2 in) in diameter that had a 2.54-cm (1-in) opening at the flanges, as shown in Figure 1. The fabric was clamped between the flanges. After all openings had been sealed, a vacuum of 64 cm (25 in) of mercury was applied to the permeameter to ensure that air did not remain entrapped within the fabric. The permeameter was filled with deaired, distilled water from the bottom with the vacuum applied. After the temperature had been noted, the time for the water level to fall from 30 to 10 cm (11.8-3.9 in) above the fabric was re-

corded. The number of timings for each sample was determined after seven runs had been performed on the first specimen. The number of runs with one specimen required to yield a mean time within 5 percent of the true mean with a 95 percent probability was calculated by using Equation 3:

$$n_t = 0.154v^2 \quad (3)$$

where n_t is the number of timings required and v is the coefficient of variation as a percentage (ASTM D2905). Two to five runs per specimen were required for the fabrics studied; three runs were most common. With the ratio of standpipe to sample of 2, the time required for the head to drop from 30 to 10 cm ranged from 1.5 to 50 s. This allowed accurate manual timing.

Deaired water was used to eliminate variations in test results due to entrapped air within the fabric. This action and application of the vacuum before filling eliminated any need for prewetting the samples to ensure saturated samples. For some samples, a fiber coating would make prewetting difficult.

Water-permeability tests should also be performed by using distilled water or filtered tap water. Tap-water impurities may plug the fabric, which results in a lower coefficient of fabric permeability.

Thickness Measurement

Thickness was measured according to the procedure described in ASTM D1777 except that a 125-g (4.3-oz) load was applied over a 25-cm² (3.88-in²) pressure plate bearing on the fabric. These values were selected so that a nominal pressure would minimize fabric compression and a fairly large area would allow for fabric irregularities.

Calculations

The apparent coefficients of permeability for the geotextiles (for water at 20°C, assuming laminar flow) were calculated from the falling-head test data by the usual falling-head equation (1):

$$k_f = [(aL)/(At)]\,[\ln(h_i/h_f)]\,(\mu_{\omega t}/\mu_{\omega 20}) \quad (4)$$

where

k_f = coefficient of permeability at 20°C measured by using water in a falling-head test,
a = area of standpipe,
A = area of fabric,
L = fabric thickness,
h_i = original height of water above fabric,
h_f = final height of water above fabric,
$\mu_{\omega t}$ = absolute viscosity of water at test temperature,
$\mu_{\omega 20}$ = absolute viscosity of water at 20°C, and
t = average time for water surface to fall from h_i to h_f.

The coefficients of permeability for the geotextiles for water at 20°C were calculated from the air-test data by the following equation (10):

$$k_a = q\left\{[(\mu_{at})L/(\Delta PA)]\,(\gamma_{\omega 20}/\mu_{\omega 20})\right\} \quad (5)$$

where

k_a = coefficient of permeability at 20°C measured by using air,
ΔP = pressure difference across fabric,
q = air volume rate of flow at mean pressure,
$\gamma_{\omega 20}$ = unit weight of water at 20°C, and
μ_{at} = absolute viscosity of air at test temperature.

Permittivity was calculated from the following equation:

$$P = k/L \quad (6)$$

by using either k_a or k_f.

For each fabric, the number of specimens required to obtain a mean value of the coefficient of permeability within 5 percent of the true mean at a probability level of 95, 90, and 80 percent was calculated by assuming a student's t-distribution as follows (ASTM D2905):

Probability (%)	No. of Samples Required
95	$0.154v^2$
90	$0.108v^2$
80	$0.066v^2$

The test results are summarized in Tables 2 and 3.

DISCUSSION OF RESULTS

For the geotextiles tested, apparent coefficients of permeability from falling-head water tests (k_f) ranged from 0.2×10^{-2} to 37.8×10^{-2} cm/s. Permittivity values ranged from 0.03 to 1.44 s^{-1}. The relationship between apparent permeability and permittivity is illustrated by considering fabrics NW-4(8) and NW-2(4). Fabric NW-4(8) ($k_f = 3.38 \times 10^{-1}$ cm/s) is about four and one-half times as permeable as NW-2(4) ($k_f = 0.78 \times 10^{-1}$ cm/s), but both have the capacity to pass nearly the same quantity of water per unit time with permittivities of 1.15 s^{-1} and 1.07 s^{-1}, respectively. Considering all the fabrics tested, the maximum apparent permeability coefficient is 189 times the minimum, but the maximum permittivity is only 48 times its corresponding minimum. The orders also change. The most permeable geotextile in terms of coefficient of permeability is only fourth in terms of permittivity.

The effect of gradient on the apparent coefficient of permeability measured in the falling-head test is indicated in Figure 2. These data are obtained from tests run by using from one to five layers of fabric in the permeability device. When more layers are used, the total thickness increases and, with other conditions being equal, the gradient through the geotextile decreases. The resulting increase in apparent permeability is probably due to reduced turbulence. The apparent coefficient of permeability increases until a constant value is approached. This corresponds to the maximum gradient for which flow is laminar and Darcy's law is valid. For the two fabrics tested, the true coefficient of permeability is approximately twice the apparent value obtained by using one layer of geotextile.

Experimentally, the problem of turbulence in tests that use water may be overcome either by increasing the number of fabric layers within the laminar range of flow or by performing tests at very low gradients. As mentioned previously, both these alternatives present problems. Another possibility may be to test by using a gas rather than a liquid.

The relationship between permittivities of the geotextiles to water as measured by air- and water-permeability tests is shown in Figure 3. There is a very good linear correlation between the two sets of data. The air-determined permittivity, however, is approximately twice the value measured in the

Table 2. Summary of air-permeability test results.

Fabric No.	Coefficient of Permeability: k_a (cm/s x 10^2)	Coefficient of Variation (%)	Required No. of Samples[a]: n_{95}	n_{90}	n_{80}	Permittivity p_a (s^{-1} x 10)
Nonwoven						
NW-1(3)	22.1	5.0	4	3	2	25.9
NW-2(4)	15.8	10.3	17	12	7	21.8
NW-3(4)	2.2	15.8	39	27	17	5.7
NW-4(8)	64.3	4.4	3	3	2	21.5
NW-5(13)	65.5	13.1	27	19	12	12.8
Woven						
W-1(4)	0.3	6.9	8	6	4	0.5
W-2(7)	4.2	11.9	22	16	10	10.4
W-3(8)	0.3	13.4	28	20	12	0.7
Combination						
C-1(4)	1.9	13.4	28	20	12	2.0

Note: 1 cm/s = 0.39 in/s.

[a]Required to yield a mean within 5 percent of the true mean at probability levels of 95, 90, and 80 percent.

Table 3. Summary of falling-head permeability test results.

Fabric No.	Coefficient of Permeability: k_a (cm/s x 10^2)	Coefficient of Variation (%)	Required No. of Samples[a]: n_{95}	n_{90}	n_{80}	Permittivity p_f (s^{-1} x 10)
Nonwoven						
NW-1(3)	12.3	8.4	11	8	5	14.4
NW-2(4)	7.8	8.3	11	8	5	10.7
NW-3(4)	1.3	12.3	24	17	10	3.4
NW-4(8)	33.8	17.0	45	32	20	11.5
NW-5(17)	37.8	9.8	15	11	7	7.4
Woven						
W-1(4)	0.2	9.3	14	10	6	0.4
W-2(7)	1.8	16.2	41	29	18	4.5
W-3(8)	0.2	14.7	33	24	15	0.3
Combination						
C-1(4)	1.0	23.4	85	60	37	1.1

Note: 1 cm/s = 0.39 in/s.

[a]Required to yield a mean within 5 percent of the true mean at probability levels of 95, 90, and 80 percent.

Figure 2. Relationship between total fabric thickness and coefficient of permeability for two geotextiles.

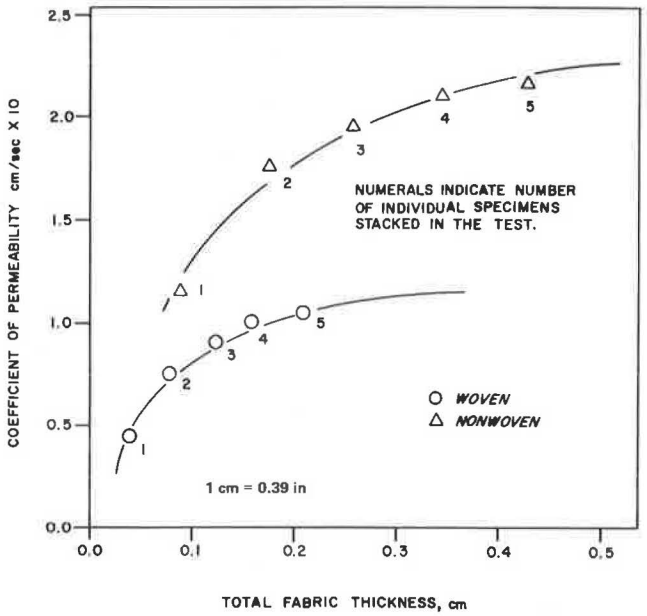

falling-head test by using water. This ratio of the air-determined to water-determined values is close to the ratio of multilayer to single-layer specimen values. It appears that the air-permeability test may be a simple, practical means of measuring geotextile permeability. Also the air-permeability test can be performed more quickly. However, initial expenditures are higher. This test deserves additional study to confirm the results of this investigation.

Data obtained in this study allow the evaluation of specimen variability, sample variability, operator variability, and the number of specimens required for desired accuracies.

Table 4 identifies the effects of sample selection on air-permeability test results. For two of the three fabrics, the coefficient of variation was essentially independent of where specimens were cut, provided that they were taken from the same lot. However, for the other fabric, the coefficient of variation was much greater when specimens were selected randomly over a large area than when they were taken from one localized area. This indicates that fabric variability may be high over a large area; therefore, specimens should be taken over a large area to obtain a representative value of permeability.

The variation in air-permeability results between

Figure 3. Relationship between air-test and water-test permittivities.

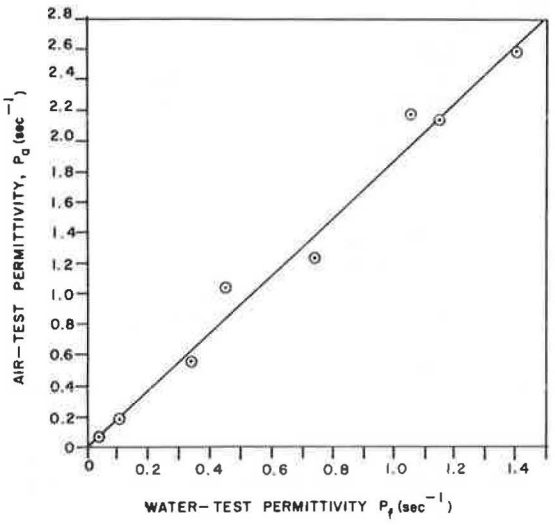

Table 4. Effect of sampling on air-permeability results.

Fabric Samples	Mean Flow Rate ($ft^3/ft^2/min$)	Standard Deviation	Coefficient of Variation (%)
NW-4(4)			
A	458.3	49.80	10.87
B	425.6	43.32	10.18
C	319.7	12.03	3.76
W-2(7)			
A	146.2	18.5	12.7
B	147.4	15.08	10.64
C	109.4	34.77	31.78
NW-3(6)			
A	23.3	1.85	7.92
B	20.6	3.00	14.57
C	27.5	4.47	16.30

Notes: 1 ft^3 = 0.028 m^3; 1 ft^2 = 0.092 m^2.
A and B were taken from the same lot. The A specimens were cut from a large area. The B specimens were randomly selected from a large area. The C specimens originated from a different fabric lot. There were seven specimens in each sample.

Table 5. Effect of operator variance on falling-head test results on one fabric specimen.

Parameter	Operator		
	A	B	C
Calculated mean permeability k_f (cm/s)	0.113	0.114	0.120
Standard deviation	0.0087	0.0143	0.0077
Coefficient of variation (%)	2.91	4.77	2.42
Number of timings	7	7	7

Note: 1 cm = 0.39 in.

different lots of fabric is also exemplified in Table 4. In all cases, there is a 30-45 percent variation in the mean flow rate between lots. In addition, for two cases the higher flow rates corresponded to fabrics that had greater thicknesses. This combination of high flow rates and greater thicknesses results in even greater variability between coefficients of permeability. For example, the coefficient of permeability varied by almost a factor of 3 between lots for NW-4(4). It cannot be assumed that the mean permeability will be constant for all fabric lots. Values of permeability should be checked each time new fabric is introduced.

Specimen size logically should have an effect on the coefficient of variation. Larger specimens should tend to represent a more-average value of permeability and therefore have a smaller coefficient of variation. Attempts were made to identify such a trend between the air-permeability sample area of 6.99-cm (2.75-in) diameter and the falling-head sample area of 2.54-cm diameter. However, no such trend was apparent for the geotextiles tested. Therefore, a recommendation of sample size on the basis of coefficient of variation cannot be made from these data.

Since the coefficient of variation shows no consistency between fabric types, the number of samples required to achieve a given accuracy cannot be generally specified. For the tested fabrics, the number of samples required to achieve a mean within 5 percent of the true mean at a 95 percent probability level ranged from 4 to 69. Woven fabrics were not better as a group than nonwoven fabrics. Sample size should be chosen as discussed in ASTM D2905 for each application.

Since the specific falling-head test is a newly developed method for geotextiles, it is necessary to consider the variability in results as a function of operator. Table 5 presents test results obtained for one fabric sample tested by three different operators. A small variation of 10 percent occurs, probably as a result of timing errors. Based on this evidence, it appears that operator variance does not significantly affect the overall test results.

Some of the thick fabrics are compressible. The permeabilities can be expected to change as a function of the pressure on the geotextile, but this was not investigated in this study.

CONCLUSIONS AND RECOMMENDATIONS

Water-permeability tests should use deaired distilled or filtered water and care should be exercised to deair the specimen. Even with care, simple water tests on only a few specimens and with relatively high gradients may only be accurate within an order of magnitude. In many instances, soil permeability and other data are not precisely known and this accuracy is satisfactory. If, however, the permeabilities of geotextiles are to be measured accurately, special procedures must be followed to assure laminar flow and adequate samples. Laminar flow may be assured by testing with very small differences in pressure across the specimen or by testing stacks of geotextile specimens to increase thickness. Each creates special testing problems.

Air-permeability testing shows potential for providing accurate results and for solving the turbulent-flow problem in a simple, economical way. Additional research should be conducted on this method.

Geotextiles are quite variable both within and between lots. Samples should consist of specimens from widely spaced locations within lots. Samples should be tested from each lot. The number of specimens in a sample should be determined according to ASTM D2905 to give the desired accuracy.

Often it is more informative to know the ease with which water will flow through a geotextile as a function of the head loss across the fabric than to know the coefficient of permeability per se. The permittivity, defined as the flow velocity divided by the head loss and which is equal to the coefficient of permeability divided by the fabric thickness, indicates this characteristic. If permittivity is used, it also eliminates the need to determine geotextile thickness.

Geotextile permeability is an important property. Approximate values may be determined from simple rapid permeability tests; however, accurate permeability determination requires care and specialized equipment. Permeability testing of geotextiles needs and deserves additional research.

ACKNOWLEDGMENT

The work reported in this paper was sponsored by the Federal Highway Administration. Their support is gratefully acknowledged. They have not reviewed the findings presented.

REFERENCES

1. H.A. Cedergren and K.A. Godfrey. Water: Key Cause of Pavement Failure. Civil Engineering Journal of ASCE, Vol. 44, No. 9, Sept. 1974, pp. 78-82.
2. J.R. Bell, R.G. Hicks, J. Copeland, G.L. Evans, J.J. Cogne, and P. Mallard. Evaluation of Test Methods and Use Criteria for Geotechnical Fabrics in Highway Applications. FHWA, U.S. Department of Transportation, Rept. RD-81-020, June 1980.
3. P.R. Vaughn. Design of Filters for the Protection of Cracked Dam Cores Against Internal Erosion. Presented at ASCE Convention and Exposition, Chicago, IL, Oct. 1978, ASCE Meeting Preprint.
4. J.A. Copeland. Fabrics in Subdrains: Mechanisms of Filtration and the Measurement of Permeability. Department of Civil Engineering, Oregon State Univ., Corvallis, Transportation Res. Rept. 80-2, 1980.
5. M. Bourdillon. Utilization of Non-Woven Fabrics for Drainage (in French). Ministère de L'Equipment, Laboratoire des Ponts et Chaussées, Paris, France, Rept. 54, June 1976.
6. C.O. Calhoun. Development of Design Criteria and Acceptance Specifications for Plastic Filter Clothes. U.S. Army Corps of Engineers, Waterways Experiment Station, Vicksburg, MI, Tech. Rept. S-72-7, June 1972.
7. W.J. Rosen and B.D. Marks. Investigation of Filtration Characteristics of a Nonwoven Fabric Filter. TRB, Transportation Research Record 532, 1975, pp. 87-93.
8. B.D. Marlar. Investigation of Mechanisms Re-

lated to Nonwoven Fabric Filtration. Univ. of Tennessee, Knoxville, M.S. thesis, 1975.
9. H.R. Cedergren. Seepage, Drainage and Flow Nets, 2nd ed. Wiley, New York, NY, 1967.
10. M. Muskat. Darcy's Law and the Measurement of the Permeability of Porous Media. In Flow of Homogeneous Fluids Through Porous Media, 1st ed., McGraw-Hill, New York, NY, 1937, pp. 55-120.
11. H.J.M. Ogink. Investigation of the Hydraulic Characteristics of Synthetic Fibers. Delft Hydraulics Laboratory, Delft, Netherlands, Publ. 146, May 1975.
12. J. Ball. Design Parameters for Longitudinal Filter Cloth Lined Subsurface Pavement Drainage Systems. State of Alabama Highway Department, Montgomery, Quarterly Rept. (Jan. 1-March 31, 1978), March 31, 1978.
13. J. Masounave, R. Denis, and A.L. Rollin. Prediction of Hydraulic Properties of Synthetic Nonwoven Fabrics Used in Geotechnical Work. Canadian Geotechnical Journal, Vol. 17, No. 4, Nov. 1980, p. 517.

Publication of this paper sponsored by Committee on Subsurface Drainage.

Performance of Soil-Aggregate-Fabric Systems in Frost-Susceptible Roads, Linn County, Iowa

J.M. HOOVER, J.M. PITT, L.D. HANDFELT, AND R.L. STANLEY

Results of a three-year laboratory and field evaluation of a first-generation geotechnical construction fabric applied in soil-aggregate and granular-surfaced low-volume roadways indicate that fabric systems can, under certain circumstances, reduce thaw-induced deformations and improve field performance. Eleven test sections that involved different soil-aggregate-fabric systems were constructed on subgrades that displayed varying degrees of frost-related performance. Field evaluations were conducted over three cycles of spring thaw plus summer healing. Laboratory simulation of freeze-thaw action along with strength and deformation parameters obtained through the Iowa K-test were used on a fabric-reinforced, frost-susceptible soil to provide insight into soil-fabric mechanisms and the potential for predicting field performance. Variation in the constructed soil-aggregate-fabric systems was achieved by locating fabric at different positions relative to layers of soil-aggregate or existing roadway materials, a choked macadam base course, and a thick granular backfill. Improvement was most noticeable where fabric was used as a reinforcement between a soil-aggregate surface and a frost-prone subgrade. Fabric used in conjunction with granular backfill, macadam base, and non-frost-susceptible subgrade did not appear justifiable.

Among the economic losses incurred by frost action are costs of repair and maintenance of the damaged roadway. Economic implications affect highway users if a weight-limit embargo is imposed or more severely if complete closure of the roadway is dictated by thaw-induced lack of support capacity.

In the spring, downward melting of ice lenses causes a supersaturated condition in the soil, and the diminishing layer of ice impedes gravitational drainage. During this period, a secondary roadway is vulnerable to severe traffic rutting or loss of support, skid-resistant surface aggregate is pushed into the supersaturated region, and displaced subgrade may be pumped to the surface.

It was the purpose of this investigation to evaluate the laboratory and in situ performance of a first-generation nonwoven polypropylene fabric as an interlayer reinforcement in the construction and maintenance of soil-aggregate-surface and granular-base roadways that overlie frost-susceptible fine-grained subgrades.

TEST SECTIONS

In the fall of 1976, fabric was placed in seven test sections located at two sites in Linn County, Iowa. Each section was paired with an adjacent control section constructed in the same manner as the test section except that it lacked fabric (1).

In sections 1A, 1B, 2A, and 2B at the Alburnett site (Figure 1), fabric was combined with a commonly used method to combat frost action in which the existing soil-aggregate surface course was removed, the frost-susceptible subgrade was undercut about 0.6 m (2 ft) and backfilled by using a coarse aggregate, and the soil-aggregate surface course was replaced and compacted.

Following removal of the soil-aggregate surface, the subgrade of sections 3 and 4 was shaped by using a blade grader and compacted by using a sheep's-foot roller. In section 3 a layer of fabric was placed on the subgrade prior to replacement of the soil-aggregate surfacing (Figure 2).

Sections 5 (fabric) and 6 were constructed in a manner identical to that used for sections 3 and 4, except on a frost-stable subgrade as a means of overall comparative control between stable and frost-prone subgrades and fabric-treated and untreated systems. All test sections at the Alburnett site were constructed by Linn County maintenance personnel by using conventional county-owned equipment.

Fairfax site test sections were constructed following a contracted geometrical change of the embankment that consisted primarily of widening the ditch and the shoulder, with little or no change in longitudinal profile or elevation. Fabric was incorporated between the subgrade and a contracted macadam-base surface course. Test sections 1 and 2, by using the granular-backfill-replacement method, were eliminated because of the expense incurred by using a force account for a nearly completed contract.

Fairfax sections 3 and 4 were built in an area that presumably contained frost-susceptible subgrade soils (Figure 3). Sections 5 (fabric) and 6 were built on frost-stable subgrades. A layer of fabric was placed on the subgrade in sections 3 and 5; then all sections were overlaid with 203 mm (8 in) of an open-graded macadam stone of 102-mm (4-in) top

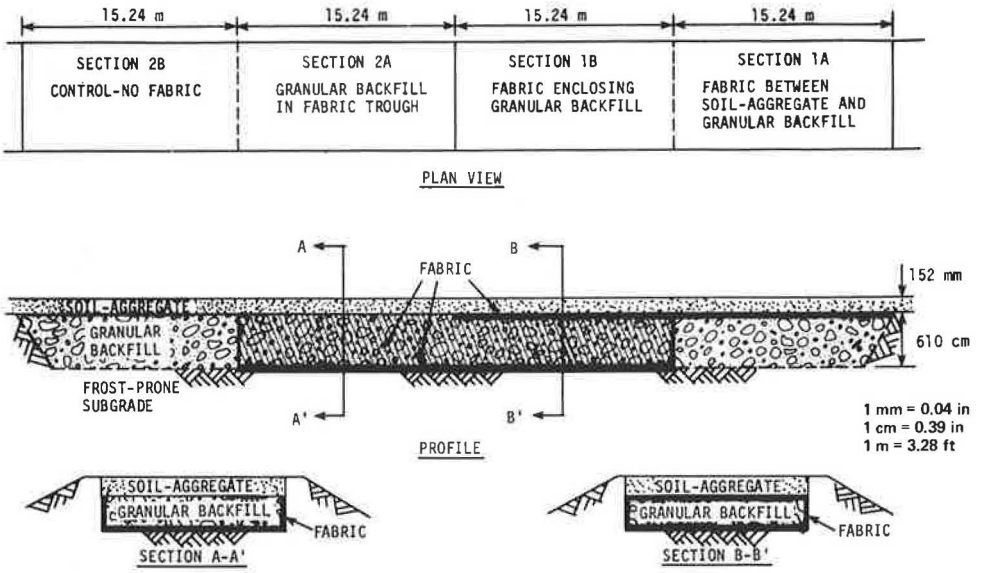

Figure 1. Fabric test sections 1A, 1B, 2A, and 2B, Alburnett.

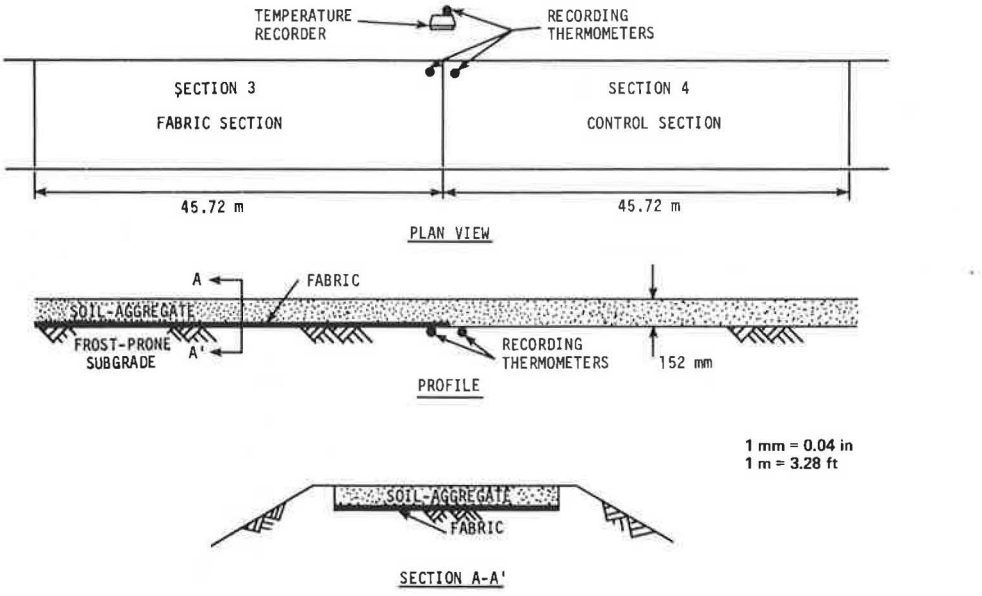

Figure 2. Fabric test sections 3 and 4, Alburnett.

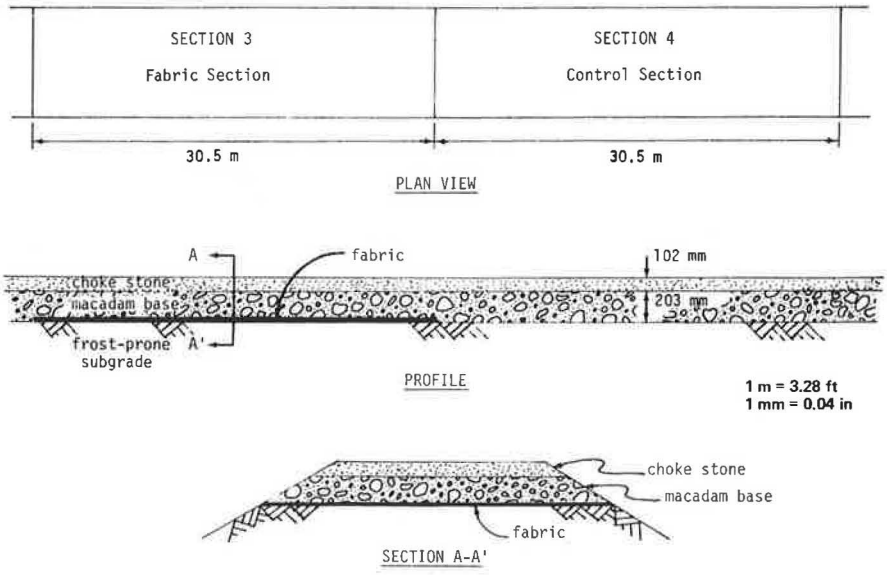

Figure 3. Fabric test sections 3 and 4, Fairfax.

Table 1. Classification of Alburnett test sections: soil-aggregate surfaces and subgrades, October 1976.

Physical Property	Subgrade			Surface		
	Sections 1 and 2	Sections 3 and 4	Sections 5 and 6	Sections 1 and 2	Sections 3 and 4	Sections 5 and 6
Percentage of						
Gravel (76.2-4.76 mm)	0	0	0	18	28	20
Sand (4.76-0.074 mm)	52	34	39	63	56	59
Silt (0.074-0.005 mm)	32	41	42	14	10	14
Clay (<0.005 mm)	16	25	19	5	6	7
Atterberg limits						
Liquid	26.0	37.1	29.1	-	-	-
Plastic	17.4	19.5	18.1	-	-	-
Plasticity index	8.6	17.6	11.0	NP[a]	NP[a]	NP[a]
AASHTO classification	A-4(1)	A-6(9)	A-6(4)	A-1-b	A-1-b	A-1-b
Unified classification	SC	CL	CL	SW	SP	SW
Uniformity coefficient C_u	170	410	78	55	95	92

Note: 1 mm = 0.04 in.
[a]NP = nonplastic.

Table 2. Classification of Fairfax test sections: base and subgrade, October 1976.

Physical Property	Subgrade		Macadam Base
	Sections 3 and 4	Sections 5 and 6	
Percentage of			
Gravel (76.2-4.76 mm)	0	0	86[a]
Sand (4.76-0.074 mm)	44	40	7
Silt (0.074-0.005 mm)	39	19	7
Clay (<0.005 mm)	17	21	
Atterberg limits			
Liquid	22.8	33.6	-
Plastic	15.6	18.6	-
Plasticity index	7.2	15.0	NP[b]
AASHTO classification	A-4(1)	A-6(6)	A-1-a
Unified classification	CL	CL	GP
Uniformity coefficient C_u	131	114	17

Note: 1 mm = 0.04 in.
[a]Gravel size, 101.6-4.76 mm. [b]NP = nonplastic.

size. The macadam base was topped with 102 mm of choke that consisted of 19-mm (0.75-in) maximum-size road stone. In June 1977, a seal-coat wearing surface was applied, followed by a thin asphaltic-concrete overlay in spring 1978. Both sites thus provided a range of comparative subgrade test and control sections underlying (a) a commonly used soil-aggregate surface or (b) a higher type of base and surface system.

INVESTIGATIONS

Fabric Properties

The first-generation nonwoven fabric used in this study is trademarked Mirafi 140. The fabric is composed of two continuous artificial fibers--one a polypropylene, the other a polypropylene core sheathed in nylon (2). The fibers are heat-bonded into a random arrangement that produces a fabric that has equal strength in all directions (2). The fabric is claimed to be rotproof, mildewproof, insectproof, and rodentproof, and chemicals normally encountered in civil engineering applications produce no noticeable effect on the fabric (2).

Laboratory Investigation

Tables 1 and 2 present representative classification data, including those from the American Association of State Highway and Transportation Officials (AASHTO), for the materials in each section immediately prior to construction. Variability of each section was most evident with the Alburnett surface materials; this variability stemmed from periodic maintenance operations, including frequent spot spread of aggregate within a deteriorating surface.

Subgrade soils at both sites could be classified as nonuniform due to their high uniformity coefficients. More than 3 percent of the particle sizes of each subgrade soil was smaller than 0.02 mm (0.000 78 in), a particle-size distribution criterion set by Casagrande (3) for considerable ice segregation to occur in a nonuniform soil. Alburnett sections 1A through 2B and Fairfax sections 3 and 4 were classified in group A4, which represents frost-prone silty soils of high capillarity. Each was identified as frost-susceptible on the basis of past performance. Alburnett sections 3 and 4 were classified A-6 but were identified by past performance as being frost-prone.

Freeze-Thaw Tests

A limited investigation was undertaken by using a silty clay soil to determine whether inclusion of the fabric reduced cyclic and/or residual heave during freezing and thawing due to assimilation of capillary moisture. A modification of the Iowa freeze-thaw test (4) was used to measure heave of both untreated and fabric-treated specimens. Basically this test duplicates field conditions of freezing from the top while water is available at the bottom of the specimen for upward capillary moisture movement. Standard ASTM D698 soil specimens were molded at maximum density and optimum moisture content. For fabric-treated specimens, single-thickness disks of fabric 102 mm in diameter were inserted horizontally between compacted layers during molding. Elongation, or change in specimen height following freeze or thaw, was expressed as a percentage of the original height (Figure 4).

Regardless of the location of a single disk, similar elongation characteristics were observed for specimens that contained only one layer of fabric. Fabric disks at each third point significantly reduced expansion. The lower heaving observed with fabric-layered specimens may have resulted from a partial cut-off by the fabric of capillary water to the remainder of the specimen. Since the fabric was designed for use as a filter, its average pore size is equivalent to that of a medium-fine sand, a material that generally has a lower capillary conductivity than that of the silty clay soil. Surface attraction between the fabric and the water should be considerably less than that between the soil and the water, which thus inhibits the rise of capillary water. With the inclusion of fabric, any reinforcement may inhibit growth of ice lenses, which in turn may result in smaller elongations.

Figure 4. Freeze-thaw elongation-test results.

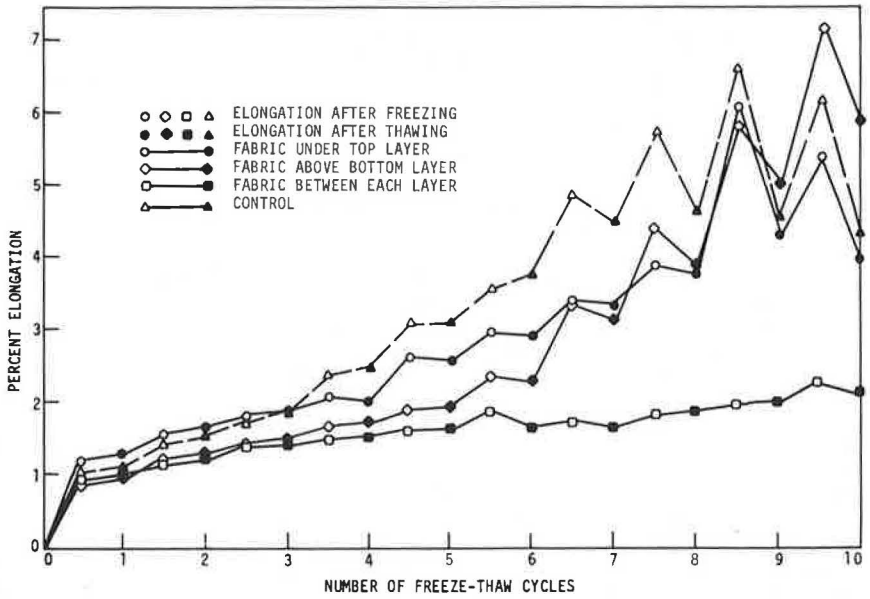

Table 3. Mean moisture density and Iowa K-test parameters for silty clay soil specimens with and without fabric.

Treatment	Moisture Content (% dry soil wt)	Dry Density (kN/m^3)	Vertical Deformation Modulus E_v (kPa)	Cohesion c (kPa)	Angle of Internal Friction ϕ (degrees)	Lateral Stress Ratio K
Control (untreated)						
Near standard moisture and density	20.6	15.42	14 740	98.6	22.7	0.337
After freeze-thaw cycle	30.9	14.24	12 080	56.5	0.0	0.777
One fabric layer						
Near standard moisture and density	20.8	15.13	14 010	102.0	23.7	0.317
After freeze-thaw cycle	31.9	14.10	12 755	68.3	5.1	0.648
Two fabric layers						
Near standard moisture and density	21.0	15.03	11 183	113.1	23.4	0.317
After freeze-thaw cycle	29.3	14.42	12 300	69.6	8.7	0.574

Note: 1 kPa = 0.145 lbf/in^2, 1 kN/m^3 = 6.37 lbf/ft^3.

Stability Tests

All specimens except those that had fabric under the top layer were recovered after the freeze-thaw cycle, combined with additional freshly molded specimens at near-optimum moisture and maximum density, and tested by using the Iowa K-test to determine various shear and stability parameters (5-7), which are presented in Table 3.

Incorporation of fabric during compaction created a slight reduction in dry density, even in specimens that had similar moisture content. A soil must be sheared to be compacted (7). If the fabric tended to confine development of internal shear surfaces, it would thus contribute to a lowering of density.

Under standard conditions of moisture and density only, the vertical deformation modulus E_v was slightly reduced through inclusion of one fabric disk; two layers markedly decreased E_v. The much-lower E_v was due to high values of vertical strain associated with the two-layer fabric specimens during testing. After 10 freeze-thaw cycles, E_v was slightly improved due to the presence of fabric.

Near standard optimum moisture and density there was minor improvement in cohesion c and angle of internal friction ϕ of the treated specimens. Following the freeze-thaw cycle, slight improvements in c were coupled with increased ϕ, although densities were reduced and moisture content had increased. The increase in c may result from tensile strength added by the fabric; use of two layers gives the greatest improvement. The zero ϕ obtained with the control is typical of saturated clays. Higher friction angles obtained with the treated specimens appear to indicate that fabric tended to confine the propagation of continuous shear planes. Use of c-ϕ in an analysis of bearing capacity would generally indicate improved support, particularly where two fabric layers were used.

Values of lateral stress ratio K should never exceed 1.000; the smaller the K value, the greater the lateral stability of a material. Only a slight reduction in K was obtained with fabric-treated specimens near standard moisture and density. A larger reduction in K occurred with an increased number of fabric disks following the freeze-thaw cycle. Both test and treatment conditions reflect radial reinforcement provided by the fabric. However, the magnitude of reinforcement may also be indicative of the amount of elongation provided by the fabric.

In the analysis of the composite effect of the fabric-reinforced soil, only properties of the fabric should be considered. It is a composite of thermoplastic fibers that are not very resilient and have a low tensile deformation modulus. The tangent modulus at 120 percent elongation is about 20 700 kPa (3000 lbf/in^2). Since slippage may occur at

the soil-fabric contact, the effective modulus of the fabric is probably lower then 20 700 kPa.

The vertical modulus E_v decreased with an increased number of fabric layers for specimens not subjected to the freeze-thaw cycle. After the soil had been degraded through capillary moisture absorption during the freeze-thaw cycle, the presence of fabric provided a slight improvement, which indicated the importance of the properties of the composite constituents. First, the effective fabric modulus, which includes its ability to bond, may have been small compared with that of the soil, which created a situation in which the soil may have reinforced the fabric. When the soil modulus was reduced by freeze-thaw action, presence of the fabric caused a slight improvement, which indicated that the roles of the individual moduli may have been reversed, and the net result was some composite reinforcement.

Composite reinforcement is affected by the degree to which fabric properties are transferred to the soil and depends on the bond achieved at the interface between the two materials. Casual observation indicated that bonding may have been achieved through partial intrusion of the soil into the fabric mesh. The more plastic the soil, the better the probable bond. This may explain why values of E_v were nearly the same for both the specimen that had one fabric layer and the specimen that had two layers following the freeze-thaw cycle; some level of bonding was established, and hence a limiting amount of reinforcement was provided.

The limiting equilibrium parameters c and ϕ were more sensitive to the effect of reinforcement before and after subjection to the freeze-thaw action. At impending failure, c and ϕ represent the shear stress on a plane oriented at an angle of $45 + (\phi/2)$ degrees with the horizontal. The fabric was thus oriented to have considerable influence on these parameters. However, fabric reinforcement did not appreciably influence the friction angle for specimens not subjected to the freeze-thaw cycle, a condition that is potentially related to soil-fabric bonding.

Table 4. Comparison of dry density and moisture content of test-section subgrades, October 1976 and June 1978.

Location	October 1976		June 1978	
	Dry Unit Weight (kN/m^3)	Moisture Content (% dry wt)	Dry Unit Weight (kN/m^3)	Moisture Content (% dry wt)
Alburnett				
Fabric section 1A	16.89	17.7	15.63[a]	18.0[a]
Fabric section 1B	17.80	9.1	-	-
Fabric section 2A	-	-	18.07[b]	11.3[b]
Control section 2B	14.26	24.6	17.72	15.7
Fabric section 3	15.88	21.4	16.93	15.8
Control section 4	17.08	16.3	11.12	45.5
Fabric section 5	14.41	14.7	16.49	17.7
Control section 6	15.27	11.2	17.28	16.2
Fairfax				
Fabric section 3	19.86	11.8	17.94	12.8
Control section 4	17.96	8.6	17.37	14.5
Fabric section 5	19.36	8.8	14.92	27.1
Control section 6	20.23	13.7	14.08	32.1

Note: 1 kN/m^3 = 6.37 lbf/ft^3.
[a]Top of stone backfill. [b]Base of stone backfill.

Table 5. Comparison of subgrade fines content prior to construction, October 1976, versus fabric-subgrade contact zone, June 1978.

Location	Section No.	Fines That Passed No. 200 Sieve (%)		Remarks
		Oct. 1976 Subgrade	June 1978 Fabric-Subgrade Contact Zone	
Alburnett	1A	48	60	Fabric between soil-aggregate surface and granular backfill
	2A	48	59	Granular backfill in fabric trough
	2B	48	59	Control (granular backfill only)
	3	66	64	Fabric over frost-prone subgrade
	4	66	67	Control (frost-prone subgrade)
	5	61	63	Fabric over stable subgrade
	6	61	77	Control (stable subgrade)
Fairfax	3	56	59	Fabric over frost-prone subgrade
	4	56	55	Control (frost-prone subgrade)
	5	41	68	Fabric over stable subgrade
	6	41	66	Control (stable subgrade)

Field Investigation

In Situ Moisture and Density Tests

Considerable variation in both density and moisture content existed within the subgrades of both sites at the time of construction (Table 4). Such variations occur in most county or local roads because of variability in transpiration and evaporation rates, subgrade drainage, and other material properties due to use of locally available materials only. Subgrade drainage is highly dependent on ditch conditions. The Alburnett site was fairly flat and had shallow ditches, whereas at the Fairfax site ditches had been widened and deepened.

In situ moisture and density tests were again performed in the subgrades of each test and control section approximately 20 months after construction (Table 4). With the exception of Alburnett sections 3 and 4 and Fairfax sections 5 and 6, no consistent trends between fabric and control sections or between times of testing were observable. At least a limited degree of moisture and density stability was indicated within fabric section 3. Control section 4 indicated a significant decrease in subgrade density coupled with a severe increase in moisture content.

Fairfax sections 5 and 6 (Table 4) indicate significant decreased density and increased moisture content. Comparison of sections 3 and 4 and 5 and 6 indicates a probable loss of stability within sections 5 and 6. This loss, however, was only partly reflected in other in situ data obtained on the roadway surface, which is due at least in part to the rigidity of the macadam base that bridges a potentially weakened subgrade. Control sections 4 and 6 showed slightly lower density and greater moisture content than their respective fabric sections.

Movement of Fine-Grained Particles

Particle size tests were performed on soil samples removed in June 1978 from the fabric-subgrade contact zone or an equivalent depth in the control sections. Table 5 presents a comparison of the total fines content of the subgrade soils prior to construction versus that of the fabric-subgrade contact zone in June 1978. No evidence was obtained to suggest that the fabric prevented migration of fines due to capillary and/or percolation water movement. However, the data indicate that a movement and/or entrapment of fines from either the soil-aggregate surface or subgrades occurred within several of the test sections during the 20-month period. In addition, the data suggest no greater entrapment of fines through use of fabric than through use of either the granular backfill at

Alburnett or the macadam base at Fairfax.

Samples of those sections that indicated a potential of silt and clay movement were subjected to x-ray diffraction analysis to discern any variability of mineralogy in the fabric-subgrade contact soils due to intrusion, particularly of the soil-aggregate surface or the macadam base. No minerals characteristic of either were observed. The traces were characteristic only of the two site subgrade materials. Therefore it may be assumed that movement of fines was predominantly from the subgrades through capillary activity.

Climatic Conditions

Ambient air and subgrade temperatures were recorded at Alburnett sections 3 and 4 in order to observe any insulating effect attributable to the fabric. No differences were observed in temperature recorded at the surface of the subgrades during the 1976-1977 freeze-thaw season, a period that coincided with the coldest fall experienced in Iowa in this century and the coldest winter since 1936 (8). Data generated during the second winter (1977-1978) seemed to indicate a subgrade-insulating effect due to the fabric. Whether or not such an effect was valid was relatively inconclusive, since operational problems occurred with the recorder during this period.

Average monthly precipitation near the test sites showed that by the end of February 1977, drought had reduced available subsoil moisture to an average 98 percent less than normal (8). Above-normal rainfall was recorded in March 1977, rainfall remained below normal until July and was significantly greater than normal through October, and by December 1977 available subsoil moisture was only 12 percent below normal. Through September 1978, precipitation was nearly normal.

The above discussion makes evident the extreme variability that may exist in central Midwestern climatic conditions from year to year, especially subsurface moisture. Extended periods of subfreezing temperatures occur during the winter months. Yet with low subgrade moisture conditions, freezing temperatures may not create detrimental frost action in a roadway. Such conditions existed during the winter of 1976-1977. No heaving or boiling was visible in any of the test or control sections at either site.

Precipitation received during the fall of 1977 provided subgrade-moisture conditions that created both heave and boil softening in the second winter following fabric placement, although no heave or boil was evident at the Fairfax site. During April 1978, Alburnett section 3 showed some alligator checking within the soil-aggregate surface. Considerable alligatoring and checking were visible within control section 4 coupled with slight rutting and shoving of the surface course. No surface signs of boil softening were visible within the non-frost-susceptible sections 5 and 6.

In April 1979, heave and boil conditions were nonexistent at Fairfax and similar to those of 1978 at Alburnett. The area immediately adjacent to section 2B was significantly softened and rutted. Alligator cracking, checking, rutting, and shoving were visible in both sections 3 and 4. Sections 5 and 6 also showed slight evidence of heave and boil conditions.

Field Performance

Performance evaluation consisted of K-tests on undisturbed roadway samples and periodic in situ spherical-bearing-value tests, Benkelman-beam tests, and plate-bearing tests. Only limited portions of the Benkelman-beam and plate-bearing tests will be reported here, since each was indicative of the support capacity of the roadway during the most severe periods of thaw activity.

Benkelman-Beam Tests

The Benkelman beam measures roadway surface deflections under a slowly moving wheel load and essentially evaluates the flexural capabilities of the composite vertically profiled components. Each rear dual tire of a loaded test truck was maintained at an air pressure of 520 kPa (75 lbf/in^2), which supported a 76.9-kN (17 300-lbf) single-rear-axle wheel load; maximum allowable single-axle loading in Iowa is 80 kN (18 000 lbf). All deflection measurements were averaged for each individual section.

As a qualitative measure of flexibility of the vertical profile of each section, a relative stiffness factor was computed by dividing the load on one set of dual wheels by the average maximum deflection. The more flexible the profile components, the greater the deflection but the lower the relative stiffness. Figures 5 through 7 illustrate the range of variability of stiffness versus time for both sites.

Deflections and stiffness of sections 1A through 2B were respectively lower and higher than those of other Alburnett sections, which indicated that added strength was provided by the granular backfill 0.6 m (2 ft) thick. Deflections in sections 5 and 6 were consistently lower than those in sections 3 and 4, a condition compatible with the assumption that sections 5 and 6 were founded on less-frost-susceptible subgrades. If sections 5 and 6 were a datum for comparison with all other sections, the granular backfill and/or backfill coupled with fabric increased stability and performance characteristics of the frost-susceptible subgrade above those attainable within the non-frost-susceptible subgrade. Likewise, use of the fabric within frost-susceptible sections 3 and 4 did not improve deflection and stiffness performance to that of the non-frost-susceptible sections 5 and 6.

Immediately following a spring thaw, deflections of a secondary roadway may be high while stiffness values are low; each characteristic reverses and improves with time as gravitational moisture movement and/or capillary transpiration and evaporation occur. In general, such conditions were noted each season within each site. The principal exception occurred in August 1977 when exceptionally high rainfall finally broke the preceding drought.

Performance of a roadway will usually be increased following any subgrade, base, or surface improvement. The improvement slowly diminishes with time due to various combinations of traffic density, loading, environmental factors, and material fatigue and deterioration. In general, Figures 5 through 7 intimate such a diminution of support performance. A linear regression of relative stiffness versus time data within the Alburnett sections would indicate a slight slope downwards and to the right by using the data of each succeeding season, beginning in the spring of 1977. It cannot be concluded, however, that a seasonal decrease in performance was due strictly to the previously noted material factors, since the effect of both low and high subgrade moisture during the study period may not have provided a normal data base for such conditions.

During the three seasons of study, deflection and stiffness performance within Alburnett sections 1A through 2B indicated that sections 1A and 1B were generally superior and that performance decreased from section 2A to control section 2B (Figure 5). Section 1A contained fabric between the soil-aggre-

gate surface and granular backfill, whereas fabric encapsulated the granular backfill within section 1B. If it may be assumed that the subgrade moisture of the 1977 season was atypical, section 1A could be regarded as generally providing the best benefits of cost versus stability for the granular-backfill treatment of this frost-prone subgrade soil.

It is apparent from Figure 6 that use of fabric improved deflection and stiffness characteristics over each of the three seasons of study. Disregarding the earlier data of August 1977, improvement of deflection and stiffness values through fabric use ranged from a low of about 6 percent in July 1978 to a high of 90 percent in April 1979. Although the latter percentage of improvement in fabric section 3 is significant, it should be noted that average maximum deflections recorded at this time were in excess of 6.35 mm (0.25 in) for section 3 and approached 12.7 mm (0.5 in) for section 4. These values are higher than the limiting deflection criteria for several methods of flexible pavement design.

Alburnett sections 5 and 6 showed basically no variability during the 1977 boil and heal season, a slight variability during 1978, and some definite variation in 1979, particularly following thawing. Healing occurred rather quickly, however, within both the 1978 and 1979 seasons.

Relative stiffness for each Fairfax section versus time showed a range similar to that obtained for Alburnett sections 1A through 2B and may be attributed to a similarity between the Alburnett granular backfill and the Fairfax macadam base. Unlike the Alburnett sections, however, use of

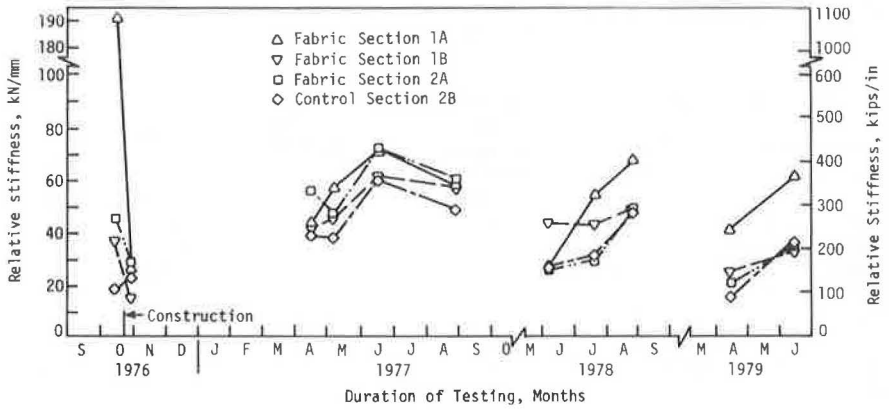

Figure 5. Benkelman-beam relative stiffness versus time, Alburnett sections 1A-2B.

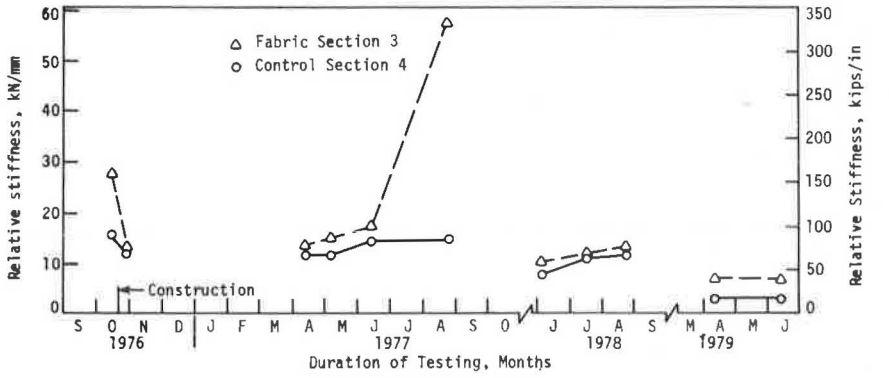

Figure 6. Benkelman-beam relative stiffness versus time, Alburnett sections 3 and 4.

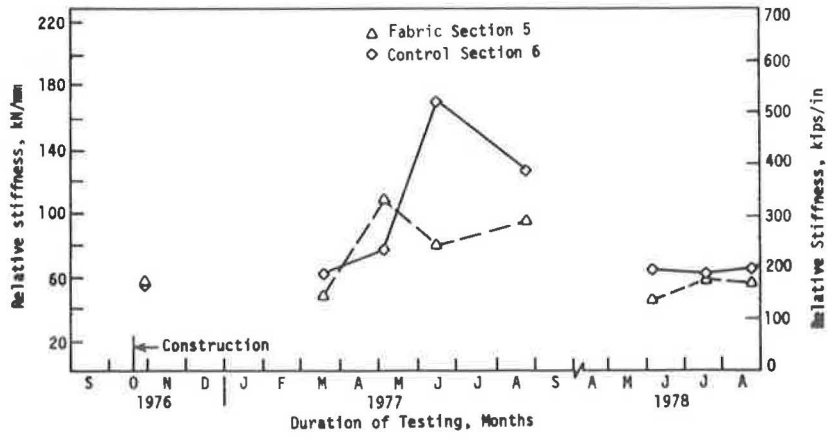

Figure 7. Benkelman-beam relative stiffness versus time, Fairfax sections 5 and 6.

fabric between the Fairfax subgrade and macadam base provided no basic improvement in deflection and stiffness, particularly at the critical stage of frost-boil development following spring thaws. It is thus apparent that use of fabric within the macadam-based Fairfax site provided no improvement in deflection and stiffness performance of the roadway, regardless of subgrade variations.

With the primary exception of Alburnett sections 3 and 4, most Benkleman-beam rebound measurements at both sites were nearly equivalent to maximum deflections, which indicates that each roadway is undergoing predominantly elastic strain during loading. Use of elastic theory, in which deformations are dirctly proportional to applied stress, thus appeared reasonably valid in analysis of deflection results. By using the 1977 Alburnett data, fabric sections 1A, 1B, and 2A decreased average deflection by 10 percent compared with control section 2B, which indicates that the stress at the subgrade surface was about 10 percent less in these sections. Alburnett sections 3 and 4 indicated about 25 percent reduction in potential subgrade stress by the use of fabric, whereas sections 5 and 6 indicated only a 7 percent stress reduction by the use of fabric on a stable subgrade.

By making assumptions of the Poisson ratio and the configuration of wheel loadings, values of the modulus of elasticity could be back-calculated for each of the Alburnett sections through use of Boussinesq theory. Values of the modulus of elasticity for the 1977 Alburnett sections thus ranged from about 24 138 to 107 586 kPa (3500-15 600 lbf/in²); the latter value was found in the granular-backfill sections. The higher value is within a typical range for dense sand and gravel, whereas the lower value is typical of silty or sandy clays, each of which existed within the Alburnett sections.

Trends regarding the laboratory stability tests and in situ fabric use as a structural reinforcement were obtained. The K-test vertical deformation modulus E_v and lateral stress ratio K (Table 3) are in principle related to Benkelman-beam relative stiffness. Laboratory stability tests indicated that fabric should produce a slight reduction in composite stiffness. Figures 5 and 6 indicate a decrease in relative stiffness following construction. After subjection to the freeze-thaw cycle, laboratory tests predicted a slight increase in E_v; field tests made in April 1977 showed some nominal improvements in relative stiffness. Incorporation of fabric predicted an improved c-ϕ relationship following the freeze-thaw cycle, which should then tend to improve as moisture content was reduced through healing. However, portions of the soil matrix and/or soil-matrix-fabric bond might be expected to reduce gradually through continued freeze-thaw cycling and moisture absorption, which reduce K and c-ϕ capabilities, an action not unlike the gradual reduction of field relative stiffness values versus time. Fluctuations of relative stiffness due to changes in field moisture content could also be anticipated on the basis of the data in Table 3. Thus the laboratory and in situ data emphasize that simple laboratory testing methods may provide predictive criteria for designed in situ use of a soil-aggregate-fabric system.

Plate-Bearing Tests

Plate-bearing tests 33 cm (12 in) in diameter were used in conjunction with the Benkelman beam during the latter phases of performance evaluation of the Alburnett sections. The modulus of subgrade reaction k was defined by

$$k = P/\Delta \quad (1)$$

where P is the plate stress at 70 kPa (10 lbf/in²) and Δ is the corresponding deformation value (9). Values of k are presented in Table 6.

Deformation moduli were computed from the Burmister (10) relation

$$E = \pi p D(1 - \nu^2)/4W \quad (2)$$

where

p = plate stress,
D = plate diameter,
ν = Poisson ratio (estimated at 0.33), and
W = plate settlement at 520 kPa (75 lbf/in²) plate stress (Table 6).

This expression was developed for a rigid plate on a homogeneous material. However, the resulting deformation modulus was thought to be a valid indicator of net response of the composite system.

Table 6 also presents values of deformation modulus as calculated from Equation 2 for Benkelman-beam deflections under 520 kPa contact pressure, since both plate and tire contact areas were equivalent.

Although loading rates of beam and plate tests were different, Table 6 indicates a high degree of correlation between deformation values at 520 kPa stress and modulus of deformation E determined from the two tests. Three exceptions are noted, in which

Table 6. Comparison of plate-bearing and Benkelman-beam test results, Alburnett sections.

			Plate-Bearing Test			Benkelman-Beam Test	
Section	Date	Subgrade Reaction (N/cm³)	Deformation Modulus E (kPa)	Deformation (mm) at 520 kPa	Permanent Deformation (mm)	Deformation Modulus E (kPa)	Deformation (mm) at 520 kPa
3	4/13/79	51	7 240[a]	15.24	6.35	25 220	4.37
4	4/13/79	18	3 570[b]	20.32	10.16	8 694	12.67
5	4/13/79	271	36 200	3.05	4.57	38 050	2.90
6	4/13/79	194	30 164	3.66	7.11	31 433	3.10
1A	6/14/79	603	124 100	0.89	1.27	111 240	0.99
1B	6/14/79	388	76 200	1.45	1.27	65 734	1.67
2A	6/14/79	388	72 400	1.52	1.27	58 626	1.88
2B	6/14/79	543	94 460	1.17	0.25	81 860	1.35
3	6/14/79	90	7 690	14.35	11.43	10 500	10.49
4	6/14/79	42	3 530[c]	20.83	12.70	8 294	13.51
5	6/14/79	453	51 710	2.13	1.02	51 035	2.16
6	6/14/79	453	57 915	1.91	1.52	55 620	1.98

Note: 1 N/cm³ = 3.684 lb/in³; 1 kPa = 0.1450 lbf/in²; 1 mm = 0.04 in.
[a]Determined at 414 kPa. [b]Failure occurred at 138 kPa. [c]Determined at 345 kPa.

plate deformations exceeded the capacity of the measuring device before a 520-kPa stress could be achieved. In one test (section 4, April 1979), stress levels above 138 kPa (20 lbf/in^2) could not be attained. The section failed; thus a state of limiting equilibrium was achieved.

The magnitude of permanent deformation that occurs after unloading of secondary roads (Table 6) is affected by the use of local soil-aggregate systems, which will nearly always undergo some permanent deformation. Acceptable permanent deformation has not been universally resolved, but experience suggests that 13 mm (0.5 in) represents an upper limit. The April tests for sections 3 and 4 tend to substantiate this limit, since section 3 was performing adequately whereas section 4 was near the threshold of unsatisfactory performance.

Relative performance of comparable fabric versus nonfabric sections was indicated by nearly all parameters developed from the plate-loading tests. The April tests on frost-prone subgrade sections 3 and 4 showed a 2.8 improvement factor for both k and E. On the less-frost-susceptible subgrade sections 5 and 6, fabric increased k by a factor of only 1.4 and E by 1.2, which supports the contention that fabric benefits may not be realized until the soil is weakened through frost action or lack of drainage. Further support for this concept was evident for sections 3 through 6 in June 1979 (Table 6), which represents performance after the frost boils had at least partly healed. Improvement factors for both k and E on frost-prone subgrade sections 3 and 4 were reduced to 2.2. For sections 5 and 6 (non-frost-prone subgrade), k indicated no improvement, whereas E-values suggested that fabric actually decreased system stiffness. In addition, permanent deformations were smaller when fabric was present, and a more pronounced difference in corresponding sections occurred when the system was soft.

Section 1A produced improvement factors of only 1.1 for k and 1.3 for E. For sections 1B and 2A, k- and E-values were lower than those for the comparable nonfabric section. Thus little was gained by using fabric in conjunction with a thick granular backfill under subgrade and environmental conditions similar to those prevalent for this field study.

CONCLUSIONS

The following general conclusions are based on both laboratory and field performance parameters:

1. Laboratory and in situ data indicate a reinforcement capability when fabric is interlayered between a soil-aggregate surface and a frost-susceptible subgrade.
2. Laboratory freeze-thaw tests of a fabric-interlayered frost-susceptible fine-grained soil indicate a reasonable control of freeze-thaw elongation.
3. Laboratory stability and strength tests of a fabric-interlayered frost-susceptible fine-grained soil indicate a degree of improvement of all parameters due to reinforcement both prior to and after subjection to the freeze-thaw cycle.
4. The fabric performed most favorably during the three-year study as a reinforcement between a soil-aggregate surface and frost-prone subgrade.
5. Use of the fabric in conjunction with granular backfill in an undercut frost-susceptible subgrade soil did not appear significantly justifiable.
6. Use of the fabric did not appear justifiable as a reinforcement (a) between a soil-aggregate surface and non-frost-susceptible subgrade or (b) between a macadam base and either frost-susceptible or non-frost-susceptible subgrade.
7. Field soil moisture may be a highly relevant factor in soil-fabric bonding characteristics and should be studied in much greater detail.
8. Laboratory investigations similar to those performed in this study should be expended in order to increase performance predictability of in situ fabric reinforcement effectiveness in frost-susceptible secondary road materials.

ACKNOWLEDGMENT

Funds for support of this project were provided by Celanese Fibers Marketing Company and the Engineering Research Institute, Iowa State University. We extend our sincere appreciation to each for such sponsorship. In addition, we gratefully acknowledge W.G. Harrington and Jerry Nelson, Linn County Engineers, and their engineering and maintenance staffs for their exceptional cooperation during the construction and investigative phases associated with this project.

REFERENCES

1. J.M. Hoover, J.M. Pitt, L.D. Handfelt, and R.L. Stanley. Performance of Soil-Aggregate-Fabric Systems in Frost-Susceptible Roads, Linn County, Iowa. Celanese Fibers Marketing Co., Charlotte, NC, Final Rept., May 1980.
2. Celanese Fibers Marketing Company. Mirafi 140 Construction Fabric. Celanese Corporation, Charlotte, NC, Publ. PM-5, 1975.
3. A. Casagrande. Discussion of paper, A New Theory of Frost Heaving, by A.C. Benkelman and F.R. Olmstead. HRB, Proc. Vol. 11, 1931, pp. 168-172.
4. K.P. George and D.T. Davidson. Development of a Freeze-Thaw Test for Design of Soil-Cement. HRB, Highway Research Record 36, 1963, pp. 77-96.
5. R.L. Handy and J.M. Hoover. Testing Device for Measuring Lateral Pressure Induced on a Material by a Vertical Applied Pressure. U.S. Patent 4,047,425, U.S. Government Printing Office, Sept. 13, 1977.
6. R.L. Handy, A.J. Lutenegger, and J.M. Hoover. The Iowa K-Test. TRB, Transportation Research Record 678, 1978, pp. 42-49.
7. J.M. Hoover and R.L. Handy. Chemical Compaction Aids for Fine-Grained Soils, Volumes 1 and 2. Office of Research and Development, FHWA, U.S. Department of Transportation, Rept. FHWA-RD-79-63, June 1978.
8. Climatological Data, Iowa Section, Volumes 87 and 88. National Climatic Center, Asheville, NC, 1976 and 1977.
9. E.J. Yoder and M.W. Witczak. Principles of Pavement Design. Wiley, New York, 1975.
10. D.M. Burmister. The Theory of Stresses and Displacements in Layered Systems and Applications to the Design of Airport Runways. HRB, Proc. Vol. 23, 1943, pp. 126-148.

Publication of this paper sponsored by Committee on Low-Volume Roads.

Pavement Cracking

CHESTER McDOWELL

Data are presented for some field and laboratory experiments that have been conducted periodically over 45 years and that involved cracking of pavements constructed over high-volume-change soils in Texas. The reports of others are coordinated with these findings. A graphic solution is presented for estimating the width of the granular base behind the curb necessary to prevent excessive dry-weather cracking. The same criteria are applicable to estimating the width of shoulders for roads and highways. The theory for this procedure is based on experience and the calculation of the values of potential vertical rise.

The purpose of this paper is to call attention to publications that pertain to pavement cracking and to offer some suggestions relative to design widths of base materials behind curbs. It is intended that use of the suggestions will materially reduce damage due to volume change of soils.

A completely analytical approach to the problem of street-pavement cracking is difficult for any one person. There are several reasons for this: (a) No one has enough experience with soils, paving materials, design, construction, and maintenance, and (b) sometimes pavement cracking is caused by one factor and develops to a point at which other factors appear to be the cause of the trouble. This is a most unfortunate circumstance because pavement cracks tell an interesting story about mistakes that we are not capable of comprehending. Perhaps research should be directed to studies of the life of pavement cracks from their first appearance until rehabilitation of pavement is necessary. One of the 10 most important research needs identified by the Workshop on Structural Design of Asphalt Concrete Pavement Systems in December 1970 contained the following statement (1):

> The problem: Pavement failures are related to the development of cracks and/or excessive deformation due to repetitive loads or environmental conditions. The analysis and prediction of failure would be aided by the development of procedures for explaining the initiation, propagation, and accumulation of cracks.

Francis N. Hveem, former materials and research engineer for the California Division of Highways, issued a report in which he recognized the state of confusion by making the following statement (2): "Among those who use language for communication, engineers are not the most meticulous in their choice of terms, and it is at times difficult to clearly understand just what is being discussed."

Several years ago, I presented a paper (3) that listed the following as some of the causes for pavement cracking:

1. Excessive load deflections, including resilience deflections;
2. Subsidence, consolidation, slides, etc.;
3. Swell-shrink conditions of the subgrade;
4. Shrinkage cracking of the base and/or pavement caused by factors other than deflections or movements of the subgrade;
5. Frost and/or freeze-thaw action;
6. Brittleness of pavement due to aging and/or absence of traffic (includes the use of hard asphalts and their hardening due to oxidation--type of mix and/or construction procedures may contribute to oxidation); and

Figure 1. Street cross sections showing variations due to seasonal changes.

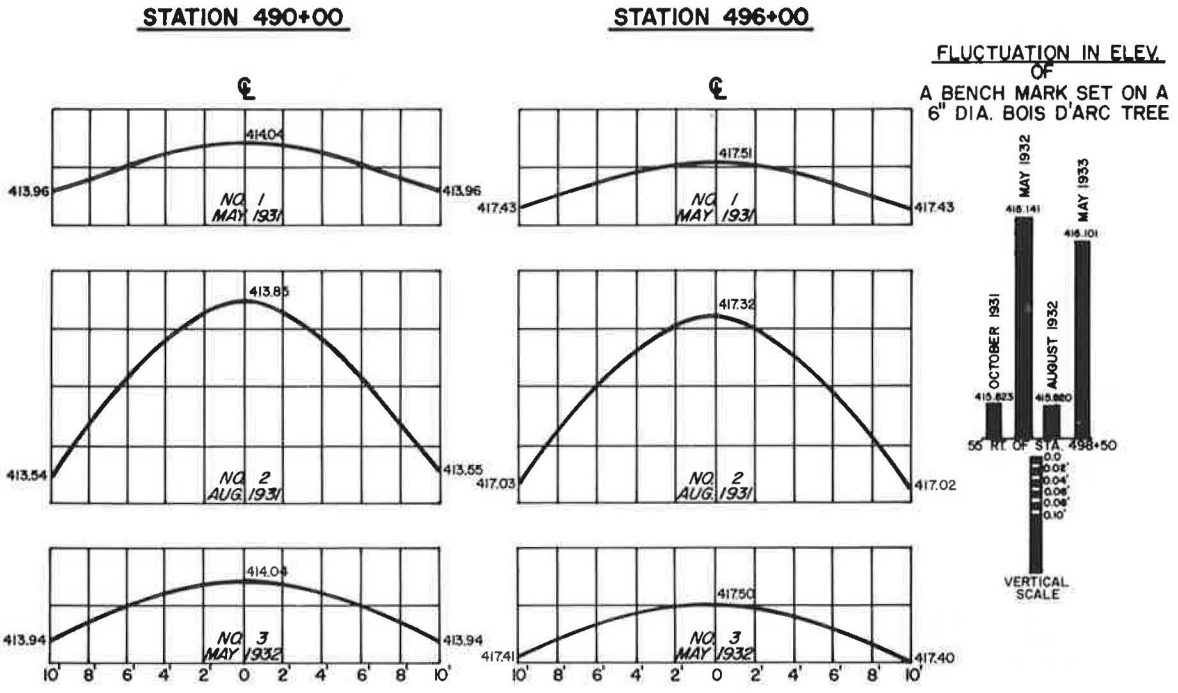

7. Thermal expansion and contraction.

These factors were discussed somewhat in detail in my earlier paper (3). From a maintenance standpoint, factors that involve slippage (lack of bond), reflection cracking (joints or old cracks coming through overlays), and tree-root damage are others that should be added to the above list. The foregoing shows why groups of engineers fail to agree as to the reasons for cracking or the proper remedial procedures to use. The mere fact that disagreement about pavement performance exists should not be embarrassing to anyone, but rather it should be considered a sign of interest that could lead to discussions pertinent to the solution of difficult paving problems.

Figure 2. Cracks in pavement when soil fill and natural soil foundation had shrunk.

I believe that my experience as state highway soils and research engineer for more than 35 years and as a member of the Committee on Flexible Pavement Design of the Transportation Research Board for 30 years qualifies me to make further contributions on this subject. During my service in the early days, highways were constructed with, but usually without, shoulders. Some history relative to the transition from the trench to the feathered type of pavement cross sections over highly expansive soils should be of interest. Figures 1 through 9, from a report submitted to the Highway Research Board in 1938 (4) by the late Henry C. Porter, engineer of research, Texas State Highway Department, are used for illustrative purposes. Figure 1 is a graphic representation used by Porter to illustrate how the elevation of the ground surface of swelling clays fluctuates with seasonal changes. The data were obtained during the observation of the performance of a concrete pavement (probably a 9-6-9 section) that had grass shoulders and had been constructed in the early 1930s. Some observations are as follows:

1. Although the center-line elevations fluctuated, it should be noted that they moved far less than the edges did. The edges of the pavement fluctuated up and down about 2 in more than did the center line.
2. After seasonal changes for a period of one year, the pavement elevations returned to their original positions.
3. Note similar movements for the bench mark set on a tree of 6-in diameter (right-hand side of Figure 1).

The report does not tell how well or poorly this pavement performed, but cracking of such an unevenly supported pavement must have been inevitable when heavy loads were frequently applied by army trucks during World War II. Cracking of rigid pavements progresses differently from that of flexible pavements. Usually the tensile strength of narrow concrete slabs is sufficient to prevent cracking of un-

Figure 3. Typical cross section of plan for coarse-grained material to be placed in trench in clay soil.

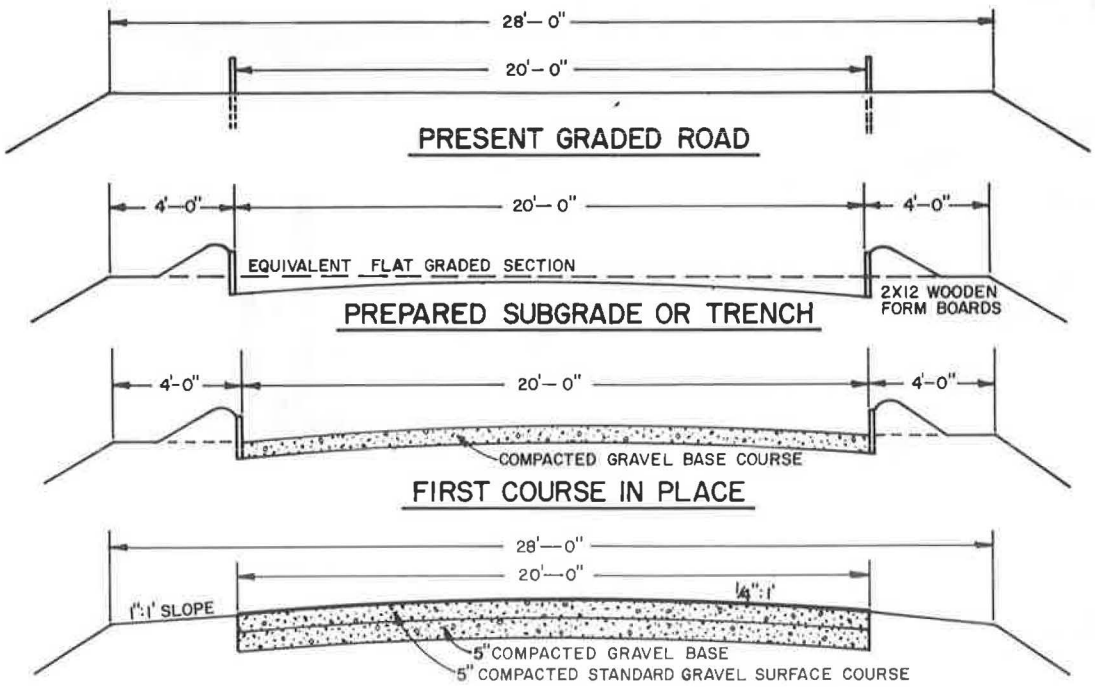

evenly supported slabs until heavy loads are applied. During this time a few cracks may occur in a random fashion even at the center line. When wheel loads are applied to poorly supported slabs, cracking often begins halfway between the center line and the edge of the pavement (Figure 2) rather than in wheel paths as is the case for flexible pavements. The deterioration of concrete pavements laid over high-volume-change soils was reduced materially when construction of granular or stabilized shoulders was adopted as standard practice by the Texas Highway Department. This practice caused dry-weather shrinkage cracks of the supporting soil to occur farther out from the edges of the pavement.

Figures 3 through 9 from Porter's report illustrate the benefits of changing from the trench to feathered design sections for flexible pavements to be placed over high-volume-change soils. Figure 3 shows the design cross section of a crushed conglomerate base to be placed in a trench. Figures 4, 5, and 6 show the poor condition of the pavement after only five years of service. It cannot be substantiated that dry-weather shrinkage cracking aggravated the development of the distress shown, but it is most likely that it did. Figure 7 shows the cross-section design of a feathered-type crushed-stone section to be constructed on the same type of expansive subgrade that was beneath the trench-type section. Figures 8 and 9 show the condition of the pavement after three and six years, respectively, of heavy traffic. Note the absence of any dry-weather cracks in the pavement. Other photographs not shown here indicate that dry-weather cracks did occur in the shoulders but did not injure the pavement. Similar experiences noted on many other projects helped convince the Texas Highway Department that money spent for shoulders was a good investment, especially when the pavement was placed over high-volume-change soils. Additional benefits consist of increased lateral support and room for motorists who have car trouble to park off the pavement. Most other highway departments adopted the use of granular shoulders many years ago.

In recent years, the city of Austin has grown toward the east so as to require the construction of many streets over high-volume-change soils such as the Taylor Geological Formation and others. This fact, plus the extensive drying period in 1977, has caused new streets to begin cracking before they had carried any appreciable amount of traffic. Figure 10 shows shrinkage cracks that formed in 1977 only a few months after completion of paving. This street is a cul-de-sac and no homes had been constructed or lawns established at the time this photograph was taken. Figures 11 through 15 show the behavior of some older streets located on similar soils and with similar drainage conditions as those shown in Figure 10. Figures 11 and 12 show some alligator cracking, produced in part by heavy traffic loads on Montopolis Drive in east Austin. It is believed that dry-weather cracking could have occurred initially and that load cracking appeared after water had penetrated and softened the subgrade. Figure 12 shows separation of gutter from pavement, which indicates some shrinkage cracking. The pavement section for this street is the same as that shown in Figure 10 except that the base does not extend beyond the back of the curb.

Figures 13, 14, and 15 were taken on Vargas Street, which is parallel to and one block from the portion of Montopolis Drive shown in Figures 11 and 12. This street carries much less traffic than does Montopolis Drive. Figure 13 shows rather extensive cracking in the foreground, probably caused by volume changes of the subgrade for the regular curb and gutter paving section. The background of Figure 13 shows a road section that has granular shoulders that drain into ditches. Figure 14 shows a close-up of the background of Figure 13. It may be noted that few, if any, cracks appear in the roadway section. Figure 15 (same location as Figure 13) shows some separation of pavement from curb and gutter. Possibly this was reduced somewhat by maintenance of

Figure 4. Failures and patching along edges of pavement where crushed conglomerate base material was placed in trench cut in tight clay soil.

Figure 5. Rainwater in rut in shoulder soil.

Figure 6. Rainwater in traffic depression caused by movement of underlying clay soil previously overly wetted.

Figure 7. Typical cross section of crowned clay soil with coarse-grained material placed as blanket across crown.

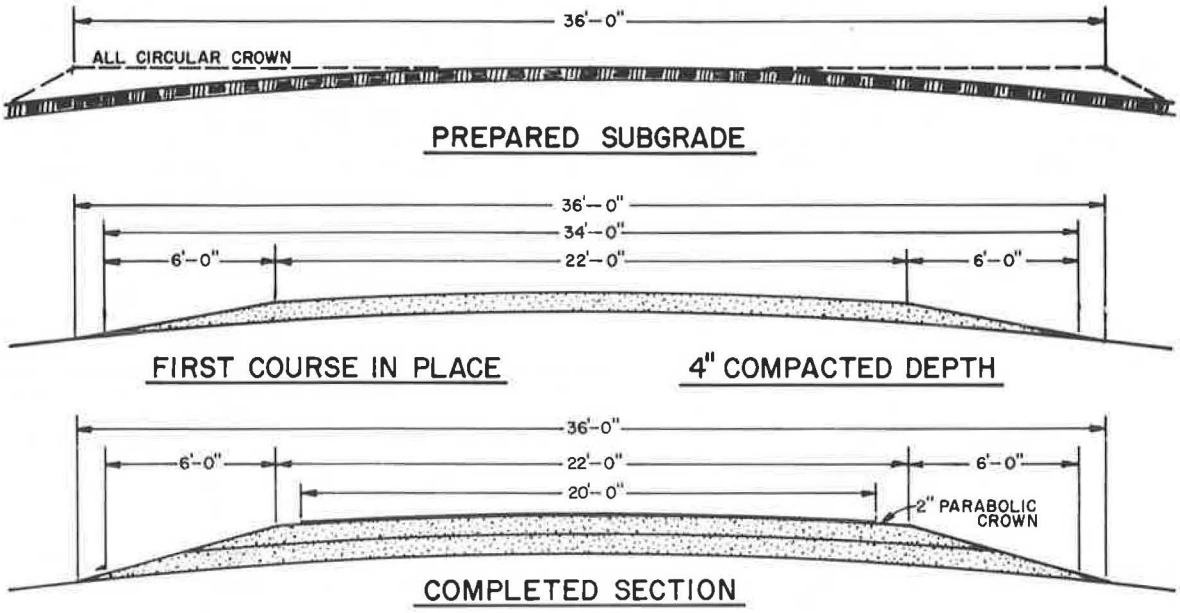

Figure 8. Riding surface after three years of heavy traffic where rain or gravity water moved from base material to ditches.

Figure 9. Same section of highway as in Figure 8 after six years.

Figure 10. Dry-weather shrinkage cracks on Galen Court, cul-de-sac street in southeast Austin.

Figure 11. Alligator cracking on Montopolis Drive in east Austin.

Figure 12. Alligator cracking and possibly some shrinkage cracking on Montopolis Drive.

Figure 13. Extensive cracking of pavement on Vargas Street (parallel to and one block from Montopolis Drive).

moisture under the sidewalk. The pavement section for this street is somewhat similar to that shown for Figure 10 except that the subgrade was not stabilized with lime and the flexible base was not extended beyond the back of the curb.

Figures 1 through 15 show the tremendous effect that change in the volume of the subgrade has on the life and performance of pavements. Others may have had experiences that differ from those presented here. It is possible that roads or streets constructed on identical soil conditions as those given in this paper, where preconstructed lawns are watered frequently, may not show any abnormal pavement distress. It is also possible that the use of the old "stand-up" curbs, which penetrated to a considerable depth into the subgrade, could have performed differently from that indicated in this paper. Sometimes cracking may not occur for several years or until a radical cycle in the weather has taken place.

In order to diminish the cracking of pavements constructed over subgrades of high-volume-change soil, I propose that a layer (4-6 in) of subbase or base be extended in back of the curb as indicated in Figure 16. The presence of well-watered lawns and existing sidewalks should be considered as exceptions in that the suggested widening shown in Figure 16 may not be necessary. The position and shape of

Figure 14. Closeup of background in Figure 13.

Figure 15. Left curb shown in Figure 13.

the curves shown in Figure 16 are based somewhat on observations and considerably on the volume-change characteristics of the subgrade soil in terms of its potential-vertical-rise (PVR) computations (5). The following PVRs are shown:

Curve (in)	PVR (in)
24	0.5
36	1.0
48	1.5
60	2.0

Calculations of PVR values were based on the presence of a thick layer of subgrade soil with average subgrade moisture conditions. Calculations of PVR were made in accordance with the THD-test method Tex-125-E. There are probably other methods of protecting subgrade moisture, such as the use of plastic sheeting or asphalt- and/or tar-treated paper, but chances of their proper replacement after utility excavations are questionable. Vertical trenches filled with granular material may also serve the purpose, but when they interrupt the natural flow of moisture, results can be very unsatisfactory.

Figure 16. Width of base behind curb.

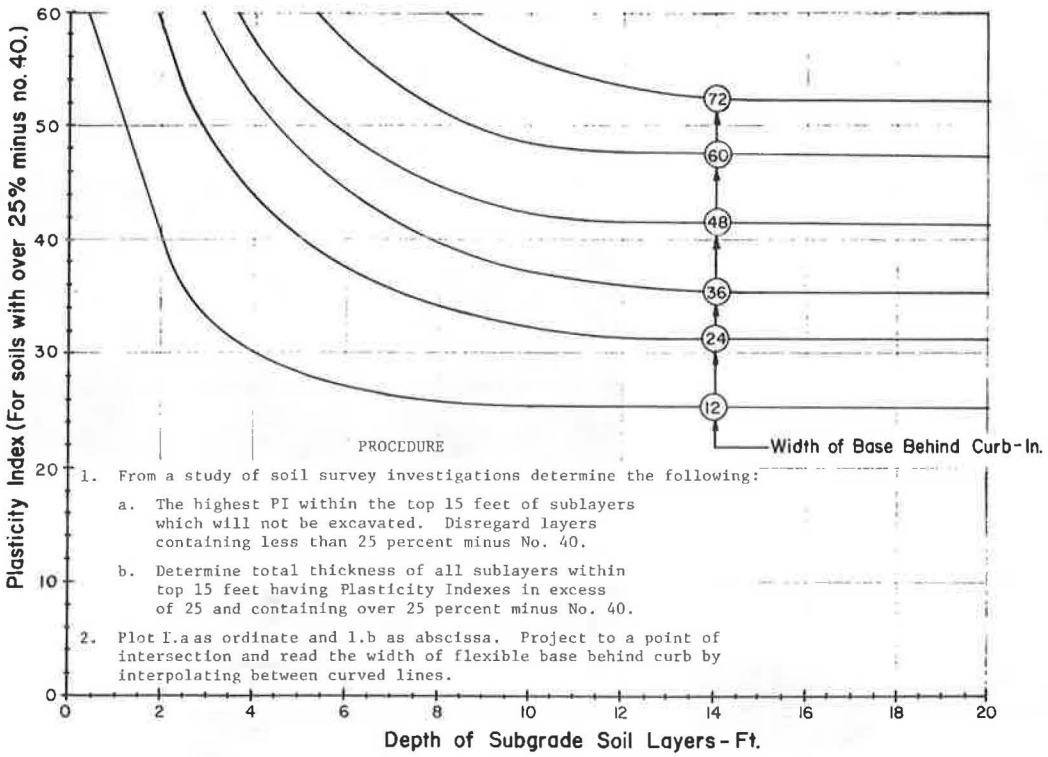

It is believed that use of the widening curves given in Figure 16 will materially reduce pavement cracking of streets in the city of Austin, but its use will not prevent cracking altogether. There will still be pavement cracking due to overloading, settling, and heaving.

Pertinent references have been used to show the complexity of the pavement-cracking problem. Fifteen figures have been presented that indicate pavement damage caused by subgrade-volume change. Some of these figures indicate how the use of granular shoulder materials reduced the severity of the problem. A new figure shows proposed widths of the base behind the curbs, which, if used, would reduce the severity of pavement cracking (Figure 16). If attention is not directed to this problem on highly plastic subgrades, extensive cracking will continue to increase until corrective maintenance is performed.

ACKNOWLEDGMENT

I am indebted to Norman L. Wood, contract administrator, and Charles B. Graves, Jr., director of engineering for the city of Austin, Texas, for their help and encouragement during the preparation of this paper. The aid received from other city employees, especially those in the Engineering Department, is also gratefully acknowledged.

REFERENCES

1. Structural Design of Asphalt Concrete Pavement Systems. HRB, Special Rept. 126, 1971.
2. F.N. Hveem. Types and Causes of Failure in Highway Pavements. HRB, Bull. 187, 1958, pp. 1-52.
3. C. McDowell. Pavement Cracking: Causes and Some Preventive Measures. HRB, Special Rept. 101, 1969, pp. 154-162.
4. H.C. Porter. The Preparation of Subgrades. HRB, Proc. Vol. 18, 1938, pp. 324-331.
5. C. McDowell. Inter-Relationship of Load, Volume Change, and Layer Thicknesses of Soils to the Behavior of Engineering Structures. HRB, Proc. Vol. 35, 1956, pp. 754-772.
6. Manual of Testing Procedures, 100E Series. State Department of Highways and Public Transportation, Austin, TX, 1980.

Publication of this paper sponsored by Committee on Low-Volume Roads.

Pavement Design of Unsurfaced Roads

JACOB GREENSTEIN AND MOSHE LIVNEH

In some tropical countries, such as Thailand and Ecuador, unpaved soil-aggregate roads are normally constructed when the average daily traffic is less than 300. These pavements are generally constructed of a single layer of subbase, which varies in depth from 5 to 14 in. Currently, various empirical models give different results for the pavement design of unsurfaced roads. This study presents a design model that has been developed to provide a rational design methodology for low-volume unsurfaced roads. This methodology is based on the theory of plasticity. It has been found to be computable with the up-to-date experience in Ecuador and Thailand, according to which 8 in of gravel and 6 in of laterite carried about 25 000 and 5000 equivalent standard axles per lane in Ecuador and Thailand on silty sand and silty subgrade, respectively.

The pavement design for low-volume unsurfaced roads, particularly in tropical areas, has not received the benefit of the detailed research and studies that have been carried out to provide design methodologies for high-volume roads. In Thailand, unpaved (soil-aggregate) roads are normally constructed when the average daily traffic (ADT) is less than 300. These pavements are generally constructed of a single layer of laterite, which varies in depth from 5 to 14 in and has a California bearing ratio (CBR) that ranges between 7 and 60 percent (1). The local experience with laterite roads and other experience with unpaved roads (2,3) has shown that maintenance is difficult when an inappropriate design method is used, which indicates the necessity of the development of a rational model for unsurfaced roads. This necessity is illustrated by the different results obtained by the application of various empirical models available (4-6). These results are indicated in Figure 1, which shows the relationship between subgrade CBR and the number of coverages to failure of given equivalent single-wheel load (ESWL) and tire pressure. The data given in Figure 1 are restricted to equivalent wheel loads of 28 and 40 kips and tire pressures of 65 and 97 lbf/in^2, respectively. Figure 1 shows that for a subgrade CBR of 8 percent (typical local plastic laterite in Thailand) and an ESWL of 28 kips, the number of coverages to failure are 25, 40, and 500 (4-6). Similar results that show a meaningful difference exist for other values of subgrade CBR and wheel load. Therefore, this study presents a design model developed to provide a rational design methodology for low-volume unsurfaced roads. This methodology is based on the following parameters:

1. Traffic (ranging from 10 to 300 ADT),
2. CBR design of the subgrade, and
3. CBR design of the subbase material.

BASIC ASSUMPTIONS

Design thickness of flexible pavements is usually based on the theory of elasticity. However, for low-cost structures that have a permissible rut depth of more than 3 in, the theory of plasticity seems to be a more-compatible choice (7) and is therefore the one chosen for this study. The assumptions behind the theoretical model are delineated in Equations 1-3.

A rational model for unsurfaced roads must represent the relationship among wheel load, engineering properties of the soil and materials, and the number of coverages to failure. The general definition of such a model is given in the following equation:

$$f(P; p; CBR_s; CBR_L; N; H) = 0 \quad (1)$$

where

P = ESWL,
p = tire pressure,
CBR_S = CBR of subgrade,
CBR_L = CBR of subbase (generally laterite in Thailand),
N = number of coverages to failure, and
H = depth of subbase.

According to Foster's observations (8), the in situ CBR values of a single granular layer vary with depth; there are high values on the surface and low

Figure 1. Relationship between subgrade CBR and number of coverages to failure.

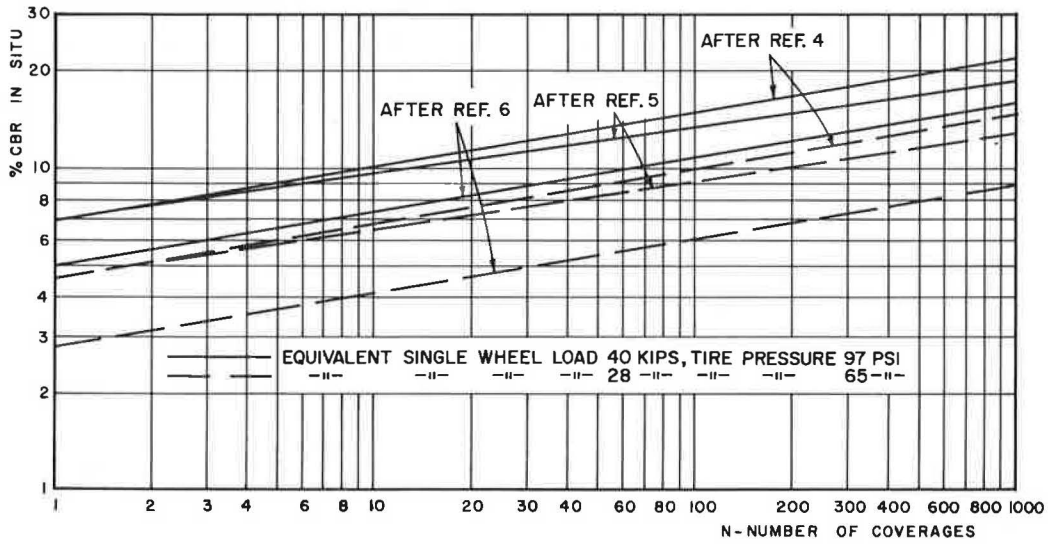

values at the bottom. Similar results were obtained from existing single-layered pavements (H = 6-8 in) in service (7). Table 1 presents these in situ CBR results (7).

It should be noted that Foster's finding and the results of Greenstein and Livneh (7) are compatible with the variation of the ratio E_G/E_S with depth, where E_G is the resilient modulus of the granular material and E_S is the resilient modulus of the subgrade material. This variation of E_G/E_S with depth is taken into consideration when the theory of elasticity is used to determine the thickness of flexible pavements.

Summing up, the variation in in situ CBR with depth is given according to the following expression (see Figure 2):

$$\log CBR_Y = \left(\log CBR_L \left\{1 - [(20 + y - H)/20]\right\} [\log(CBR_L/CBR_S)] + \log CBR_S\right) \rightarrow H - 20 > Y > 0 \rightarrow H \geq Y \geq (H - 20) \quad (2)$$

where

CBR_Y = in situ CBR of laterite subbase as a function of depth Y;
CBR_L = CBR on surface of laterite subbase material, i.e., for Y = 0 (or over an 8-in single layer of subbase, as shown in Figure 2);
CBR_S = CBR of subgrade; and
H = thickness of laterite subbase, which is thickness of pavement (see Figure 2).

Equation 2 is valid only for $0 < Y < H$. When $Y > H$, CBR_Y is actually equal to CBR_S.

Finally, the results by Wiseman and Zeitlen (9) are expressed by the following equation:

$$S = \lambda \cdot CBR \quad (3)$$

where S is the shear strength of the material and λ is the material constant.

DEVELOPMENT OF DESIGN CRITERIA FOR EARTH PAVEMENT

The models from material cited for pavement design of unsurfaced roads are empirical. Such a model (10), is given below:

$$\text{Log } CBR_S = -1.574\,55 + 0.581\,14 \log P + 0.490\,26 \log p + 0.171\,90 \log N - 0.001\,23 \log CBR_L - 0.654\,71 \log H - 0.382\,51 \log SN \quad (4)$$

where SN denotes the "shape number," i.e., the geometric dimensions and deflection of the tires, and the other variables are as previously described. For this case--a single-layer earth road without a subbase cover--the design model must include the following design parameters: P; p; N, where $CBR_S = CBR_L = CBR$.

For a given wheel size (a given contact area), the following relationship can be obtained by partial differentiation of Equation 4 between the CBR and the tire pressure (which is, in the first approximation, equal to the contact pressure between the tire and the earth):

$$[(\partial \log CBR)/(\partial \log p)] = \left\{[(\partial \log CBR)/(\partial \log p)]\right\} + \left\{[(\partial \log CBR) \div (\partial \log P)]/[(\partial \log P)/(\partial \log p)]\right\} = 0.580\,426 + 0.489\,66 = 1.07 \quad (5)$$

Equation 5 indicates that an approximate linear relationship exists between the CBR and the tire pressure given by the following:

$$CBR \cong Cp \quad (6)$$

where C is a constant obtained by integration of Equation 5.

Equation 5 is equivalent to Equation 3 and is compatible with the plastic theory of cohesive medium, which was used successfully by Greenstein and Livneh (7) for pavement design of a base course covered by surface treatment. Therefore, the conclusion under discussion is that it is possible to adopt Equation 5 as a submodel.

The relationship between CBR and N (coverages to failure) is obtained by partial derivation of Equation 4, i.e.,

$$(\partial \log CBR)/(\partial \log N) = 0.1716 \quad (7)$$

According to Womack (4) and Brabston and Hammitt (5), the values of this factor [(∂ log CBR)/∂ log N)] are 0.17 and 0.14, respectively. Brabston and Hammitt (5) deal with a subbase pavement covered by a thin asphalt membrane. Therefore, for unsurfaced pavement, the CBR is expected to have higher sensitivity to N. In other words, [(∂ log CBR)/(∂ log N)] > 0.14. Thus, for this study, Equation 7 is compatible with the empirical results found by Womack (4).

Table 1. In situ CBR results.

Thickness of Granular Layer (cm)	CBR of Subgrade (%)	CBR in Middle of Granular Layer (%)	CBR on Surface of Granular Layer (%)
15.0-17.0	9	25-40	>80
14.5-16.0	12	28-44	>80

Note: 1 cm = 0.39 in.

Figure 2. Variation in CBR value with depth.

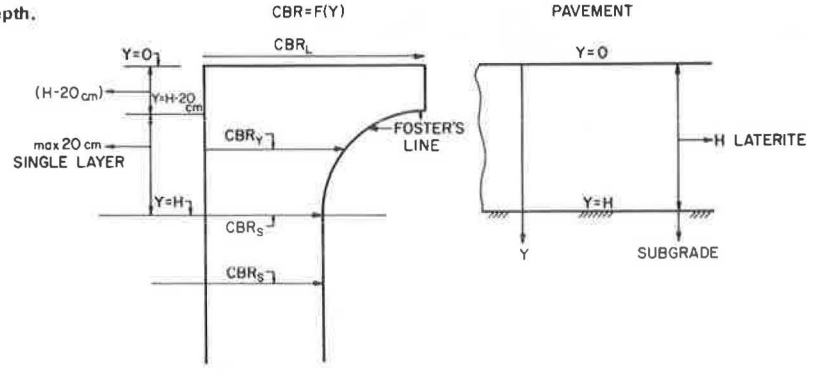

Table 2. Test results on earth pavement.

Source	In Situ Test Results: CBR In Situ (%)	ESWL (lbf 000s)	Tire Pressure (lbf/in^2)	No. of Coverages to Failure	Calculated Values from Equation 6: K	CBR	N[a]
Unpublished data from Livneh and Greenstein	6.3[b]	27	70	8	-2.831	6.6	6.0
	7.9	36	90	11	-2.882	9.3	4.2
	7.9[c]	27	70	21	-2.804	7.8	22.6
	7.9[c]	27	70	18	-2.793	7.6	22.6
Womack (4)	3.7	23	60	1	-2.834	3.9	0.7
	7.5	23	60	40	-2.802	7.4	44.6
	3.7	29	40	1	-2.806	3.7	1.0
	7.5	29	40	70	-2.816	7.6	64.7
	7.5	29	60	16	-2.792	7.2	20.3
	3.7	23	40	3	-2.830	3.9	2.3
Turnbull and Burns (11)	4.0	10	40	40	-2.780	3.7	60.8
	4.5	10	100	3	-2.730	3.7	8.8
	8.3	10	100	27	-2.628	5.5	313.0
	7.5	10	200	2	-2.625	4.9	24.0
	15.5	10	300	30	-2.600	9.5	519.0
	4.0	25	40	10	-2.906	5.0	2.7
	4.5	25	100	2	-2.930	5.9	0.4
	10.5	25	100	40	-2.930	9.9	55.6
	11.5	25	200	20	-2.842	12.4	13.1
	18.3	25	200	147	-2.789	17.4	195.8
	17.0	25	300	75	-2.857	18.9	40.1
	12.5	50	100	30	-2.863	14.1	14.7
	19.5	50	200	120	-2.921	25.1	27.2
	22.5	50	300	35	-2.853	24.8	19.6

[a] K = -2.8102. [b] Site 1. [c] Site 2.

Figure 3. Distribution of in situ CBR.

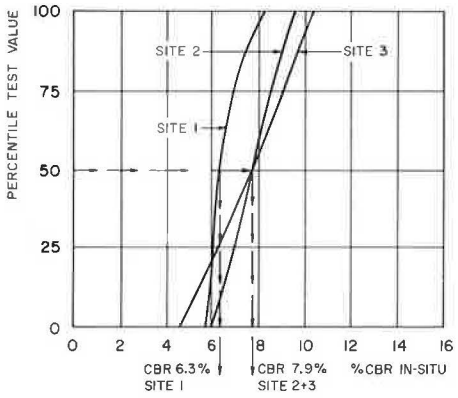

Figure 4. Distribution of K_i-values (according to Equation 8).

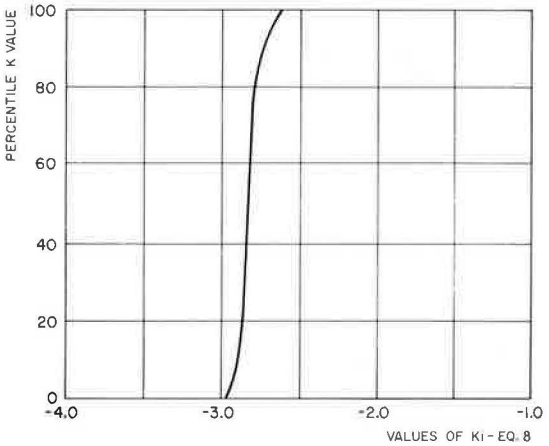

In conclusion, the solution of Equations 5 and 7 is given in the following:

$$0.489\,66 \log p + 0.580\,426 \log \underline{P} + 0.1716 \log N - \log CBR + K = 0 \quad (8)$$

where K is a constant parameter determined by the site investigation presented in the following section.

EVALUATION OF IN SITU INVESTIGATION (EARTH PAVEMENT)

A summary of empirical in situ test results is given in Table 2 (4,11). The parameters included in Table 2 are subgrade CBR, ESWL ($\underline{P}$), tire pressure (p), and number of coverages to failure (N). For example, tests were run on three sites that had a silty-sand subgrade classified A-2-4 by the American Association of State Highway and Transportation Officials (AASHTO). The distribution of the in situ CBR for the three sites is shown in Figure 3. This figure shows that in situ CBR corresponds to the 50th percentile, is 6.3 percent on site 1, and 7.9 percent on sites 2 and 3. The earth pavement failed after N = 8, 21, and 18 coverages on sites 1, 2, and 3, respectively. The ESWL was 27 kips and the tire pressure was 70 lbf/in^2 (see Table 2). Another study (4) was carried out on uncompacted sandy subgrade (CBR = 3.7 percent) and on silty subgrade (CBR = 7.5 percent). In this case, the earth pavement failed after N = 1 and 40 coverages (by ESWL = 23 kips and p = 60 lbf/in^2), respectively.

The experimental data given in Table 2 enabled us to study the reliability of the model developed in the previous section (Equation 8) and to determine the K-values. The results of this computation are given in Table 2. For example, in the experiment carried out on site 1 with a subgrade CBR of 6.3 percent, the calculated K-value is K_i = -2.831. The distribution of K_i (according to Equation 8) is given in Figure 4. This distribution has a standard deviation of 0.0879, which is an indication of the reliability of the developed model. Finally, the value of K in Equation 8 is based on the K_i-values given in Table 2, i.e.,

$$K = \sum_{0}^{24} K_i/24 = \sum_{0}^{24} (\log CBR_i - 0.489\,66 \log p_i - 0.580\,426 \log \underline{P}_i - 0.1716 \log N_i)/24 \quad (9)$$

where

CBR_i = in situ CBR of each study i (according to Table 2, 24 studies exist),
$\underline{P}_i$, p_i = ESWL and tire pressure in each study i, and
N_i = number of coverages to failure in each study i.

Substituting the calculated K_i-values (shown in Table 2) into Equation 9 gives K = -2.8102. Substituting this value into Equation 8 enables the determination of the required CBR (or coverages for a given ESWL, p, and N or CBR). The results of this calculation are given in Table 2. For example, in the investigation carried out on site 1 (subgrade CBR = 6.3 percent; ESWL = 27.000 lb; p = 70 lbf/in²; N = 8), the calculated CBR (by using Equation 8) is 6.6 percent. The relationship between the in situ measured subgrade CBR and calculated CBR by the model developed in this study is a statistical test of this model's reliability. This statistical correlation (linear regression) is given in the following:

$$\text{Calculated CBR} = -0.63 + 1.09\text{CBR in situ} \quad R^2 = 0.89 \quad (10)$$

Equation 10 is plotted in Figure 5, which contains the measured and calculated CBR values. The important conclusion derived from Figure 5 is that in the practical range of the in situ CBR (3-30 percent), Equation 10 coincides with the line of equality of in situ CBR and calculated CBR. This is additional proof of the validity of the model developed for this study.

Relative lower correlation (which is expected for the number of coverages to failure, $R^2 = 0.77$) is obtained for the calculated and measured coverages (Figure 6). In this case also, the correlation line (Equation 11) coincides with the line of equality (calculated log N = in situ log N):

$$\log N \text{ (calculated)} = 0.95 \log N \text{ in situ} + 0.0688 \quad (11)$$

Figure 5. Relationship between calculated CBR (Equation 10) and measured CBR in situ.

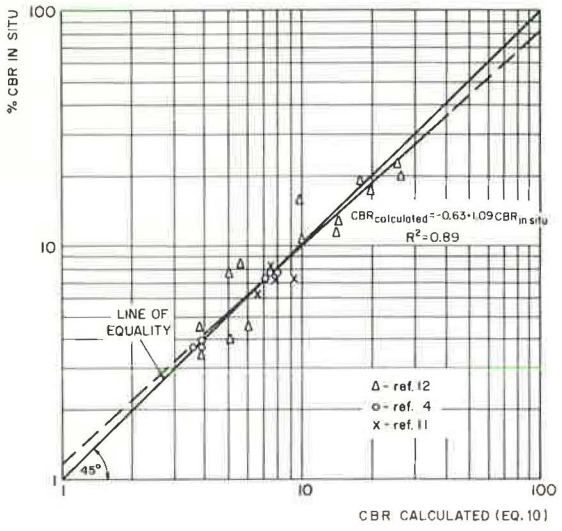

DEFINITION OF METHODOLOGY FOR LATERITE SURFACE PAVEMENT

Studies by the U.S. Army Corps of Engineers and others (3,6,12) have shown that the maximum practical coverages per lane to failure for a soil-aggregate surface are in the region of 10×10^3 to 15×10^3 equivalent standard axles (ESA), which is equivalent to approximately 25 000 applications of ESA. Therefore, since it is normal practice in Thailand to reconstruct the surface annually or every two years, the most economical pavement section should have the minimum thickness required to carry the estimated traffic through this period and

Figure 6. Relationship between calculated N (Equation 8) and N measured in situ.

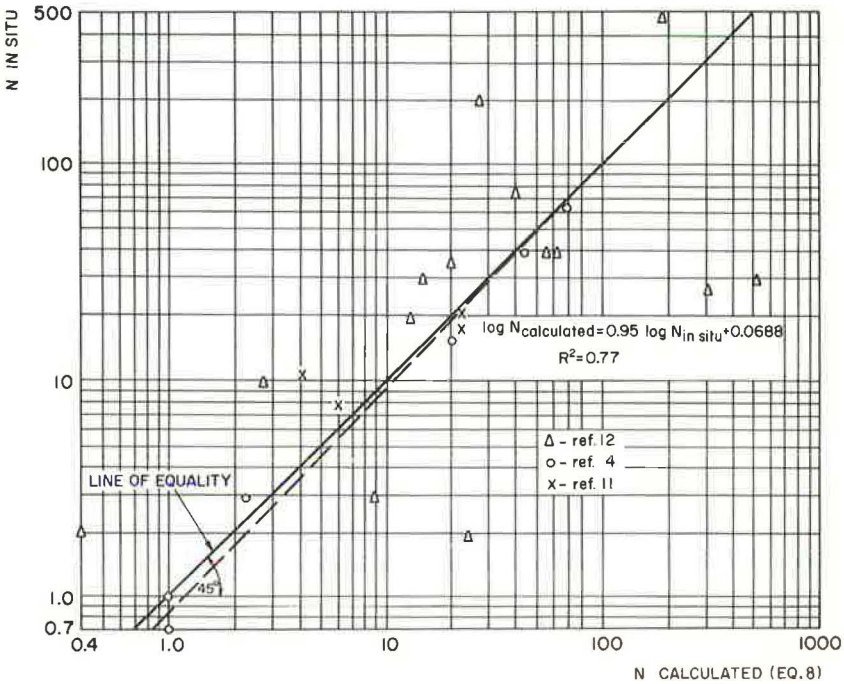

Figure 7. Stress distribution beneath surface of flexible pavement.

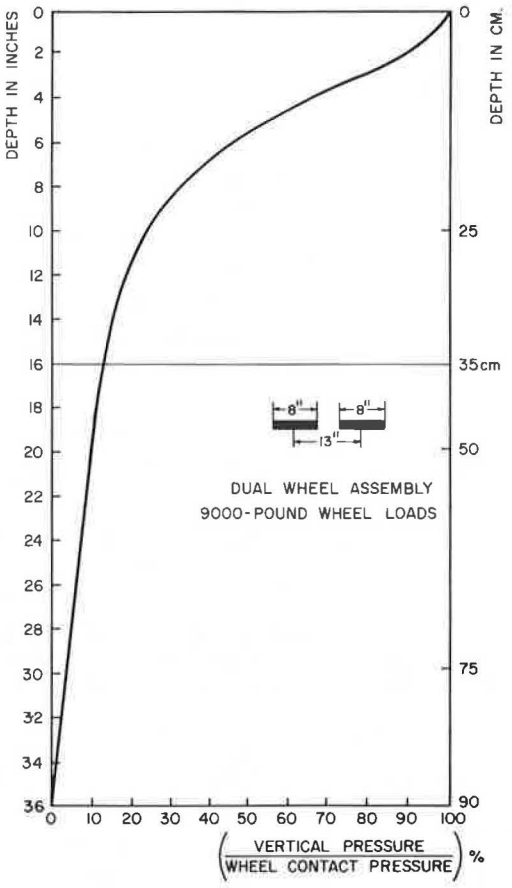

Figure 8. Equivalent wheel factor (α) versus depth of pavement.

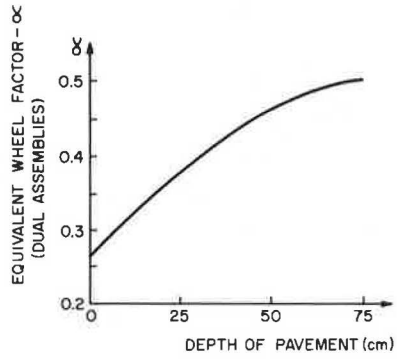

less than 25 000 applications of ESA per lane.

As stated in the section on basic assumptions, the plastic theory was adopted for this study for the analysis of the pavement design. In other words, Equations 2 and 8 (with K = -2.8102) are the basic equations that govern the pavement design for laterite roads. Therefore, in this case (two-layer analysis), an equivalent CBR of the two-layer system must replace the CBR of the one-layer system given in Equation 8. This equivalent CBR is defined in the following equation:

$$CBR_{eq} = (1/h) \int_o^h CBR_y dy \quad (12)$$

where

CBR_{eq} = equivalent CBR of two-layer system (subgrade and subbase), which replaces subgrade CBR of one-layer analysis in Equation 8;
CBR_y = in situ CBR of pavement system as a function of depth y (see Figure 2 and Equation 2); and
h = depth of pavement that supports standard axle load (9000 lb, dual-wheel assembly).

In this study, it is assumed that h is the depth beneath which the vertical stress is less than 15 percent of the tire contact pressure. Therefore, based on Figure 7 [adapted from Martin and Wallace (13)], h = 14 in.

Finally, the use of Equations 8 and 12 for the 18 000-lb axle load (p = 70 lbf/in²) yields the following equation for the pavement design of unsurfaced subbase roads:

$$-2.8102 + 0.489\,66 \log (70) + 0.580\,426 \log (\alpha \times 18\,000) + 0.1716 \log (N) = \log CBR_{eq} = \log [(1/35) \int_0^{35} CBR_y dy] \quad (13)$$

where α denotes ESWL, i.e., α (axle load) = ESWL, and α is a function of the type of axle and pavement depth. For the dual assembly, the values of α are given as a function of the depth of pavement in Figure 8 [modified from Livneh, Ishai, and Uzan (14)].

APPLICATION

Earth Roads

The nomogram shown in Figure 9 is used for the application to earth roads of the model (Equation 8 with K = -2.8102) developed in this study. In this figure, Equation 8 has been solved for a range of values of ESWL, tire pressure, subgrade CBR, and number of coverages to failure.

Figure 9. Design charts for earth roads.

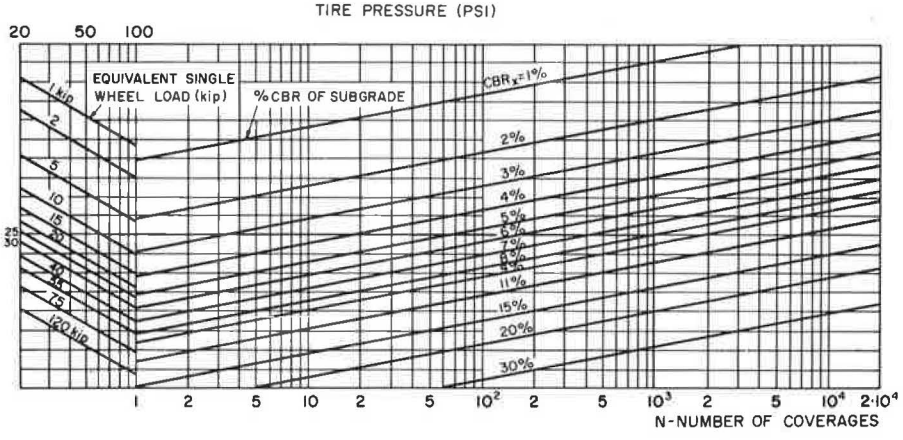

Figure 10. Pavement design of unsurfaced laterite roads.

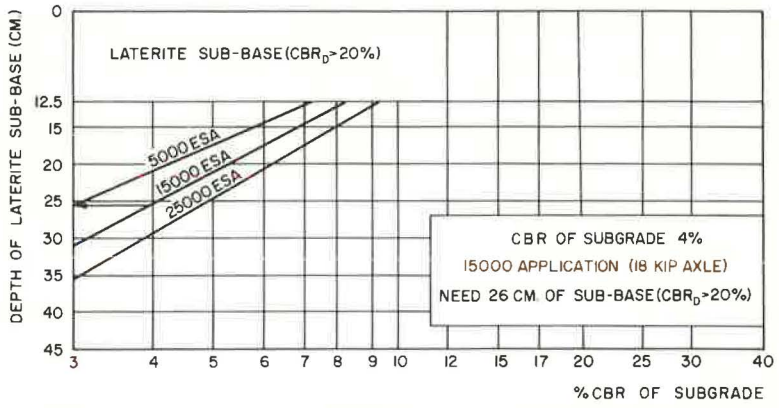

By entering the tire pressure and ESWL (as shown by the arrows in Figure 3), the number of coverages to failure for any given subgrade CBR design value can be determined. The example in Figure 9 shows that a subgrade that has a CBR of 8 percent permits 1000 coverages of 9000-lb equivalent wheel loads with a tire pressure of 70 lbf/in^2.

Unsurfaced Subbase Roads

The nomogram shown in Figure 10 is used for the application of the model (Equation 13) developed in this study for unsurfaced subbase roads. In this figure, Equation 13 has been solved for a range of subbase thicknesses, subgrade CBR values, and number of applications (5000-25 000 applications of ESA, which is equivalent to 2500-12 500 coverages) for an 18 000-lb axle. Therefore, for a given subgrade CBR design value, the required subbase thickness can be determined. For example, for a CBR value of 4 and estimated loading of 15 000 ESAs, the required subbase thickness is 10 in (see Figure 10).

It is important to note that the conclusions from Figure 10 are compatible with the up-to-date experience in Ecuador (3). According to Greenstein and Garcia (3), an unpaved gravel road 8 in thick on a silty-sand subgrade (CBR 6-7 percent) carried about 25 000 ESAs (18 kips) per lane until reconstruction of the surface was required. This is an indication of the reliability of the developed model.

An additional indication of the validity of this model is the local experience in Thailand for rural roads, according to which a minimum pavement depth of 6 in is used over silty subgrade (CBR ≈ 5-6 percent) for approximately 5000 ESAs, which is nominally the minimum design traffic load.

The following three limitations should be observed when Figure 10 is used:

1. Figure 10 can be used for local laterite subbase with a CBR design value that ranges between 20 and 40 percent.
2. For subbase CBR values greater than 40 percent, the required thickness may be reduced by approximately 30 percent to a practical minimum of 5 in.
3. For subgrade CBR values greater than 15 percent, local subgrade can be used as the pavement layer.

REFERENCES

1. T. Ruenkrainagsa. Soil Materials and Improvement of Their Properties in Thailand. Presented at Symposium of Geotechnical Aspects of Highway Engineering, Bangkok, Thailand, 1979.
2. F.N. Hveem. Pavement Deflections and Fatigue Fractures. HRB, Highway Res. Bull. 119, 1955, pp. 43-73.
3. J. Greenstein and J. Garcia. Estudio de Caminos Vecinales. In Study of Low-Volume Roads in Ecuador, World Bank, Washington, DC, 1979.
4. L.M. Womack. Tests with a C-130 E Aircraft on Unsurfaced Soils. Air Force Systems Command, U.S. Air Force, Camp Springs, MD, Paper 4-712, n.d.
5. W.N. Brabston and G.M. Hammitt II. Soil Stabilization for Roads and Airfields in the Theater of Operations. U.S. Army Corps of Engineers Waterways Experiment Station, Vicksburg, MS, 1974.
6. R.G. Ahlvin and G.M. Hammitt II. Load-Supporting Capability of Low-Volume Roads. TRB, Special Rept. 160, 1975, pp. 198-203.
7. J. Greenstein and M. Livneh. Design Thickness of Low-Volume Roads. TRB, Transportation Research Record 702, 1979, pp. 39-46.
8. C.R. Foster. Strength of Bases and Subbase. Proc., 3rd International Conference on Structural Design of Asphalt Pavements, Univ. of Michigan, Ann Arbor, 1972.
9. G. Wiseman and J.G. Zeitlen. A Comparison Between the CBR and the Shear Strength Methods in the Design of Flexible Pavements. Proc., 5th International Conference on Soil Mechanics and Foundation Engineering, Vol. 2, Paris, 1961, pp. 359-363.
10. G.M. Hammitt II. Structural Design of Unsurfaced Roadways and Airfields. HRB, Highway Research Record 362, 1971, pp. 96-97.
11. W.J. Turnbull and C.D. Burns. Strength Requirements of Unsurfaced Soils for Aircraft Operations. Proc., 5th International Conference on Soil Mechanics and Foundation Engineering, Paris, 1961.
12. S.P. Peter. Development in Highway Pavement Engineering. Applied Science Publishers, Barking, Essex, England, 1978.
13. R.J. Martin and H.A. Wallace. Design and Construction of Asphalt Pavement. McGraw-Hill, New York, 1967.
14. M. Livneh, I. Ishai, and J. Uzan. Load Equivalency Factors for Mixed Traffic Using the CBR Equation. Technion-Israel Institute of Technology, Haifa, Israel, 1979.

Publication of this paper sponsored by Committee on Low-Volume Roads.

Lime-Soil Mixtures for Low-Volume Road Construction in Egypt

SAMIR A. AHMED

Some experimental research findings on the application of hydrated lime to the superficial soils of the valley and delta of the Nile River for the purpose of low-volume road construction are described. Eight soil samples and one type of commercial lime were included in the experimental program. Statistical techniques were used to analyze the effects of lime content, curing temperature, curing time, and soil type on the increase in the unconfined compressive strength of lime-soil mixtures. Suggestions and guidelines for the use of hydrated lime to improve the properties of local soils and nearby paving materials are given in the conclusion.

The construction of low-volume, low-cost rural roads is receiving growing emphasis among the transportation officials in Egypt as part of its national development policy. These roads are planned and designed to encourage the economic development of rural localities, improve the mobility of rural residents, and help redistribute the population in order to relieve the severe urban problems that exist in large cities. Because of limited capital funds for road construction programs, highway engineers have sought the use of available low-cost stabilization materials to improve the properties of local soils and the nearby paving materials. The fact that limestone is an abundant resource in Egypt made hydrated lime a desirable stabilizing material in low-volume road construction.

This paper presents some experimental research findings on the application of hydrated lime to the soils of the valley and delta of the Nile River. The potential improvements in strength, plasticity, volume changes, durability, and workability that result from the addition of small amounts of lime to almost any fine-grained soil have been the subject of extensive research efforts and are reviewed and summarized elsewhere (1-3). However, the effects of applying lime to a particular soil cannot be exactly predicted without testing the individual soil in question. This is particularly relevant to the alluvial soils of the Nile River, which have experienced extensive advanced weathering during the trip from mideast Africa to the Mediterranean.

Four reactions are reported in the literature to explain the mechanisms of lime-soil stabilization (4,5). These are the cation-exchange, flocculation, carbonation, and pozzolanic reactions. The first two reactions influence soil plasticity, volume changes, and workability, whereas the pozzolanic reaction is responsible for strength increase (4,5). Soil properties that affect the rate and magnitude of the pozzolanic reaction include clay mineralogy, organic carbon, percentage of clay fraction, exchange-complex characteristics, soil pH, and amounts of silica, alumina, iron oxide, free carbonates, free sulfates, and sodium enrichment (6-10). Other factors that influence the strength increase of lime-soil mixtures are lime content, curing conditions, and mixture density (2-4,11).

MATERIALS, TEST SPECIMENS, AND EXPERIMENTATION

Eight soil samples that represented the superficial soils of the Nile valley and delta were included in this study. The samples were taken from a depth of approximately 1 m (3.3 ft) below the ground surface and shipped to the laboratory in sealed containers to permit evaluation of the natural moisture content. Soils were air dried, hand crushed, sieved to finer than 4.75 mm (0.2 in) (no. 4 sieve), and stored for subsequent analysis. The engineering and mineralogical properties of the different soil samples are summarized in Table 1, and the chemical properties are presented in Table 2.

The lime used is a commercial-grade, high-calcium hydrated lime manufactured by the Cairo Sand Bricks Company. Analysis of the single lime batch used in this study showed 70.41 percent available calcium oxide and a maximum particle size of 0.037 mm (0.001 in) (no. 400 sieve).

Three levels of lime content--3, 5, and 7 percent by weight of the dry soil--were used in the experimental program. Test specimens from the natural soils and lime-treated soils were prepared by using a mold 10 cm high by 5 cm in diameter (4 by 2 in). Natural soils were thoroughly mixed with the appropriate amount of water and molded. Lime-treated soils were mixed in the dry state, and mixing continued while the proper amount of water was added. All specimens were compacted at optimum moisture content determined in accordance with ASTM C593. Compacted specimens were sealed and cured in a constant-temperature cabinet at 21°C and 60°C (70°F and 140°F). Curing periods were 3, 7, 14, 21, 35, and 56 days.

At the end of each curing condition, the specimens were tested for unconfined compressive strength by using a Farnell compression-testing machine. Loads were applied at a constant rate of deformation of 0.12 cm/min (0.05 in/min), and the maximum load was recorded for each specimen. The unconfined compressive strength was estimated by the average strength of a series of six specimens.

RESULTS AND DISCUSSION

Table 3 summarizes most of the results of tests for unconfined compressive strength for the eight soil samples used in this study. Soils II, IV, V, and VII showed remarkable increase in strength with the addition of lime, whereas soils I, III, VI, and VIII were not reactive to lime. The major clay minerals in soil types II, IV, V, and VII are kaolinite and montmorillonite, whereas in soils I, III, VI, and VIII the predominant minerals are illite, chlorite, and quartz.

To investigate the statistical significance of lime content and soil type on the unconfined compressive strength of lime-soil mixtures, a randomized complete block design was used that had three percentages of lime (3, 5, and 7 percent) that represented the treatment levels and four lime-reactive soils that formed the blocks. Only lime-reactive soils (types II, IV, V, and VII) were included in the analysis, since strength is not a major factor in determining the appropriate treatment for nonreactive soils. Results of the analysis of variance indicated that lime content has a significant effect on the average strength of lime-reactive soils at the 0.05 level of significance. Soil type, on the other hand, was found to be not significant at the same level. In general, for a given soil type and set of curing conditions the relationship between lime content and strength peaks at a certain optimum

Table 1. Engineering and mineralogical soil properties.

Soil No.	Drainage	Atterberg Limits (%)			Classification		Specific Gravity	Moisture-Density		Clay <2 μm (%)	Major Clay Minerals[a]
		Liquid Limit	Plastic Limit	Plasticity Index	AASHTO	Unified		γ_d max (t/m^3)	W_{opt} (%)		
I	Poor	55	34	21	A-7-5 (15)	MH	2.67	1.52	24	0	A,F,Q
II	Poor	55	28	27	A-7-6 (17)	CH	2.69	1.54	23.5	22	K,M,Q
III	Poor	44	25	19	A-7-6 (13)	CL	2.75	1.59	22.7	14	I,C,G,Q
IV	Moderate	70.5	42	28.5	A-7-5 (19)	MH	2.63	1.42	28	23	K,M,I,Q
V	Moderate	54.4	28.7	25.7	A-7-6 (16)	CH	2.71	1.64	18.3	27	K,M,Q
VI	Poor	73.5	34.5	39	A-7-5 (20)	CH	2.75	1.47	25	8.5	I,C,A,Q
VII	Poor	79.5	33	46.5	A-7-5 (20)	CH	2.75	1.48	27.5	20	K,M,Q
VIII	Poor	48	30	18	A-7 (13)	ML	2.61	1.52	25	0	I,A,G,Q

Note: 1 ton = 0.9 Mg.
[a]Symbols used are as follows: A = albite, C = chlorite, F = feldspars, G = gibbsite, I = illite, K = kaolinite, M = montmorillonite, Q = quartz.

Table 2. Chemical soil properties.

Soil No.	pH	Organic Carbon (%)	Cation Exchange Capacity (meq/100 g)	Exchangeable Cations (meq/L)					Exchangeable Anions (meq/L)				
				Ca	Mg	Na	K	Total	CO_3	HCO_3	CL	SO_4	Total
I	6.0	1.60	38.0	8.9	2.5	8.4	0.2	20.0	0	1.8	10.0	8.2	20.0
II	7.7	0.25	28.5	75.5	369.0	960.0	0.2	1404.7	0	1.4	1314.0	89.8	1405.2
III	6.7	1.16	42.5	31.6	57.2	12.0	0.3	101.1	0	0.5	82.0	18.7	101.2
IV	8.2	0.00	53.5	19.2	30.2	25.0	0.3	74.7	0	0.7	12.0	62.0	74.7
V	8.9	1.15	44.5	6.8	11.9	34.0	1.0	53.7	0	0.9	10.0	42.8	53.7
VI	5.5	1.73	34.0	4.7	7.7	50.0	1.0	63.4	0	1.8	37.0	24.6	63.4
VII	8.0	0.52	38.0	50.7	54.4	230.0	3.0	338.1	0	1.2	245.0	91.9	338.1
VIII	7.9	1.80	18.0	33.0	21.2	45.0	1.0	100.2	0	1.8	36.0	69.4	100.2

Note: 1 L = 0.264 gal; 1 g = 34 oz.

Table 3. Results of tests for unconfined compressive strength.

Soil No.	Natural Soil (kg/cm^2)	3 Percent Lime (kg/cm^2)						5 Percent Lime (kg/cm^2)						7 Percent Lime (kg/cm^2)					
		21°C			60°C			21°C			60°C			21°C			60°C		
		7-Day	35-Day	56-Day	7-Day	35-Day	56-Day	7-Day	35-Day	56-Day	7-Day	35-Day	56-Day	7-Day	35-Day	56-Day	7-Day	35-Day	56-Day
I	22.4	11.9	21.0	19.5	19.8	22.7	23.0	10.8	19.7	21.3	17.5	21.5	21.8	10.1	14.7	17.2	13.0	17.6	18.2
II	4.4	5.7	12.3	13.9	11.7	17.5	18.9	14.5	28.2	31.9	26.8	43.3	44.0	11.1	21.6	23.4	19.9	31.4	32.6
III	13.3	8.3	13.8	14.3	13.5	14.9	15.1	12.1	15.4	15.9	14.1	16.0	16.2	7.9	10.3	11.7	10.1	12.9	13.2
IV	8.8	6.9	19.8	22.4	17.8	28.7	30.9	7.2	30.0	34.1	29.5	46.1	47.3	5.7	16.5	18.5	15.4	22.7	25.2
V	21.1	14.2	23.5	25.8	22.3	34.3	35.8	22.6	27.5	32.6	26.1	41.3	45.7	9.3	12.9	14.3	12.1	19.4	23.7
VI	15.7	8.9	15.2	16.9	13.9	17.1	17.9	5.5	8.2	8.8	9.1	13.0	15.3	5.1	7.4	8.1	8.6	11.4	12.9
VII	9.1	9.5	24.2	26.6	22.1	35.2	37.7	12.6	20.1	23.7	19.0	30.2	32.4	5.4	15.3	17.4	13.5	20.9	27.8
VIII	16.0	9.7	16.3	17.1	14.5	17.5	18.1	9.9	18.0	19.3	16.9	18.7	18.9	9.4	16.9	18.2	15.1	17.3	17.7

Note: 1 kg = 2.204 lb; 1 cm^2 = 0.155 in^2; t°C = (t°F - 32)/1.8.

lime content. Increasing the percentage of lime beyond this optimum level not only results in no additional increase in strength but also may reduce the strength to that below the strength at optimum lime content.

Figures 1, 2, and 3 depict the effects of the percentage of organic carbon, percentage of clay fraction, and soil pH on the increase in strength of lime-soil mixtures. As expected, organic carbon has a negative impact on the strength gain because it retards the long-term pozzolanic reaction (4). The results of Figure 1 indicate that soils that contained more than 1 percent organic carbon do not react satisfactorily to lime. In Figure 2, it may be noted that soils that have a clay fraction that exceeds 20 percent are the same soils that showed a remarkable increase in strength due to lime treatment. The clay fraction of a soil is the major source of silica and alumina, which react with lime to form cementing agents such as calcium silicate and calcium aluminate. The estimated coefficient of correlation between the clay fraction and the strength increase is 0.70 based on the results of Figure 2.

Soil pH, an indicator of the degree of weathering, varied from 5.5 to 8.9 for the natural soils used in this study. As the amount of absorbed hydrogen ions increases, the soil pH decreases, which implies a weathered soil. In general, a high pH value indicates that soil silica and/or alumina are available for the pozzolanic reaction. Examination of the results of Figure 3 reveals that soils that have a pH value greater than 7.0 are lime-reactive soils. The estimated correlation coefficient between soil pH and strength gain is 0.56 based on the data in Figure 3. Similar values of this correlation coefficient were found by Thompson (4) and by Harty and Thompson (9).

The analysis-of-variance techniques were also applied to study the separate effects of curing

Figure 1. Effect of organic carbon on strength increase.

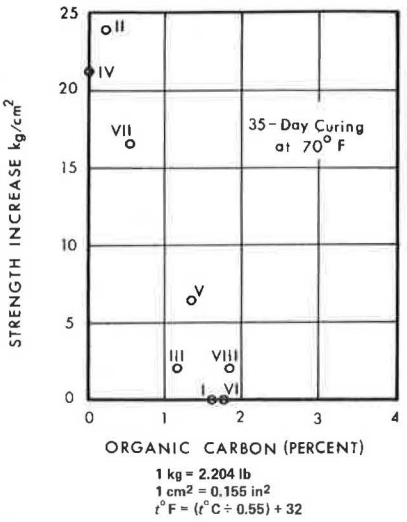

Figure 2. Effect of clay fraction on strength increase.

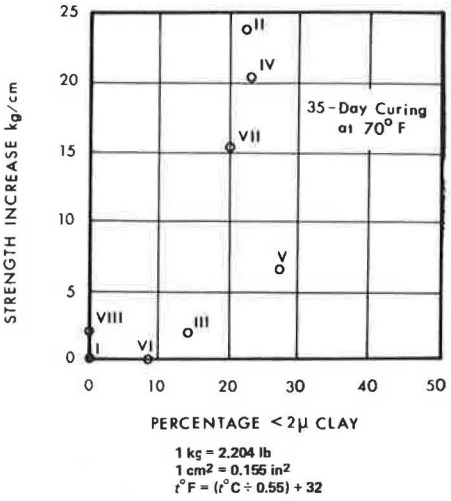

Figure 3. Effect of soil pH on strength increase.

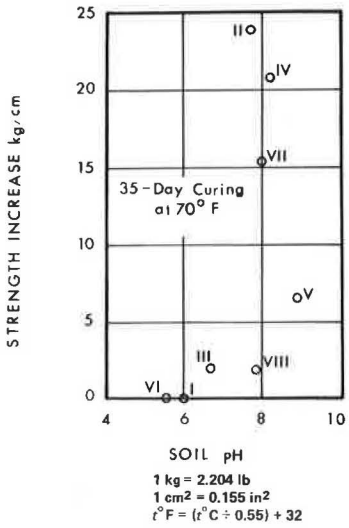

Figure 4. Relationship between compressive-strength results and curing conditions.

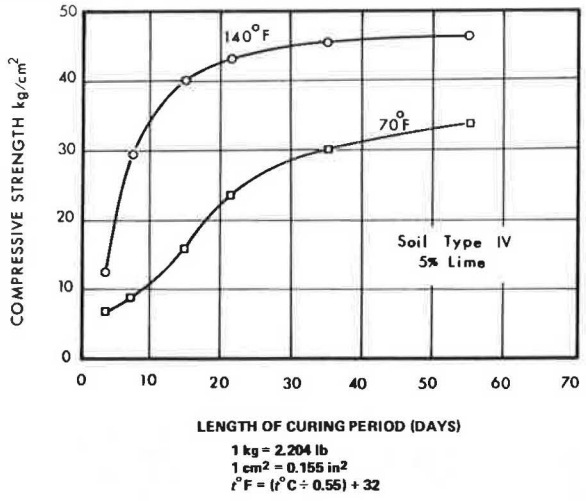

temperature and curing time on the strength increase of lime-soil mixtures. Two curing temperatures, 21°C and 60°C (70°F and 140°F), represented the treatment levels in the first randomized block design, and three curing periods--7, 35, and 56 days--made up the treatment levels in the second randomized block design. In each design, soil types II, IV, V, and VII formed the blocks. The effects of curing temperature and curing period on the strength increase were found to be statistically significant at the 0.05 level. Figure 4 shows representative plots of the unconfined compressive strength of soil type IV treated with 5 percent lime at different curing conditions.

CONCLUSIONS

The purpose of this research was to establish design criteria and guidelines for applying lime stabilization to the soils of the Nile valley and delta. The following conclusions and suggestions are based on the test results and analyses presented in this paper.

1. The basic data required by the highway engineer to evaluate the potential applicability of lime stabilization to a particular soil are soil pH, organic carbon content, percentage of clay fraction, and characteristics of the cation-exchange complex.

2. Remarkable increase in the strength of a lime-soil mixture can be expected if the following conditions are met: (a) The percentage of organic carbon is less than 1 percent, (b) the soil pH is greater than 7, and (c) the amount of clay fraction is more than 20 percent.

3. For a given lime-reactive soil, the relationship between lime content and strength peaks at a certain optimum lime content, the value of which ranges in general from 3 to 7 percent. The optimum lime content for a soil that has a relatively low pH value is greater than that required for a soil that has a high pH value. Increasing the percentage of lime beyond this optimum level not only results in no additional increase in strength but also may reduce the strength to that below the strength at optimum lime content.

4. The strength of a lime-treated soil is directly influenced by both curing temperature and curing time. In general, most of the strength gain takes place during the first five weeks at tempera-

tures of approximately 20°C to 25°C (68°F to 77°F). Higher curing temperatures help accelerate the increase in strength.

ACKNOWLEDGMENT

This study was supported by the Ministry of Transportation and Communications, Cairo, Egypt, as part of a research project on low-volume road construction. The experimental phase of this study was conducted in the Soil Mechanics Research Laboratory of the Highway Research Center, Cairo, Egypt.

REFERENCE

1. M.R. Thompson. Soil-Lime Mixtures for Construction of Low-Volume Roads. TRB, Special Rept. 160, 1975, pp. 149-165.
2. M.J. Dumbleton. Lime Stabilized Soil for Road Construction in Great Britain. Roads and Road Construction Journal, Vol. 40, No. 479, 1962, pp. 321-325.
3. O.G. Ingles and S. Frydman. The Effect of Cement and Lime on the Strength of Some Soil Minerals, and Its Relevance to the Stabilization of Australian Soils. Proc., Australian Road Research Board, Vol. 3, Part 2, 1966, pp. 1504-1528.
4. M.R. Thompson. Lime Reactivity of Illinois Soils. Journal of the Soil Mechanics and Foundations Division of ASCE, Vol. 92, No. SM5, 1966, pp. 67-92.
5. S. Diamond and E.B. Kinter. Mechanisms of Soil-Lime Stabilization. HRB, Highway Research Record 92, 1966, pp. 83-102.
6. J.L. Eades and R.E. Grim. Reactions of Hydrated Lime with Pure Clay Minerals in Soil Stabilization. HRB, Bull. 262, 1960, pp. 51-63.
7. O.G. Ingles and J.B. Metcalf. Soil Stabilization: Principles and Practice. Wiley, New York, 1973.
8. C.C. Ladd, Z.C. Moh, and T.W. Lambe. Recent Soil-Lime Research at the Massachusetts Institute of Technology. HRB, Bull. 262, 1960, pp. 64-85.
9. J.R. Harty and M.R. Thompson. Lime Reactivity of Tropical and Subtropical Soils. TRB, Transportation Research Record 442, 1973, pp. 102-112.
10. J.C. More and R.L. Jones. Effect of Soil Surface Area and Extractable Silica, Alumina, and Iron on Lime Stabilization Characteristics of Illinois Soils. HRB, Highway Research Record 351, 1971, pp. 87-92.
11. J.M. Ozier and R.K. Moore. Factors Affecting Unconfined Compressive Strength of Salt-Lime-Treated Clay. TRB, Transportation Research Record 641, 1977, pp. 17-24.

Publication of this paper sponsored by Committee on Low-Volume Roads and Committee on Chemical Stabilization of Soil and Rock.

Polymer Stabilization of Sandy Soils for Erosion Control

RAZI A. SIDDIQI AND JOHN C. MOORE

The usefulness of a number of polymeric materials in increasing the resistance of cohesionless sandy soils to wind and water erosion was studied. Erosion resistance, compressive strength, and permeability of treated soil samples were measured. Film properties of individual polymers were also studied. These properties were then related to the performance of the polymer in controlling erosion. The optimum dilution of polymer with water and the quantity of polymer required to provide a nonerosive surface were determined for three different soils. A copolymer of butadiene-styrene is suggested as an ideal polymer for controlling erosion without significantly reducing the permeability of the treated soil. Other polymers such as polyvinyl acetate and acrylic polymers were found to be water sensitive in various degrees and consequently did not perform well. From a practical viewpoint, the application of polymers to soils by spraying has an obvious advantage over mechanically mixing polymers and soils. In the study it was found that less polymer is required to provide a nonerosive surface if spraying is used. In addition, aqueous-base polymers have numerous advantages over solution-base polymers.

Various materials and methods have been proposed for controlling erosion of agricultural lands and other terrain surfaces such as highway cut-and-fill slopes. The common methods of erosion control are the application of asphaltic products or portland cement, the establishment of vegetative cover, or the provision of riprap. All these methods and materials have limited usefulness and require frequent maintenance, which increases the total cost of a project. Another possibility is the use of polymeric materials, which have great potential for use as soil stabilizers for erosion control and for other purposes. Some of these polymeric compounds have already been used in the field and have been found quite successful (1-6). In this study, the usefulness of this versatile group of materials for application in soil stabilization has been evaluated and some of the fundamental properties and characteristics related to their performance have been identified. A full account of the studies reported here has been made by Siddiqi (7).

MATERIALS

Ten different polymeric products were studied by using three different soils. The soils were essentially noncohesive sands of varying fine (< no. 200-sieve) content obtained from different locations in Oklahoma. The pattern of results for the three soils is quite similar; consequently, the results for only one of the soils are presented. Figure 1 shows the grain-size analyses of the soils. Table 1 presents general information about the polymers used in the study. All but one of these polymers were in the form of a liquid that can be diluted with water as desired. Altak 59-50, a solution-base polymer, was included in the study for comparison purposes. This polymer requires MEK peroxide for curing and styrene as thinner.

EXPERIMENTAL PROCEDURE

Some samples for the study of erosion control and permeability were prepared by spraying the diluted

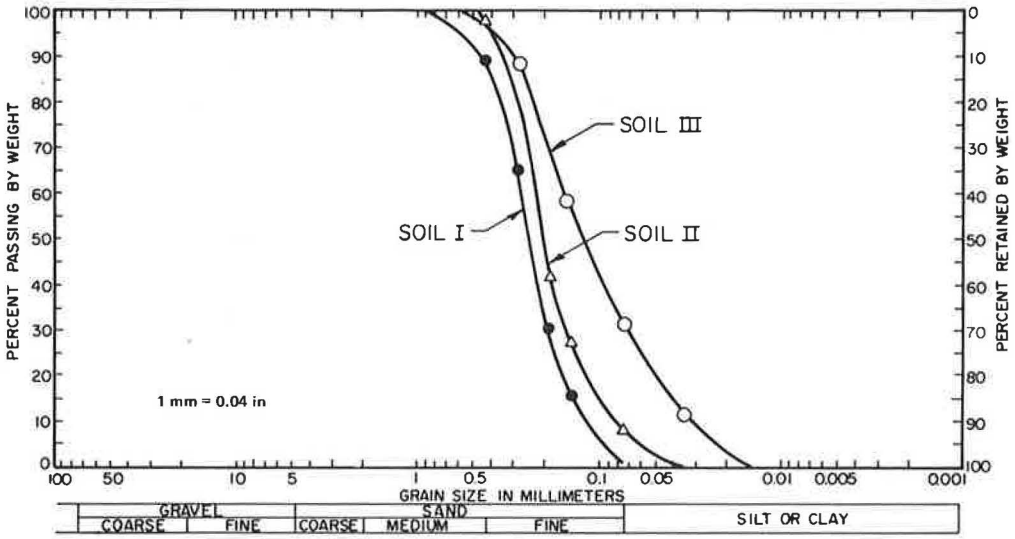

Figure 1. Grain-size analyses of soils.

Table 1. General information on polymers used.

Name	Manufacturer	Type of Polymer	1977 Cost ($/L)
Petroset SB	Phillips Chemical Co.	Butadiene styrene copolymer	0.63
Aerospray 70	American Cyanamide	Polyvinyl acetate	0.63
Terra Krete	Kingman Chemical Co.	Fermented extract of malt and vanilla (wort) and citric acid + metallic sulfates	2.12
NeoCryl 601A	Polyvinyl Chemical Industries	Vinyl polymer	0.53
Rhoplex H-8	Rohm and Has	Acrylic polymer	0.54
Altak 59-50[a]	Alpha Chemical Corp.	Polyester in styrene	
Corexit 7730	Exxon Chemical Co.	Partially neutralized polyamide	0.93
Norlig 41	American Can Co.	Calcium lignosulfonate	
Orzan GL-50	Crown Zellerbach Corp.	Ammonium lignosulfonate	
Latex XP-4026	Hooker–Ruco Division	Polyurethane latex	3.36

Note: 1 L = 0.264 gal.
[a]Solution-base polymer.

polymer solution on the soil surface and others by mechanically mixing the polymer with the soil. The sprayed samples were prepared in molds that had a diameter of 134 mm (5.3 in) and a depth of 50 mm (2.0 in). The molds were open at one end and perforated at the other to permit flow of water through the sample. Mechanically mixed samples were prepared in molds that had a diameter of 71 mm (2.8 in) and a depth of 25 mm (1.0 in) and were open at both ends. Samples were removed from the molds immediately after compaction. Samples for the study of unconfined compressive strength were prepared by mechanically mixing the soil and polymer and compacting the mixture in Harvard miniature molds by using a standard American Association of State Highway and Transportation Officials (AASHTO) compaction effort by means of a drop hammer. All samples were cured at 35°C (95°F) for seven days before being tested.

The effects of 10 freeze-thaw cycles and 10 wet-dry cycles were investigated. In the former, the samples were subjected to alternate freezing at -10°C (14°F) for 16 h and thawing at 25°C (77°F) for 8 h in an ambient relative humidity of 100 percent. Before the first freeze, the samples were immersed in water for 24 h. The wet-dry cycles consisted of 8 h of soaking at room temperature and 16 h of drying at 35°C (95°F).

The effects of exposure to ultraviolet light were also investigated. Samples half-covered with a 2-mm (0.08-in) aluminum plate were placed 254 mm (1 ft) below a 275-W sunlamp. Samples were first exposed for 8 h in a dry condition, soaked in water for 24 h, and then exposed again to the light for 8 h. Following this, the samples were further soaked for 24 h and then subjected to water-erosion testing. Total exposure was roughly equivalent to two months' exposure to sunlight.

Resistance to wind erosion was evaluated by subjecting dried samples to wind velocities of 72 km/h (45 miles/h) produced 50 mm (2 in) from the discharge snout of a blower. The velocity was measured by a pendulum anemometer that had been calibrated in a wind tunnel. The sample was positioned to simulate a horizontal wind striking a IV:2H slope with a velocity of 72 km/h.

Resistance to water erosion was measured by subjecting the soaked samples to a uniform water spray. The spray applicator produced jets that had a diameter of 0.6 mm (0.02 in) and were spaced 6.0 mm (0.24 in) apart. The jet velocity was maintained at 3.1 m/s (10 ft/s). The energy supplied by the water jets per unit area of sample surface was about four times that of a natural storm (1).

Film properties of the polymer were investigated by using a film formed by drying 20 mL of a 1:1 mixture of polymer and water in Pyrex glass dishes 89 mm (3.5 in) in diameter. Film properties such as cohesion, adhesion to the substrate (Pyrex glass) or to another layer of the same polymer or to a different one, brittleness, and swelling due to soaking in water were observed quantitatively. Some of the polymer films could be peeled from the glass by using a fingernail, whereas others required a knife blade. It was noted whether the film could be peeled intact from the glass or whether it came off in fairly large pieces or small flakes. If pieces were large enough, they were flexed and folded to

Table 2. Quality of spray-treated surface.

Name	Suitability of Polymer for Erosion Control[a]				
	Dilution Ratio	Rate of Application (L/m^2)	Solid Polymer (kg/m^2)	Cost of Treatment (1977 $\$/m^2$)	Quality of Treatment
Petroset SB	1:9	9.00	0.35	0.52	Excellent
Aerospray 70	1:12	9.00	0.34	0.47	Good
Terra Krete	1:19	9.0	0.37	0.95	Good
NeoCryl 601A	1:5	9.0	0.40	0.79	Fair
Rhoplex H-8	1:7	9.0	0.42	1.16	Fair
Altak 59-50	1:4	4.5	0.36	0.60	Fair
NeoCryl 601A and Aerospray 70	1:12	9.0	0.26	0.42	Good
Terra Krete and Aerospray[b]	1:19	9.0	0.20	0.74	Good

Notes: 1 L/m^2 = 0.264 gal/yd^2; 1 kg/m^2 = 2.2 lb/yd^2; 1 m^2 = 10 ft^2.
Excellent = no surface or internal erosion, flexible surface; very small reduction in permeability.
Good = no surface erosion, hard surface, significant reduction in permeability.
Fair = no surface erosion and significant reduction in permeability, but internal erosion is possible; or polymer is difficult to apply.
[a]Spray treatment for 38-mm (1.5-in) layer of soil.
[b](1:1) by volume.

Table 3. Permeability of spray-treated surface.

Name	Permeability of Soil (cm/s)	
	Before Spray Treatment	After Spray Treatment
Petroset SB	2.0×10^{-3}	1.3×10^{-3}
Aerospray 70	2.0×10^{-3}	3.1×10^{-4}
Terra Krete	2.0×10^{-3}	5.5×10^{-4}
NeoCryl 601A	2.0×10^{-3}	4.8×10^{-4}
Rhoplex H-8	2.0×10^{-3}	3.2×10^{-4}

evaluate pliability and brittleness (soaked films were dried before flexure).

The optimum proportion of water to polymer in a solution to be used for spray applications and the minimum amount of solution needed to provide a nonerosive surface were determined by trial and error for each polymer. A fixed quantity of the polymer was mixed with varying amounts of water for the trials, and each batch was sprayed onto a sample of the soil. The samples were allowed to dry and were then cut into a few pieces to permit the depth of penetration to be observed. In early trials, dye was used to facilitate this observation, but since the filtering effect of the fine granular soils permitted the dye to penetrate farther than it did in the polymer, this procedure was abandoned. The effective penetration depth was finally taken as the thickness of the surface layer that remained intact after the samples had been gently tapped. The optimum dilution for the polymer was considered (perhaps somewhat arbitrarily) to be that which provided a 38-mm (1.5-in) effective depth of penetration. If the solution was too dilute, greater penetration was obtained, but the treated layer was too weak to survive the tapping test. If the dilution was less than optimum, the intact layer was less than 38 mm in thickness, although it was stronger than that corresponding to the optimum dilution. The thinner but stronger surface layer was rejected as unacceptable because its permeability was too low and because the risk of internal erosion of the soil below it, with consequent loss of support for the treated layer, was deemed too great.

RESULTS

For the soils and polymers used in this study, the quantity of polymer required to prevent wind erosion was invariably much less than that required to control water erosion. It was also found that 10 cycles of wetting and drying affected erosion resistance more adversely than did 10 freeze-thaw cycles. Consequently, test results are presented only for those polymeric materials that provided significant resistance to water erosion after 10 wet-dry cycles. Petroset SB, Aerospray 70, Terra Krete, Rhoplex H-8, NeoCryl 601A, Altak 59-50, and two combinations of the foregoing are of that category. The two-polymer combinations were tried with the idea of either suppressing some of the undesirable properties of one polymer with the help of another or reducing the cost of an expensive polymer by incorporating a cheaper one without sacrificing the quality of treatment. The other polymers studied were found to be unsuitable, either because they did not make the soil resistant to erosion or because any benefits gained were lost after the polymers had been soaked in water.

The samples treated with Norlig 41, Orzan GL-50, and Corexit 7730 showed very poor resistance to water erosion and fell apart when immersed in water. Neither Norlig 41 nor Orzan GL-50 formed a film but changed into powder after drying and dissolved immediately when immersed in water. Similarly, Corexit 7730 did not form a dry film after curing but remained in the form of viscous liquid that was easily leached away by water. Only those polymers that formed water-resistant films were found to be suitable for erosion control.

The optimum dilution and minimum quantity of polymer solution required to provide a nonerosive surface for soil II are given in Table 2. It was found that 9 L/m^2 (2 gal/yd^2) is sufficient to provide a treated surface layer 38 mm (1.5 in) thick. The 1977 cost of the material is given in the same table. Although the cheapest treatment is a combination of NeoCryl 601A and Aerospray 70, the quality of treatment is best for Petroset SB, and the reduction in permeability is also the least. Permeability of spray-treated samples is given in Table 3. It may be observed that all the polymers except Petroset SB reduce the permeability quite substantially.

The minimum amount of polymer required to provide a nonerosive surface in premixed samples is given in Table 4. It may be observed that the cost of polymer to provide a nonerosive surface by premixing is two to three times that of spray treatment. Samples for compression tests were prepared through a considerable range of polymer content, and the results of strength tests for soil II are given in Table 4 and in Figure 2. It may be seen that if the object of polymer treatment is to increase compressive strength, considerable success is possible, although heavier treatments of polymer may be required than are necessary for erosion control. Petroset SB, which seems to be ideally suited for erosion control, is not very effective in improving strength.

Thus, polymers that may provide good erosion control do not necessarily provide high strength.

Regarding the water susceptibility of polymer films, it was observed that, with the exception of Petroset SB, Altak 59-50, and (possibly) Terra Krete, the polymer films were adversely affected when soaked in water for 24 h or more (Table 5). Either the film swelled, as in the case of Aerospray 70, or it lost adhesion, as in the case of NeoCryl 601A and Rhoplex H-8. It is concluded that polymers that provide short-term protection from erosion do not necessarily provide long-term protection. Surface characteristics of the spray-treated soil must also be considered. If the surface is very hard and rigid, it would inhibit the growth of vegetation. This could be an undesirable result from an esthetic point of view. For this reason, polymers that form flexible or rubberlike films may be more suitable for erosion control.

The investigation of the effect of environmental factors on these polymers was limited in scope. However, the brief exposure to ultraviolet radiation produced no observed effects on any of the polymers, and those listed in Table 2 were not intolerably damaged by the 10 freeze-thaw cycles or the 10 wet-dry cycles. It is possible--even probable--that more-extensive degradation would occur during extended field conditions. It is believed, however, that the effectiveness of the treatment may be restored from time to time, as may be required, by an additional light application of the polymer. All those in Table 2 exhibited satisfactory adhesion not only to the soil substrate but also to dried films of the same polymer. The susceptibility of these materials to biological degradation was not addressed in this study.

DISCUSSION

There are numerous polymer products available on the market that have the potential to stabilize soils. However, many of these products would be more suitable for use in soil stabilization if the material were modified to some extent. For example, most of the solution-base polymers are initially manufactured by a process called emulsion polymerization. Later, the water is removed from the emulsion and replaced by a solvent. These solution-base polymers are not only less suitable for soil stabilization but are also more expensive. They require special equipment for spraying, pollute the atmosphere, and are a fire hazard in storage. Aqueous-base polymers are less expensive, easier to apply, and generally better soil stabilizers.

Common polymers that are relatively inexpensive and can be manufactured as an emulsion or latex are acrylic polymers, polyurethanes, and copolymers of butadiene-styrene and butadiene-acronitrile. Most of the acrylic polymers and their derivatives are water sensitive and consequently have limited use for soil stabilization. Vinyl polymers are less water sensitive but lack adhesion. It has been ob-

Table 4. Cost of mechanically mixed polymer-treated surface.

Name	Solid Polymer for Nonerosive Surface (%)	Compressive Strength (N/m^2) Dry	Soaked	1977 Cost of 38-mm Treated Layer ($)
Petroset SB	1.92	0.062×10^6	0.0275×10^6	1.32
Aerospray 70	1.20	3.792×10^6	0.165×10^6	0.64
Terra Krete	0.72	2.447×10^6	0.1723×10^6	1.60
NeoCryl 601A	1.44	2.758×10^6	0.1722×10^6	1.27
Rhoplex H-8	1.57	3.310×10^6	0.075×10^6	0.97

Note: 1 N/m^2 = 0.224 lbf/yd^2; 1 mm = 0.04 in.

Figure 2. Effect of polymer content on unconfined compressive strength of soil in dry and soaked conditions.

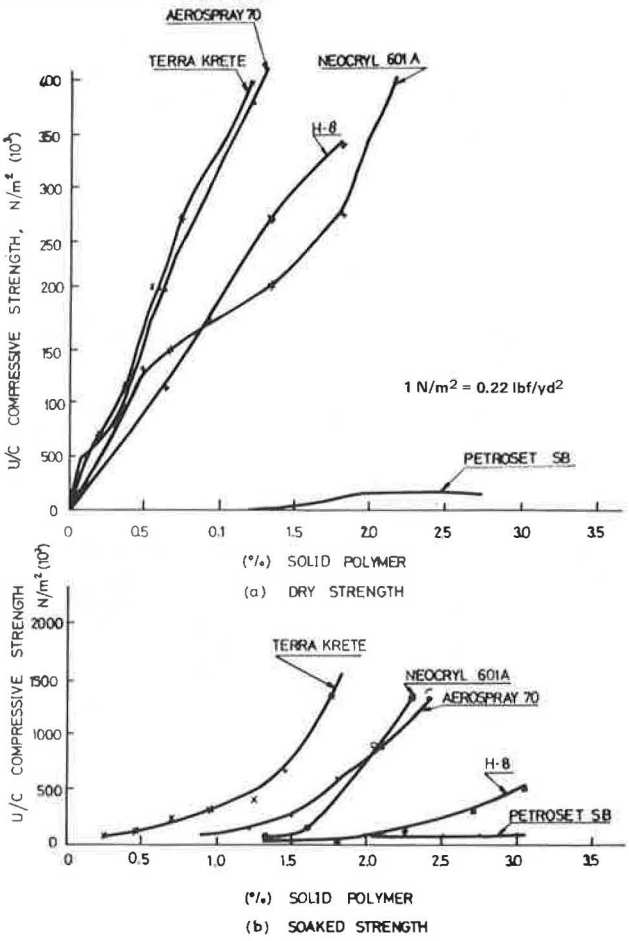

Table 5. Adhesive properties of polymer films.

Name	Adhesion to Glass: Before Soaking	After 24 h of Soaking	After 36 h of Soaking	After Redrying
Petroset SB	Good	Good adhesion, no swelling	Good adhesion, no swelling	Good
Aerospray 70	Good	Weak adhesion, swelling	No adhesion, slight swelling	Good
Terra Krete	Good	Good adhesion, no swelling	Weak adhesion, no swelling	Good
NeoCryl 601A	Good	Poor adhesion, no swelling	Poor adhesion, slight swelling	Weak
Rhoplex H-8	Good	Weak adhesion, swelling	Poor adhesion, high swelling	Weak
Altak 59-50	Good	Good adhesion, no swelling	Good adhesion, no swelling	Good
NeoCryl 601A and Aerospray 70	Good	Good adhesion, no swelling	Weak adhesion, no swelling	Good
Aerospray 70 and Terra Krete	Good	Poor adhesion, no swelling	Weak adhesion, no swelling	Good
Latex XP-4026	Poor	Poor adhesion, no swelling	Poor adhesion, slight swelling	Poor

served that lack of adhesion is a major deficiency in a polymer that is to be used for soil stabilization. Adhesion between polymer molecules and a polar substrate such as the quartz surfaces of most sandy noncohesive soils depends, among other things, on the flexibility and polarity of the polymer molecules. Water, a polar material, spreads on quartz surfaces very quickly. Similarly, natural rubber, which has very flexible molecules, is a very good adhesive. Thus a polymer that is relatively flexible, like an elastomer, and is also polar has good properties for stabilization for erosion control. Due to the polarity of molecules, there will be a strong electrical force between them and the polar substrate. This will give rise to strong adhesion. In addition, if the molecules are flexible, a large area of contact and better adsorption will result. This will increase the van der Waals forces, which in turn will improve adhesion. Flexibility in a polymer can be increased by incorporating a suitable plasticizer. Similarly, polarity can be induced or increased by combining an acid group in the polymer molecule. These functional groups can be incorporated, even after polymerization, by treating the polymer with carboxylic acid, alcohol, or amine. The resulting modifications are indicated below:

$$\text{Polymer} + \text{RCOOH} \rightarrow \text{Polymer}\begin{array}{c}\\ \text{OH}\end{array}\!\!-\!\!\text{OCOR}$$

$$\text{Polymer} + \text{ROH} \rightarrow \text{Polymer}\begin{array}{c}\\ \text{OH}\end{array}\!\!-\!\!\text{OR}$$

$$\text{Polymer} + \text{RNH2} \rightarrow \text{Polymer}\begin{array}{c}\\ \text{OH}\end{array}\!\!-\!\!\text{NHR}$$

The main disadvantage to adding an acid group is that it makes the polymer more sensitive to the effects of water.

Most of the elastomers, such as butadiene-styrene and butadiene-acronitrile, have quite flexible molecules and consequently are good adhesives. These copolymers are also less water sensitive. If such copolymers can be made polar, their adhesive and cohesive strength can be further increased. The most common acid group that can make these elastomers more polar is the carboxylic group (COOH). By incorporating this group into an elastomer, a strong and good adhesive polymer can be produced. The amount of carboxylic group in the elastomer will affect the overall properties of the polymer. It has been reported (8) that the addition of up to 20 percent of an acid group in an elastomer increases both the adhesion and the cohesive strength of the polymer because of the increased intermolecular and intramolecular forces. When the acid group exceeds 20 percent, the polymer becomes rigid and its adhesive properties decrease. Moreover, it becomes somewhat water sensitive. Thus, for controlling the erosion of noncohesive sandy and silty materials, a carboxylated elastomer of butadiene-styrene or butadiene-acronitrile in the form of latex or emulsion, which is dilutable in water, would be a promising polymer.

ACKNOWLEDGMENT

Thanks are extended to the Research and Development Division of the Oklahoma Department of Transportation for the financial assistance for the project. Thanks are also extended to the Department of Civil Engineering, Oklahoma State University, for providing research facilities. Thanks are also due the chemical manufacturers and suppliers for their fine cooperation.

REFERENCES

1. F.J. Blavia and D.E. Law. Materials for Stabilizing the Surface Clods of Cropped Soil. Proc., Soil Society of America, Vol. 35, 1979.
2. W.W. Emerson. Synthetic Soil Conditions. Journal of Agricultural Science, Vol. 47, 1947.
3. T.W. Lambe. The Effect of Polymers on Soil Properties. Proc., Third International Conference on Soil Mechanics and Foundation Engineering, Vol. 1, 1953, pp. 253-255.
4. N.R. Morrison and V.L. Kuehn. Laboratory Evaluation of Petrochemicals for Erosion Control. U.S. Government Memoranda, Denver, CO, June 12, 1973; May 31, 1974; and April 9, 1976.
5. H.A. Sultan. Soil Erosion and Dust Control on Arizona Highways, Part 2. Arizona Department of Transportation, Phoenix, Rept. ADOT-RS-141-I, 1979.
6. S.D. Voronkevich. Use of Modified Polyvinyl Alcohol for Reinforcement of Clayey Soils. Soviet Plastics, No. 7, 1973.
7. R.A. Siddiqi. Cost, Effectiveness, and Utility of Polymer Soil Stabilizers. Oklahoma State Univ., Stillwater, Ph.D. dissertation, July 1978.
8. L. Holliday. Ionic Polymers. Wiley, New York, 1975.

Publication of this paper sponsored by Committee on Chemical Stabilization of Soil and Rock.

Pore-Size Distribution and Its Relation to Durability and Strength of Shales

M. SURENDRA, C.W. LOVELL, AND L.E. WOOD

Shale durability is measured by resistance to slaking in a standard laboratory test. All slaking mechanisms (namely, air-pressure breakage, differential swelling, and dissolution of cementing agents) require that water penetrate the pore space of the shale pieces. Since it is now possible to measure the magnitude and size distribution of these pores by mercury intrusion, correlation of slaking and pore-size distribution is feasible. Testing of slake durability, pore-size distribution, and point-load strength was undertaken on eight Indiana shales of varying durability and strength. It is proposed that the shales be classified as to performance in compacted embankments by slake-durability and point-load-strength indices and that either index can be estimated from parameters of the pore-size distribution. Parameters from the pore-size distribution study (namely, cumulative porosity, median diameter, and spread

factor) were correlated with the slake durability and the point-load strength by linear regression. These Indiana shales were then classified into performance categories based on durability and strength values predicted from the measured pore-size parameters. Thus, the pore-size measurements appear to have both conceptual and practical value with respect to the design and construction of compacted shale embankments.

Use of excavated shale from cuts and borrow areas in Indiana for compacted embankments as a rock fill [in lift thicknesses of about 1 m (3 ft)] has led to various problems, namely, excessive settlement and slope failures. This initiated an extensive research program at Purdue University through the Joint Highway Research Project to study the behavior of Indiana shales. Deo (1) proposed a classification system that is currently being used by the Indiana State Highway Commission (ISHC). Chapman (2) investigated additional laboratory classification tests. Bailey (3) and Hale (4) investigated the factors relating to degradation of shales during the compaction process, and van Zyl (5) prepared a statistical analysis of the data provided by ISHC for the shales tested in their laboratory. Abeyesekera (6) investigated the stress-deformation and strength characteristics of compacted New Providence shale, and Witsman (7) investigated the effect of compacted prestress on compressibility of compacted New Providence shale. Surendra (8) investigated the potential for stabilizing compacted shales by using salts and lime. He also measured pore-size distributions of shale aggregates and developed statistical relationships among pore-size distribution parameters, slake durability, and point-load strength (PLS). The latter relationships suggest a new engineering classification for midwestern U.S. shales for use in compacted embankments.

LITERATURE REVIEW

Slaking Tests

Slaking is defined in the dictionary of geological terms (9) as follows: "Loosely, the crumbling and disintegration of earth materials when exposed to air or moisture. More specifically, the breaking up of dried clay when saturated with water, due either to compression of entrapped air by inwardly migrating capillary water, or to the progressive swelling and sloughing off of the outer layers." Slaking is measured in the laboratory by the percentage of weight retained or lost through a given sieve as a result of soaking the specimen in water. A number of tests following this concept have been developed by various investigators. A description of some of these slaking tests has been presented by Surendra (8).

Slaking Mechanisms

Terzaghi and Peck (10, p. 146) attributed the slaking phenomenon to the compression of entrapped air in the pores as water entered these pores. This air entrapped in the pores exerts tension on the solid skeleton, which causes the material to fail in tension. The behavior can be recognized in the case of soil aggregates and poorly cemented (i.e., compacted) shales and mudstones. Moriwaki (11) found that slaking of compacted kaolinite can be attributed to this mechanism. There have been cases (12;13, pp. 1-14) in which this mechanism did not satisfactorily explain the observation.

Clay surface hydration by ion adsorption has been suggested as the second mechanism that causes slaking through swelling of illite, chlorite, and montmorillonitic clays (14). Differential swelling due to hydration or osmotic swelling is reported to be the main cause of slaking in expansive materials (11). Tschebotarioff (15, p. 102) defines slaking as a surface phenomenon in the following way: "...the clay layer at the exposed surface swells first and therefore expands more than the adjoining inner layers; the induced relative displacements are liable to detach the surface layer and cause it to disintegrate and slough away. The process can then be repeated and gradually progress from the surface inward."

Removal of cementing agents in the case of shales, siltstones, and mudstones by the dissolving action of the moving groundwater is considered to be the third mechanism that causes slaking (11,12). The pH of the percolating groundwater and the presence of oxygen, carbon dioxide, and other minerals in the shales control the slaking due to this mechanism.

No single mechanism can be considered the dominant cause for slaking of shales. A combination of the above-mentioned mechanisms is most likely, either by one triggering the other or by each occurring independently. The composition and the environment in which the shale is placed determine the principal mechanism that causes the failure.

Shale Classification

Earlier classification systems were based on visual observation of physical features, namely, fissility and breaking characteristics of shales in situ and of hand specimens in the laboratory (16-18). The more-recent classification systems take into consideration the results from durability tests and observed field behavior (1,18-22). These classification systems may also employ test results in the form of Atterberg limits, pH's, rate of slaking values, and PLS. A classification system proposed by Morgenstern and Eigenbrod (23) used the unconfined compressive strength of soaked specimens. A discussion of these classification systems has been presented by Surendra (8). A summary of these classification systems and their tests is presented in Table 1.

The principal features needed in a shale-classification system are (a) a measure of durability (i.e., resistance to environmentally induced slaking cycle during service) and (b) a measure of strength or hardness (i.e., resistance to construction degradation in the field, which determines the ease with which it can be placed in an embankment).

Classification systems thus developed use measured properties in the laboratory to predict field behavior. The slake-durability test is normally used to distinguish durable and nondurable shales. Additional tests for durability are sometimes necessary (20,22,24). Visual observation of the material at the end of the slake-durability test is also useful (2,20). ISHC uses the classification system developed by Deo (1).

Indiana shales may be placed in three categories, namely, hard and durable, hard and nondurable, and soft and nondurable, as shown in Figure 1 (8). In Figure 1, the durability is rated from the slake-durability test and the hardness from the PLS test. It can be seen that increasing durability is generally associated with increased PLS. The properties of shales represented in Figure 1 are given in Table 2.

In the slake-durability test, the specimens (discrete pieces of shale) are subjected to a joint effect of abrasion caused by the tumbling action of the rotating drum and softening by water. The shale may be cycled in this test by removing the retained material from the drum, oven-drying it, and rein-

Table 1. Summary of classification tests.

Classification System	Test			
	Durability	Strength	Other	Comments
Gamble (18)	200-revolution, two-cycle slake-durability test	–	Atterberg limits (I_p)	
Deo (1)	500-revolution, one-cycle, wet and dry slake-durability test; slaking test; modified soundness test	–	–	
Morgenstern and Eigenbrod (23)	–	Unconfined compressive strength test	–	Loss of strength on soaking
Hudec (19)	200-revolution, five-cycle slake-durability test	–	–	
Strohm, Bragg, and Zeigler (20)	200-revolution, two-cycle slake-durability test; slaking test; rate-of-slaking test	–	pH; Atterberg limits (I_p)	Visual observation of fragmented material in slake-durability test
Andrews and others (21)	200-revolution, two-cycle slake-durability test	–	pH; cationic exchange capacity (CEC)	Preliminary classification based on pH and CEC determines need for any durability test
Franklin (22)	200-revolution, two-cycle slake-durability test (Id_2)	PLS	Atterberg limits (I_p)	For $Id_2 > 80$, PLS is needed; for $Id_2 < 80$, I_p is needed

Figure 1. Variation of PLS with slake-durability index.

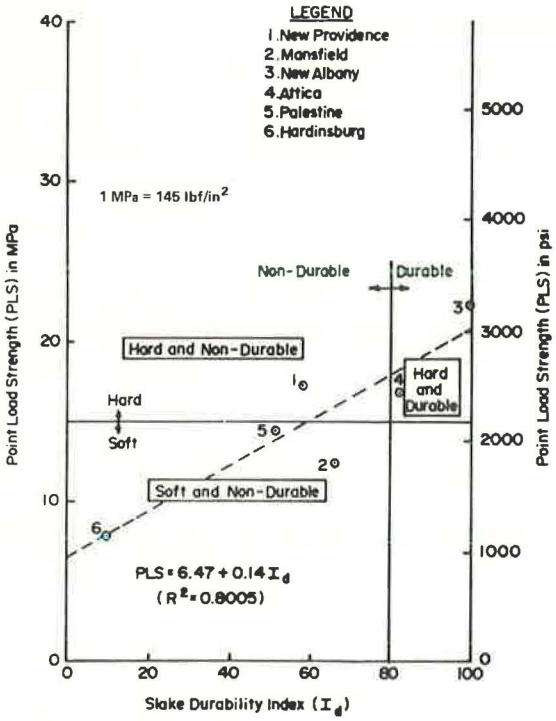

Table 2. Properties of shales shown in Figure 1.

Shale	Slake-Durability Index I_d	PLS (MPa)	Plasticity Index I_p
New Providence	58.0	17.25	11
Mansfield	66.0	12.4	10.6
New Albany	99.1	22.3	5.6
Attica	82.1[a]	16.8	5
Palestine	51.7	14.5	5.2
Lower Hardinsburg	9.8	8.30	15

Note: 1 MPa = 145 lbf/in^2.
[a]Second-cycle slake-durability index was estimated [from Abeyesekera and Lovell (25)].

serting it in the drum. The breakdown is increased by increasing the number of cycles, as shown in Figure 2 [data from thesis by Gamble (18)]. Drying the sample prior to the slake-durability test does increase the degradation. Varying reasons for this are supplied by Nakano (13) and by Bailey (3). Degradation is also a function of the number of revolutions of the drum as shown in Figure 3 (data from ISHC).

LABORATORY TESTING

Materials

Table 3 gives a brief description of all the shales studied and the investigation during which these shales were sampled. The slake-durability, PLS, and plasticity-index values were given in Table 2 for six of the shales studied.

Slake-Durability Test

The slake-durability index was determined according to the procedure of the International Society for Rock Mechanics (26, pp. 32-36). The slake-durability apparatus, developed by Franklin (27), consists of a drum that has a screen opening of 2 mm (0.08 in) (no. 10 sieve). The drum is rotated by an electric motor in a bath of slaking fluid (usually water) at a constant rate (20 rpm). The slaking samples consist of 10 equidimensional pieces of shale that each weigh about 50 g (1.5 oz) and are oven dried at 110 ± 5°C (225 ± 10°F), cooled to room temperature, and placed in the drum of the apparatus. The drum is immersed in the tub that contains the slaking fluid and is rotated for 200 revolutions. At the end of the test, the material retained in the drum is oven dried and weighed. The retained material is then subjected to another cycle of slaking in the rotating drum. The slake-durability index (Id_2) is calculated at the end of the second cycle as follows:

Id_2 = [(oven-dried weight of material retained at end of second cycle)/(oven-dried weight of sample before test)] x 100.

At least four tests were run for each shale, and average values are reported. The slake-durability indices presented in Table 4 are the average of six tests.

Figure 2. Influence of number of cycles on slake-durability index.

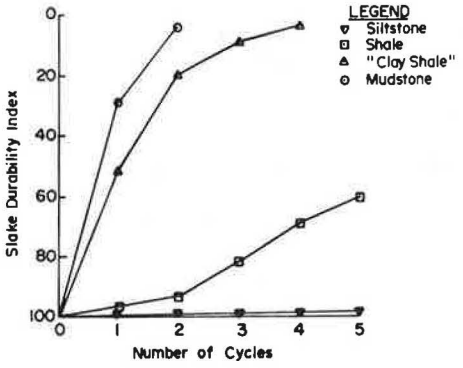

Figure 3. Influence of number of revolutions of drum on slake-durability index.

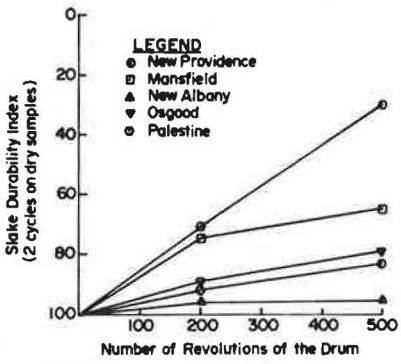

Table 3. Description of shales studied.

ISHC Laboratory No.	Shale	Deo's Classification (1)	Physical Nature	Study
75-55731	New Providence	Soil-like	Hard and nondurable	Abeyesekera (6)
79-55198				Hale (4)
74-54684	Mansfield	Soil-like	Soft and nondurable	Chapman (2)
74-54621	New Albany	Rocklike	Hard and durable	Chapman (2)
79-55199	Osgood	Soil-like	Hard and nondurable	Hale (4)
75-55564	Attica	Soil-like	Hard and nondurable	Bailey (3)
74-54716	Palestine	Soil-like	Soft and nondurable	Chapman (2)
79-55204				Hale (4)
73-51703	Lower Hardinsburg	Soil-like	Soft and nondurable	Chapman (2)
75-55315	Klondike	Rocklike	Hard and durable	Chapman (2)

Table 4. Durability and PLS properties.

Shale	Slaking Index (SI)	Slake-Durability Index (Id_2)	Deo's Classification (1)	PLS (MPa)
New Providence	50.81	58	Soil-like	16.18
Mansfield	40.78	66	Soil-like	9.32
New Albany	0.14	99.1	Rocklike	23.68

Note: 1 MPa = 145 lbf/in^2.

PLS Test

A diagram of the PLS test apparatus is shown in Figure 4 [data from reports by Bailey (3)]. The load was applied by an electrically driven compression-testing machine at a constant rate of deformation of 0.254 mm/min (0.01 in/min). The load was monitored through a 22.24-kN (5000-lbf) capacity, SR4-type load cell. The initial dial gage reading indicates the height of the guide plate, and from this the sample thickness (D) can be obtained. The sample of shale consisted of platy pieces approximately equidimensional for the plan area. The sample was loaded perpendicular to the bedding planes and the initial sample thickness of the shales tested varied from 2.56 to 13.41 mm (0.10-0.53 in). The samples were oven dried to constant weight at 110 ± 5°C and cooled to room temperature before testing (i.e., all the samples were tested at near-zero moisture content). The PLS index was computed by taking the ratio of maximum compressive load (P) to the square of the initial sample thickness (D). Table 4 presents the PLS of the New Providence, the Mansfield, and the New Albany shale samples; these are averages of several tests.

Pore-Size Distribution

The procedure used in this test, the assumptions made in the study, and the appropriate precautions and corrections have been described by Surendra (8). The determination of pore-size distribution is described briefly below.

Figure 4. Side view of PLS test apparatus.

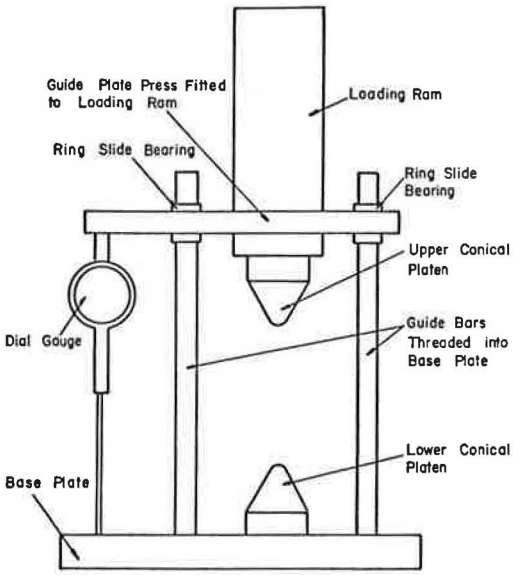

The oven-dried sample of shale (sometimes consisting of two to three discrete pieces) is initially evacuated and surrounded by mercury, the pressure is raised in small increments, and the volume of mercury that enters the sample after each increment is recorded. With each pressure increment, the mercury is forced into the accessible pores in the sample of a diameter larger than or

Figure 5. Differential and cumulative pore-size distribution for Mansfield, New Providence, and New Albany shales.

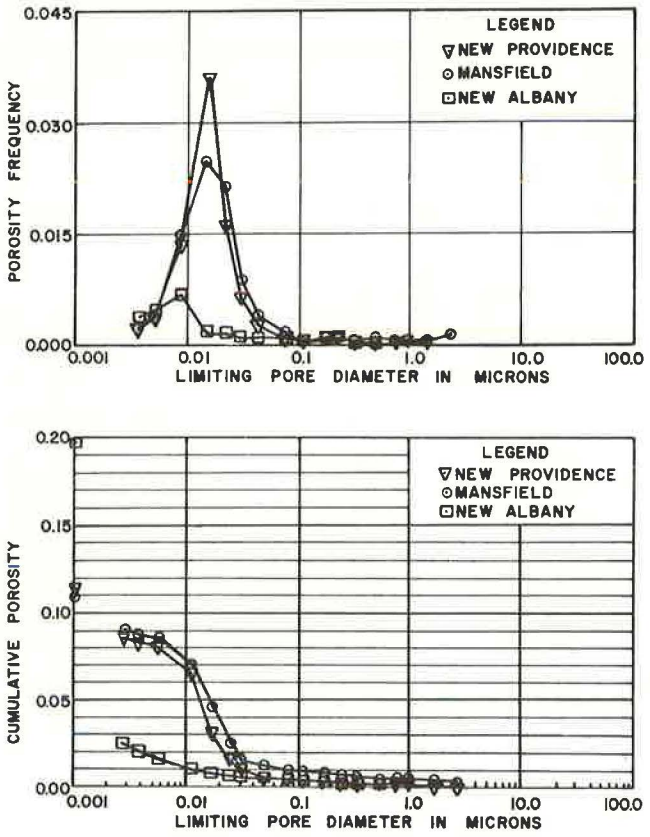

Table 5. Pore-size parameters for shales studied.

Shale	1 ÷ Cumulative Porosity	1 ÷ Median Diameter (μm)	Spread Factor
New Providence	11.83	71.43	2.00
	11.30	71.43	2.14
Mansfield	11.09	62.5	1.56
	11.16	52.63	1.42
New Albany	52.55	114.94	2.64
	55.09	100.00	3.00
Osgood	14.86	50.00	10.25
	14.94	83.33	2.58
Attica	9.29	37.04	1.52
	9.06	38.46	1.54
Palestine	8.12	3.57	2.93
	5.57	8.33	4.00
Lower Hardinsburg	12.67	125.00	1.75
	12.41	108.70	1.96
Klondike	7.69	22.20	1.78
	6.33	27.03	2.38

equal to that calculated by the Washburn (28) equation:

$$P = (4\,T_s \cos\theta)/d \qquad (1)$$

where

P = absolute pressure required for intrusion,
T_s = surface tension of intruding liquid,
θ = contact angle between solid and liquid, and
d = limiting pore diameter.

The volume of pore space between pressure increments is recorded, and from this the limiting pore diameter is computed and the pore-size distribution is generated. The pore-size distribution is presented in the form of differential-distribution and cumulative-distribution curves for this study. Figure 5 provides these curves for the three shales given in Table 4.

Figure 6. Estimated slake-durability index (Id_2) from pore-size parameters versus measured values.

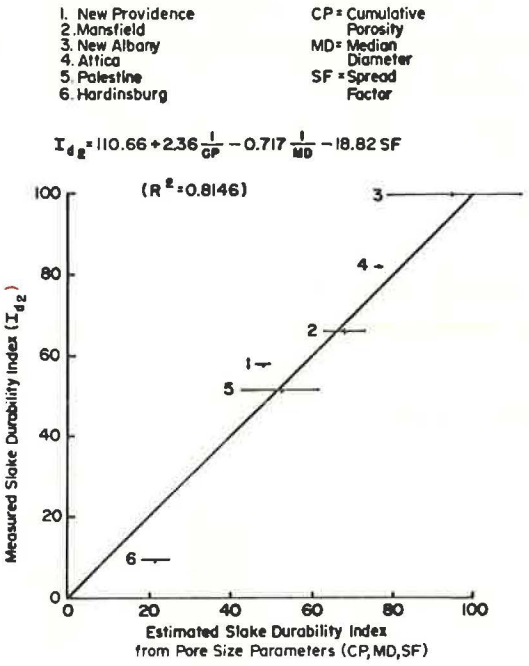

RESULTS AND DISCUSSION

Pore-Size Distribution

Pore-size studies were made on eight Indiana shales (Table 3) as described in detail by Surendra (8). The intrusion constant (Equation 1) used in this study was taken from Kaneuji (29) to be 160 (measured in microns times pounds force per square inch) or 1103.2 (measured in microns times kilonewtons per square meter). The same value was used for all the shales. Two tests were run on each shale. The parameters from these distributions used for correlation with the slake-durability index were as follows:

1. Cumulative porosity: ratio of intruded pore volume to the volume of the sample,
2. Median diameter: diameter of the pore corresponding to the 50th-percentile value of the intruded volume, and
3. Spread factor: ratio of pore diameter corresponding to the 25th-percentile value of the intruded volume to the median diameter.

The above parameters from the cumulative pore-size distribution curves for the shales studied are given in Table 5. The three parameters from the pore-size distribution study (except those for the Osgood and the Klondike shales) were successfully used in a linear regression to correlate with the slake-durability index, and a value of $R^2 = 0.8146$ was obtained. It can be seen from Figure 6 that the slake-durability index can be estimated with good reliability from the pore-size parameters.

PLS

PLS was determined in the laboratory as described earlier for six Indiana shales. All the samples tested were 6.6 mm (0.26 in) thick; they were oven dried prior to testing. The results of this test on the shale samples investigated are presented below (1 MPa = 145 lbf/in²):

Shale	PLS (MPa)
New Albany	22.30
Mansfield	12.40
New Providence	17.25
Attica	16.80
Palestine	14.50
Lower Hardinsburg	8.30

Figure 7. Estimated slake-durability index from pore-size parameters versus PLS index.

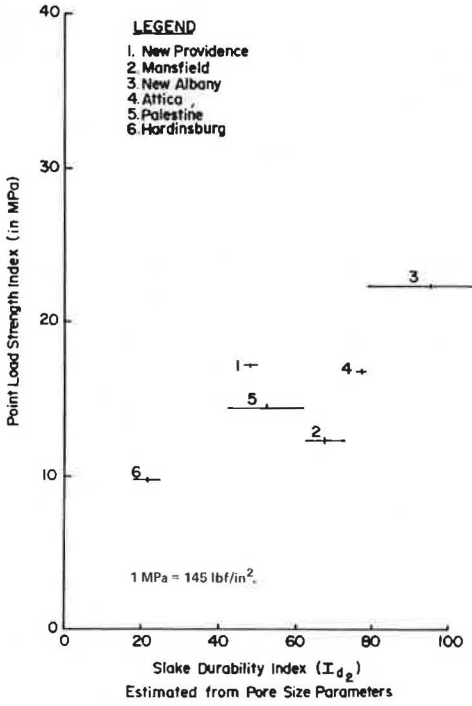

Figure 8. Estimated PLS index from pore-size parameters versus measured PLS index.

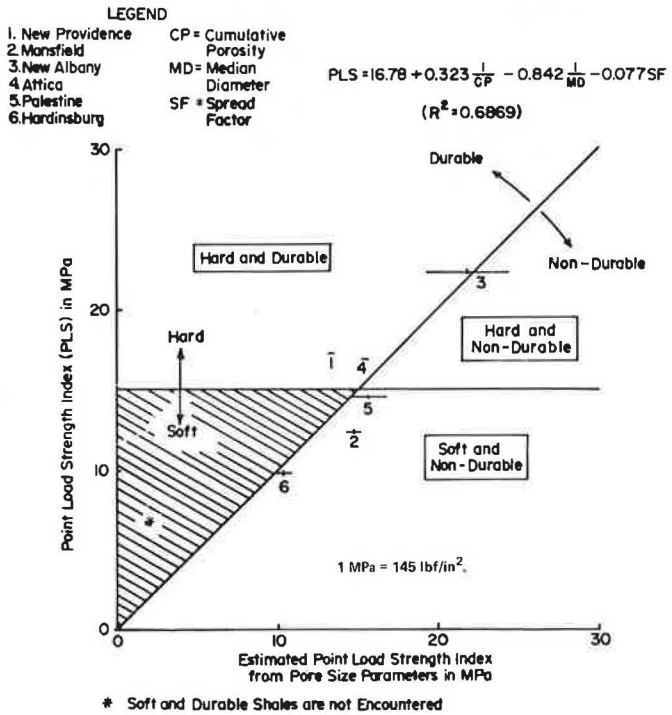

SUMMARY--NEW SHALE CLASSIFICATION

Parameters from the pore-size distribution study--namely, cumulative porosity, median diameter, and spread factor--were correlated with the slake-durability index by linear regression. The R^2-value for six shales was 0.8146. The results of this regression were presented in Figure 6.

When the predicted slake-durability index was plotted against the PLS index (Figure 7), it was found that most of the shales plotted in a narrow range of strengths and had varying durabilities. The implication is that durability is more sensitive to pore-size distribution than is strength.

PLS indices are plotted against the measured values in Figure 8. Durable shales plot above the diagonal line and nondurable shales fall below it, except in the case of the New Providence shale. The R^2-value is low, approximately 0.7. An arbitrary strength (indicated by the field behavior) can be selected to designate the shale as hard or soft. In this case, a value of 15 MPa (2175.5 lbf/in²) is used. The results from this classification and those of Deo (1) are given below (we found the New Providence shale to be nondurable since it has a slake-durability index of less than 80 from a two-cycle test):

Shale	This Classification	Deo's Classification
New Providence	Hard and durable	Soil-like
Mansfield	Soft and nondurable	Soil-like
New Albany	Hard and durable	Rocklike
Attica	Hard and durable	Soil-like
Palestine	Soft and nondurable	Soil-like
Lower Hardinsburg	Soft and nondurable	Soil-like

Thus, the parameters from the study of the pore-size distribution of shales--namely, cumulative porosity, median diameter, and spread factor--can be used to predict the durability of these Indiana shales. The pore-size parameters and the PLS index can be used to classify the shales with regard to durability and strength, respectively (Figure 8). Correlation with field performance is of course needed.

ACKNOWLEDGMENT

The financial support for this research was provided by ISHC and the Federal Highway Administration. Special thanks are extended to W.J. Sisiliano, chief soils engineer, and R. Rahn, soils laboratory section head, Division of Materials and Tests, ISHC, for their valuable comments and suggestions throughout this investigation.

REFERENCES

1. P. Deo. Shales as Embankment Materials. Ph.D. thesis and Joint Highway Res. Project Rept. 45, Purdue Univ., West Lafayette, IN, Dec. 1972, 202 pp.

2. D.R. Chapman. Shale Classification Tests and Systems: A Comparative Study. M.S. thesis and Joint Highway Res. Project Rept. 75-11, Purdue Univ., West Lafayette, IN, June 1975, 90 pp.
3. M.J. Bailey. Shale Degradation and Other Parameters Related to the Construction of Compacted Embankments. M.S. thesis and Joint Highway Res. Project Rept. 76-23, Purdue Univ., West Lafayette, IN, Aug. 1976, 208 pp.
4. B.C. Hale. The Development and Application of a Standard Compaction-Degradation Test for Shales. M.S. thesis and Joint Highway Res. Project Rept. 79-21, Purdue Univ., West Lafayette, IN, Dec. 1979, 180 pp.
5. D.J.A. van Zyl. Storage, Retrieval, and Statistical Analysis of Indiana Shale Data. Joint Highway Res. Project Rept. 77-11, Purdue Univ., West Lafayette, IN, July 1977, 140 pp.
6. R.A. Abeyesekera. Stress-Deformation and Strength Characteristics of a Compacted Shale. Ph.D. thesis and Joint Highway Res. Project Rept. 77-24, Purdue Univ., West Lafayette, IN, May 1978, 417 pp.
7. G.R. Witsman. The Effect of Compaction Prestress on Compacted Shale Compressibility. M.S. thesis and Joint Highway Res. Project Rept. 79-16, Purdue Univ., West Lafayette, IN, Sept. 1979, 181 pp.
8. M. Surendra. Additives to Control Slaking in Compacted Shales. Ph.D. thesis and Joint Highway Res. Project Rept. 80-6, Purdue Univ., West Lafayette, IN, May 1980, 304 pp.
9. American Geological Institute. Dictionary of Geological Terms. Doubleday, New York, 1976, p. 394.
10. K. Terzaghi and R.B. Peck. Soil Mechanics in Engineering Practice, 2nd ed. Wiley, New York, 1967.
11. Y. Moriwaki. Causes of Slaking in Argillaceous Materials. Ph.D. thesis, Univ. of California at Berkeley, Jan. 1975, 291 pp.
12. C.W. Badger, A.D. Cummings, and R.L. Whitmore. The Disintegration of Shales in Water. Journal of the Institute of Fuel, Vol. 29, 1956, pp. 417-423.
13. R. Nakano. On Weathering and Change of Properties of Tertiary Mudstones Related to Landslide. Soils and Foundations, Vol. 7, 1967, pp. 1-14.
14. M.E. Chenevert. Shale Alteration by Water Adsorption. Journal of Petroleum Technology, Sept. 1970, pp. 1141-1148.
15. G.P. Tschebotarioff. Soil Mechanics Foundations and Earth Structures. McGraw-Hill, New York, 1951.
16. W.H. Twenhofel. Report of the Committee on Sedimentation. National Research Council, Washington, DC, 1973, 193 pp.
17. L.B. Underwood. Classification and Identification of Shales. Journal of the Soil Mechanics and Foundations Division of ASCE, Vol. 93, No. SM6, Nov. 1967, pp. 97-116.
18. J.C. Gamble. Durability-Plasticity Classification of Shales and Other Argillaceous Rocks. Ph.D. thesis, Univ. of Illinois at Urbana-Champaign, 1971, 161 pp.
19. P.P. Hudec. Development of Durability Tests for Shales in Embankments and Swamp Backfills. Ontario Ministry of Transportation and Communications, Downsview, Ontario, Canada, April 1978, 51 pp.
20. W.E. Strohm, Jr., G.H. Bragg, Jr., and T.W. Zeigler. Design and Construction of Compacted Shale Embankments, Vol. 5: Technical Guidelines. FHWA, U.S. Department of Transportation, Rept. FHWA-RD-78-141, 1978, 207 pp.
21. D.E. Andrews, J.L. Withiam, E.F. Perry, and H.L. Crouse. Environmental Effects of Slaking of Surface Mine Spoils--Eastern and Central United States. Bureau of Mines, U.S. Department of the Interior, Draft Rept., Nov. 1979, 219 pp.
22. J.A. Franklin. Field Evaluation of Shales for Construction Projects. Ministry of Transportation and Communications, Downsview, Ontario, Canada, Res. and Development Project 1404, Final Rept., Phase II Study, March 1979, 29 pp.
23. N.R. Morgenstern and K.D. Eigenbrod. Classification of Argillaceous Soils and Rocks. Journal of the Geotechnical Engineering Division of ASCE, Vol. 100, No. GT10, Proc. Paper 10885, Oct. 1974, pp. 1137-1156.
24. D.F. Noble. Accelerated Weathering of Tough Shales. Virginia Highway and Transportation Research Council, Charlottesville, Final Rept. VHTRC 78-R20, Oct. 1977, 38 pp.
25. R.A. Abeyesekera and C.W. Lovell. Characterization of Shales by Plasticity Index, Point Load Strength, and Slake Durability. Presented at 31st Annual Highway Geology Symposium, Univ. of Texas at Austin, Aug. 13-15, 1980.
26. Committee on Laboratory Tests. Document 2, Part 2. International Society for Rock Mechanics, Pretoria, South Africa, Nov. 1972.
27. J.A. Franklin. Classification of Rock According to Its Mechanical Properties. Ph.D. thesis, Imperial College, London, England, 1970, 155 pp.
28. E.W. Washburn. Note on a Method of Determining the Distribution of Pore Sizes in a Porous Material. Proc., National Academy of Sciences, Vol. 7, 1921, pp. 115-116.
29. M. Kaneuji. Correlation Between Pore Size Distribution and Freeze Thaw Durability of Coarse Aggregate in Concrete. Ph.D. thesis and Joint Highway Research Project Rept. 78-15, Purdue Univ., West Lafeyette, IN, Aug. 1978, 142 pp.

Publication of this paper sponsored by Committee on Physicochemical Phenomena in Soils.

Eccentrically Loaded Surface Footing on Sand Layer Resting on Rough Rigid Base

BRAJA M. DAS

Laboratory model-test results are given for the ultimate bearing capacity of an eccentrically loaded rough rigid strip surface footing on sand that has a rough rigid base located at a shallow depth. For centrally loaded footing, the modified bearing-capacity factors calculated from the experimental ultimate loads are compared with the existing theory as presented by Mandel and Salencon. When the ratio of the depth of the sand layer to the width of the footing is smaller than 0.6, the experimental bearing capacity is somewhat lower than that predicted by theory by using the direct shear angle of friction. However, if the experimental variation of the bearing-capacity factor for the centrally loaded footing is assumed to be correct, Meyerhof's effective-area method may be used to estimate the bearing capacity of eccentrically loaded footing.

The ultimate bearing capacity of a shallow continuous footing in a homogeneous soil subjected to centric loading is generally expressed by the following equation:

$$q_u = cN_c + qN_q + \tfrac{1}{2}\gamma BN_\gamma \quad (1)$$

where

q_u = ultimate load per unit area of footing,
c = cohesion of soil,
γ = soil unit weight,
B = width of footing, and
N_c, N_q, and N_γ = bearing-capacity factors.

For a footing placed at the surface of a cohesionless soil, $c = 0$ and $q = 0$; hence, Equation 1 will transform to the following form:

$$q_u = \tfrac{1}{2}\gamma BN_\gamma \quad (2)$$

A number of solutions for the variation of the bearing-capacity factor N_γ with the angle of friction of the soil have been proposed in the past by such investigators as Terzaghi (1), Meyerhof (2), Caquot and Kerisel (3), and Lundgren and Mortensen (4).

If a rough rigid continuous surface footing that rests on a sand layer is subjected to a uniformly distributed load of magnitude q_u, bearing-capacity failure will take place, and the slip lines will extend to a depth H_{cr} as shown in Figure 1a. However, if we consider a condition in which a rough rigid base is located at a shallow depth H so that $H < H_{cr}$ (Figure 1b), the development of the slip lines at failure will be somewhat affected. Mandel and Salencon (5) have developed a theoretical solution for the ultimate bearing capacity for such cases, and it can be given by the following equation:

$$q_u = \tfrac{1}{2}\gamma BN'_\gamma \quad (3)$$

where N_γ' is the modified bearing-capacity factor.

According to Mandel and Salencon (5), for $H \geq H_{cr}$ the value of N_γ' becomes equal to N_γ as determined by Lundgren and Mortensen (4). On the other hand, for $H < H_{cr}$ the modified bearing-capacity factor increases with the decrease of H/B. The theoretical variation of N_γ' with H/B is shown in Figure 2 (5,6) for several values of the soil friction angle ϕ.

Experimental studies in the laboratory have been conducted by Meyerhof (6) and by Pfeifle and Das (7) to compare the experimental values of the modified bearing-capacity factor with the theoretical values presented in Figure 2. This study is not a repetition of any previous work by Das (7).

The purpose of this paper is to present some small-scale laboratory model-test results for the ultimate bearing capacity of eccentrically loaded rough rigid surface footings on sand that have a rough rigid base located at a shallow depth as shown in Figure 3 and to evaluate whether the effective-area concept as suggested by Meyerhof (8) can be used in this case. It must be pointed out that Meyerhof's effective-area concept was originally suggested for conditions in which the rough rigid base is located at great depths (i.e., $H/B > H_{cr}/B$). According to the effective-area concept, if a load is applied on a strip footing that has an eccentricity e measured from the center line, it can be assumed to be equivalent to a strip footing of width $B' = B - 2e$ that has the load applied along the center line as shown in Figure 4.

EXPERIMENTAL PROCEDURE

Model tests were conducted in a box that measured 0.915 m x 0.3048 m x 0.457 m (3 ft x 1 ft x 1.5 ft). The walls of the box were reinforced by steel channels against possible yielding during tests. The bottom of the box was a wooden plank 50.8 mm (2 in) thick. In order to make the bottom of the box rough, a sand-glue mixture was spread over a masonite panel. This was allowed to dry for several days and was then attached to the bottom of the box by means of wood screws. The sand used for the sand-glue mixture was the same sand used for the model tests.

Figure 1. Bearing-capacity failure for rough rigid surface footing on sand.

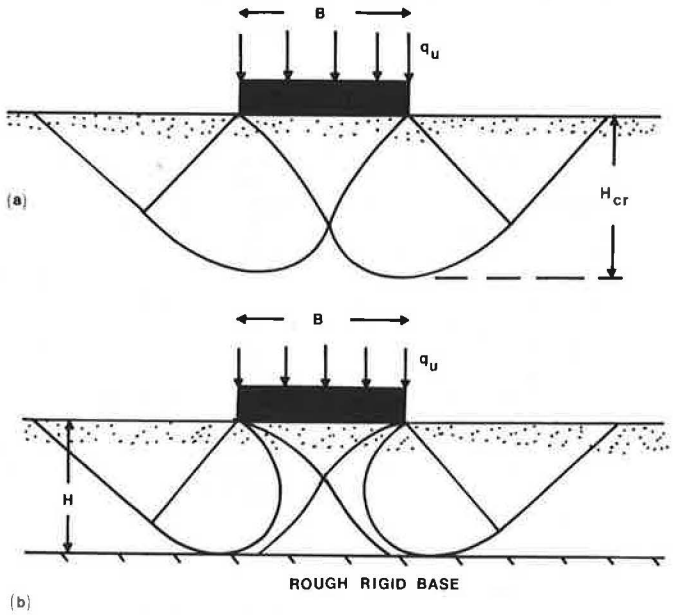

Figure 2. Variation of N_γ' with H/B and ϕ.

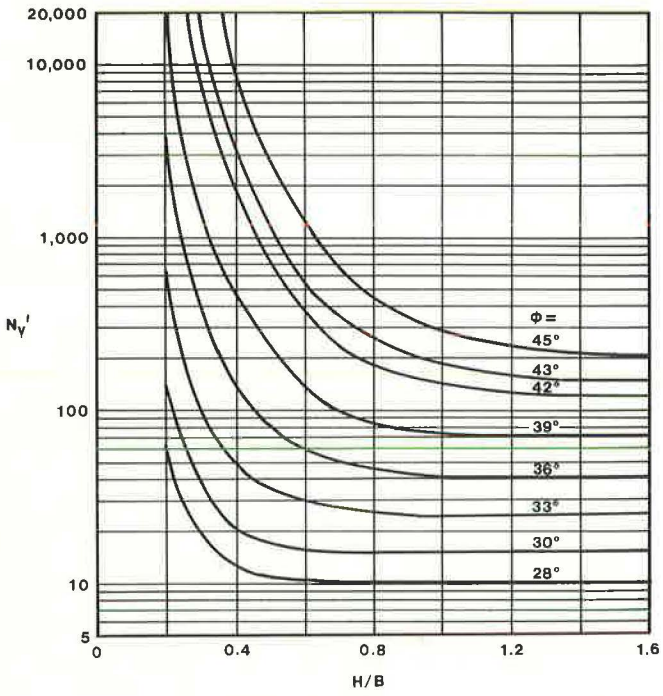

Figure 3. Geometric parameters for bearing-capacity tests with eccentric loading and rough rigid base at shallow depth.

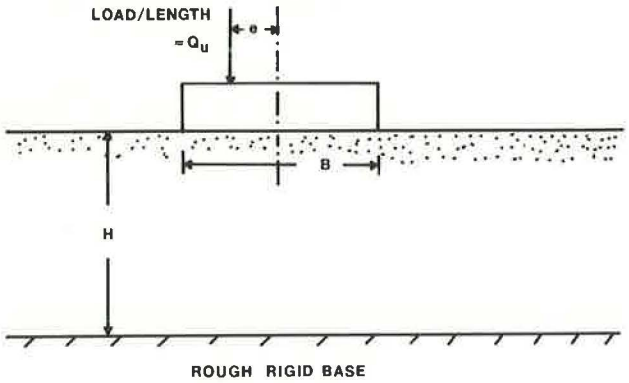

The sand used for the test had 100 percent passing through a no. 10 sieve, 52 percent passing through a no. 40 sieve, and 4 percent passing through a no. 200 sieve. For the model tests, the sand was compacted in small layers in the test box to the required depth to an average unit weight of 16.0 kN/m³ (101.8 lbf/ft³). This yielded an average relative density of compaction of 80 percent. At this compaction, the triaxial angle of friction was determined to be 39° and the direct shear angle of friction was 42°.

The model footing was made of a 12.7-mm (0.5-in) steel plate that measured 101.6 mm x 304.8 mm (4 in x 12 in). The bottom of the model footing was made rough by spreading a similar sand-glue mixture as that used for the bottom of the box and allowing it to dry.

Vertical load was applied to the model footing by a hydraulic jack through a steel shaft 38.1 mm (1.5 in) in diameter. The bottom of the shaft was enlarged and rounded. Semicircular grooves into which

Figure 4. Equivalent-area concept for eccentrically loaded strip footing.

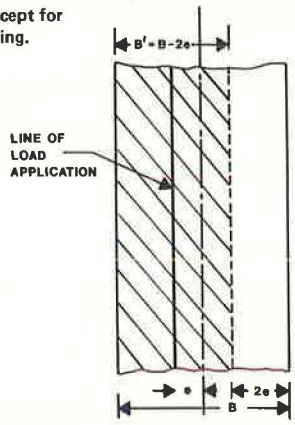

the bottom of the shaft would just fit were cut on the top of the footing. This allowed free rotation of the footing during failure. These grooves were cut parallel to the center line of the footing at distances of e = 0, 12.7 mm (0.5 in), and 19.05 mm (0.75 in). During the model tests, the load was measured by a proving ring. The deflection along the center line of the footing was measured by a dial gauge. Tests were conducted at various values of e/B and H/B. Some grain crushing occurred during the tests at lower values of H/B.

MODEL-TEST RESULTS

Diagrams of typical load per unit length versus settlement of footing for the model footing at H/B = 0.375 determined from the laboratory tests are shown in Figure 5. The ultimate load per unit length of the footing at failure Q_u was determined from these diagrams. Figure 6 shows a plot of Q_u versus H/B for all the tests conducted in this program.

For tests in which the loads on the footing were centrally applied (i.e., e/B = 0), the modified bearing-capacity factor can be given by $Q_u = q_u(B)(1) = 1/2\gamma B^2 N'_\gamma$ (Equation 3), or

$$N'_\gamma = Q_u/(0.5\gamma B^2) \quad (4)$$

By using the experimental values of Q_u (for the tests in which e/B = 0) given in Figure 6, the values of N_γ' were determined and are shown in Figure 7. For comparison purposes, the theoretical values of N_γ' (from Figure 2) for ϕ = 39°, 42°, and 43° have been plotted in Figure 7. A comparison of the experimental and theoretical values shows the following:

1. The experimental values of N_γ' are higher than those presented by theory with ϕ = 39°, which is the triaxial angle of friction. However, for tests of continuous footing, the plane strain friction angle should be used. The experimental results of N_γ' are fairly close to those predicted by using friction angles determined from direct shear tests up to a value of H/B $\geq$ about 0.6. In the region of H/B between 0.6 and 0.4, the experimental values are lower than those of the theory (by using direct shear angle of friction).

2. The experimental values of N_γ' for H/B < 0.4 are lower than those predicted by theory by using the triaxial friction angle of 39°. There can be several factors that would cause the type of experimental results obtained here and their derivations from the theory for the zone of H/B < 0.6. They are as follows: (a) the sand-placement technique makes the sand anisotropic; (b) although a

Figure 5. Typical plot of load per unit length of footing versus settlement.

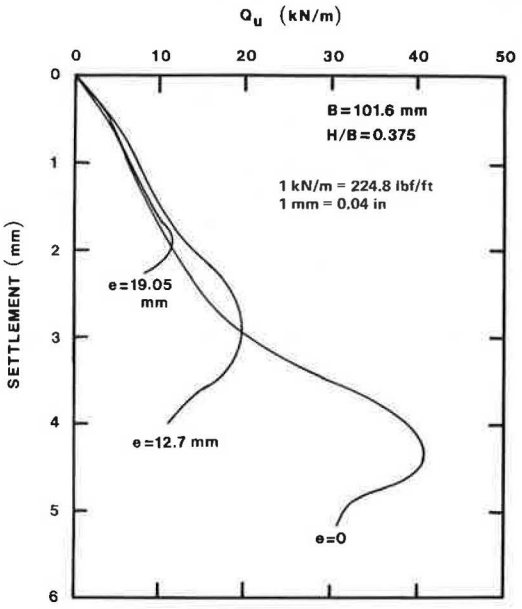

Figure 6. Q_u versus H/B obtained from laboratory tests.

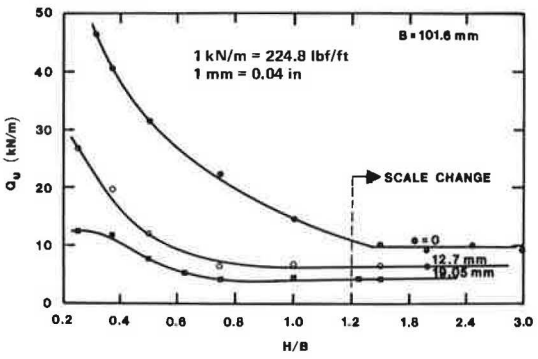

quantitative evaluation was not made, some grain crushing did occur during the tests; and (c) there was curvilinearity of the Mohr-Coulomb failure envelope at very high pressures.

However, an evaluation of the model-test results shows that, if the experimental variation of N_γ' versus H/B is assumed to be correct, the ultimate bearing capacity of the eccentrically loaded footing can be evaluated approximately by using the effective-area concept presented by Meyerhof (8) for footings in which $H/B > H_{cr}/B$. Hence,

$$B' = B - 2e \tag{5}$$

where B' is the effective width.

For surface footings, the ultimate load per unit length can be expressed as follows:

$$Q_u = \tfrac{1}{2}\gamma B' N'_\gamma (B')(1) = \tfrac{1}{2}\gamma B'^2 N'_\gamma$$

$$N'_\gamma = Q_u/(0.5\gamma B'^2) = Q_u/[0.5\gamma(B - 2e)^2] \tag{6}$$

Note that N_γ' is now a function of H/B'. For centrally loaded footings, H/B' = H/B. By using the values of Q_u and e given in Figure 6 and by using Equation 6, the experimental values of N_γ' for all tests have been determined and are shown in

Figure 7. Comparison of experimental N_γ' with theory (e/B = 0).

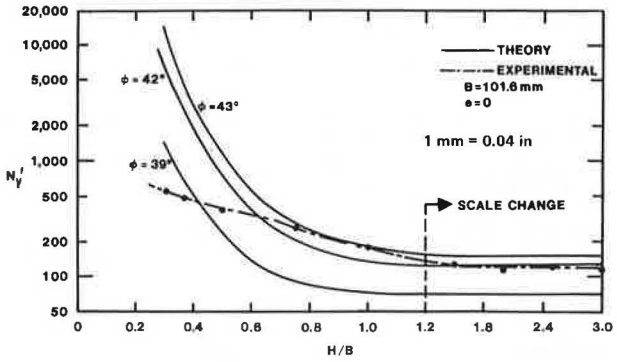

Figure 8. Variation of experimental N_γ' with H/B.

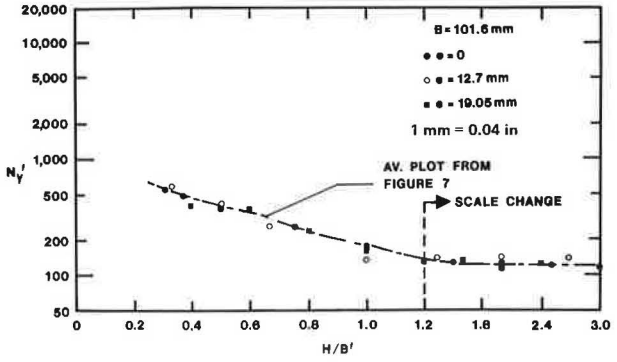

Figure 8. The average experimental plot of N_γ' versus H/B shown in Figure 7 is also replotted in Figure 8 for comparison. It can be seen that, although there is some scattering, the average N_γ' versus H/B' plot is the same for all tests.

CONCLUSIONS

Laboratory model tests have been presented for the ultimate bearing capacity of rough rigid continuous surface footings on sand that have a rough rigid base located at a shallow depth. Based on the model-test results, the following conclusions can be drawn:

1. For centrally loaded footings (i.e., e/B = 0), the experimental modified bearing-capacity factor N_γ' compares reasonably well with the theory (with the assumption that the direct shear angle of friction is valid) only in the range of H/B > 0.6. For H/B < 0.4, the experimental values of N_γ' are lower than those predicted by theory, even by using the triaxial friction angle. Grain crushing, curvilinearity of the Mohr-Coulomb failure envelope at high normal stress, and possible anisotropy in sand due to the placement technique may be responsible for such results.
2. If the experimental variation of N_γ' with H/B' for centrally loaded footings is assumed to be correct, the ultimate bearing capacity of eccentrically loaded surface footings can be reasonably estimated by using the concept of effective area for continuous footing, $Q_u = 1/2\gamma(B - e)^2 N_\gamma'$.

REFERENCES

1. K. Terzaghi. Theoretical Soil Mechanics. Wiley, New York, 1943.

2. G.G. Meyerhof. The Ultimate Bearing Capacity of Foundations. Geotechnique, Vol. 2, 1951, pp. 301-332.
3. A. Caquot and J. Kerisel. Sur le terme de surface dans le calcul des foundations en milieu pulverulent. Proc., 3rd International Conference on Soil Mechanics and Foundation Engineering, Zurich, Switzerland, Vol. 1, 1953, pp. 336-337.
4. H. Lundgren and K. Mortensen. Determination by the Theory of Plasticity of the Bearing Capacity of Continuous Footings on Sand. Proc., 3rd International Conference on Soil Mechanics and Foundation Engineering, Zurich, Switzerland, Vol. 1, 1953, pp. 409-412.
5. J. Mandel and J. Salençon. Force portante d'un sol sur une assise rigide (etude theorique). Geotechnique, Vol. 22, No. 1, 1972, pp. 79-93.
6. G.G. Meyerhof. Ultimate Bearing Capacity of Footings on Sand Layer Overlying Clay. Canadian Geotechnical Journal, Vol. 11, No. 2, 1974, pp. 223-229.
7. T.W. Pfeifle and B.M. Das. Model Tests for Bearing Capacity in Sand. Journal of Geotechnical Engineering Division of ASCE, Vol. 105, No. GT9, 1979, pp. 1112-1116.
8. G.G. Meyerhof. The Bearing Capacity of Foundation Under Eccentric and Inclined Load. Proc., 3rd International Conference on Soil Mechanics and Foundation Engineering, Zurich, Switzerland, Vol. 1, 1953, pp. 440-445.

Publication of this paper sponsored by Committee on Foundations of Bridges and Other Structures.